



UNIVERSITÀ DI SIENA

Research Doctoral School

In

Biochemistry and molecular biology-BiBiM 2.0

Cycle: XXXIV

**Induction of inflammatory response by different stimuli in a
human lens epithelial cell line**

Supervisor

Dr. Roberta Moschini

PhD student

Viola Scali

ABSTRACT	4
INTRODUCTION	6
1. Diabetes: the metabolic disorder of the third millennium	7
2. Oxidative stress and reactive aldehydes: 4-hydroxy-2-nonenal.....	11
2.1 4-HNE formation	12
2.2 4-HNE structure and reactivity	16
2.3 4-HNE metabolism	20
2.4 Enantioselectivity of 4-HNE metabolism.....	25
2.5 4-HNE in cell signalling processes.....	27
3. Glycative stress and glucotoxicity: D-glucose	31
3.1 The polyol pathway	32
4. Oxidative and glycative stress: inflammatory response	34
4.1 NF- κ B (nuclear factor kappa-light-chain-enhancer of activated B cells)	35
4.2 COX-2 (cyclooxygenase-2).....	42
5. Oxidative and glycative stress: role of two NADPH-dependent enzymes	48
5.1 Aldose reductase (AKR1B1).....	48
5.2 Carbonyl reductase (CBR1)	52
AIM OF THE THESIS	56
MATERIALS AND METHODS	58
1. Materials	59
2. Methods.....	61
2.1 Cell culture.....	61
2.2 HLE-B3 cells preparation for the experimental procedures	61
2.3 Incubation of HLE-B3 cells under three different experimental conditions.....	62
2.4 Pro-inflammatory treatment of HLE-B3 cells	62
2.5 4-HNE preparation and quantification.....	63
2.6 Spectrophotometric GSH quantification	63
2.7 GS-HNE preparation and quantification	63
2.8 4-HNE determination in the incubation medium	64
2.9 D-glucose preparation	65
2.10 DMEM (Dulbecco's Modified Eagle's Medium) preparation	65
2.11 Cell viability assays.....	65
2.12 HLE-B3 crude extracts preparation for HPCE analysis and enzymatic assays.....	66
2.13 Sample preparation for HPCE analysis	66

2.14 High performance capillary electrophoresis (HPCE)	68
2.15 NADPH-dependent enzymatic activities assay.....	68
2.16 HLE-B3 cell lysates preparation for Western blotting analysis.....	68
2.17 Protein quantification	69
2.18 Western blotting.....	69
2.19 Evaluation of NF- κ B activation through a stably transfected HLE-B3 cell line	72
2.20 Empty control vector preparation	73
2.21 Amplification of pFireflyLuc2P and empty vector in XL-1 cells	73
2.22 Stable transfection of HLE-B3 cell line	73
2.23 Pro-inflammatory treatment of stably transfected HLE-B3 cells	74
2.24 Preparation of stably transfected HLE-B3 crude extracts for Firefly luciferase assay .	75
2.25 Quantification of the Firefly luciferase expression	75
2.26 Statistical analysis.....	77
RESULTS	78
1. Optimization of experimental conditions for the treatment of HLE-B3 cells with 4-HNE .	79
2. Inflammatory effect of 4-HNE in HLE-B3 cells	82
2.1 Time- and dose-dependent effect of 4-HNE	82
2.2 Evaluation of the inflammatory effect of 4-HNE enantiomers.....	84
2.3 Determination of glutathione and glutathione adduct levels in HLE-B3 cells treated with 4-HNE	85
2.4 Evaluation of the anti-inflammatory effect of two reductase activity inhibitors in HLE- B3 cells	89
2.5 Evaluation of 4-HNE pro-inflammatory effect on stably transfected HLE-B3_F cell line	94
3. Optimization of experimental conditions for the exposure of HLE-B3 cells to hyperglycaemic conditions	96
4. Pro-inflammatory effect of hyperglycaemic treatment on HLE-B3 cells	99
4.1 Evaluation of the cytotoxic effect of high glucose levels	99
4.2 Evaluation of time-dependent and dose-dependent effect of high glucose levels on COX-2 expression	100
4.3 Evaluation of NF- κ B activation induced by high glucose levels in HLE-B3_F cells...	102
4.4 Evaluation of the inhibitory effect of sorbinil on D-glucose pro-inflammatory effect.	105

4.5 Evaluation of the inhibitory effect of DMSO on NF- κ B activation induced by D-glucose
.....
106

4.6 Evaluation of Firefly luciferase expression under D-glucose stimulation in glucose-
deprived stably transfected HLE-B3 cells
107

DISCUSSION AND CONCLUSIONS 110

REFERENCES 114

ABSTRACT

Human lens epithelial cells, due to their ocular function, are normally exposed to radiating and oxidative stress conditions. Indeed, the lens is an environment rich in endogenous sources of reactive oxygen species (ROS), among which there are the high oxygen concentration and the chronic exposure to light, that have been linked to apoptosis in lens epithelial cells. Although multiple defence systems exist to protect the lens from the toxic effects of oxidative damage, including abundant antioxidant enzymes, reduced glutathione (GSH) and the chaperone-like functions of crystallins, increasing evidence suggest that oxidative stress may predispose the lens to cataract development. In fact, ROS can attack polyunsaturated fatty acids in membranes, causing lipid peroxidation and generating highly toxic reactive aldehydes. Among them, one of the most reactive is 4-hydroxy-2-nonenal (4-HNE) which can form adducts with DNA and proteins and, for this reason, undergoes a rapid enzymatic biotransformation that regulates its free content. The major enzymatic route of 4-HNE detoxification consists in its conjugation with glutathione (GSH) to generate 3-glutathionyl-4-hydroxynonanal (GS-HNE), an adduct that in turn can be either reduced or oxidized. It is worth underlying that the reduced form of GS-HNE, namely 3-glutathionyl-dihydroxynonane (GS-DHN), a product of a reaction catalyzed by both aldose reductase (AKR1B1) and carbonyl reductase (CBR1), is reported to be a mediator of cytokines, chemokines and growth factors-induced signalling pathways that trigger the inflammatory response associated with NF- κ B activation, leading to apoptosis in human lens epithelial cells. In addition, AKR1B1, that catalyzes the rate limiting step of the polyol pathway, under hyperglycaemic conditions promotes, through the activation of NF- κ B, the synthesis of many proteins such as proinflammatory cytokines (TNF- α , IL-1, IL-8), adhesion molecules (VCAM-1, ICAM-1), inducible nitric oxide synthase (iNOS) and cyclooxygenase-2 (COX-2), establishing a chronic pathological inflammatory response associated with the onset of diabetic complications. In summary, the aim of this thesis was providing evidence that a cultured human lens epithelial cell line, HLE-B3, could respond to both 4-HNE and D-glucose, considered as two endogenous pro-inflammatory stimuli intertwined by AKR1B1 activity, that can activate the inflammatory response associated with the transcription factor NF- κ B and COX-2. The pro-inflammatory effect of both 4-HNE and hyperglycaemia was investigated in HLE-B3 cells by evaluating, through Western blotting, the increase in COX-2 expression as well as in stably transfected HLE-B3 cells by measuring NF- κ B activation. Capillary electrophoresis analysis suggested the formation, in HLE-B3 cells incubated with 4-HNE, of a

glutathionylated 4-HNE adduct that likely correspond to GS-HNE, indicating that the pro-inflammatory action exerted by the aldehyde could be mediated by its glutathionylated derivatives. Finally, the role played by the two enzymes potentially involved in mediating both 4-HNE- and D-glucose-induced inflammatory signalling, AKR1B1 and CBR1, was verified by assessing the anti-inflammatory effect of two their well-known inhibitors, sorbinil and rutin. Since these inhibitors appears not to significantly attenuate COX-2 expression induced by 4-HNE nor NF- κ B activation triggered by hyperglycaemic conditions, probably due to methodological limitations, further experiments are needed in order to clarify the efficacy of these molecules in the anti-inflammatory response. In this regard, it has also to take into account the role of the solvent used for inhibitors solubilization, which could interfere with the performed analysis.

INTRODUCTION

1. Diabetes: the metabolic disorder of the third millennium

Diabetes is a chronic multifactorial disease characterised by hyperglycaemia which occurs either for a low insulin production by the pancreas or for a reduced body capacity to use this hormone. In fact, diabetes can be divided into two main categories depending on the etiology of the hyperglycaemia: type 1 diabetes is primarily due to the autoimmune-mediated destruction of pancreatic β -cells and consequent insulin deficiency as a result of both genetic and environmental factors (Hiroaki and Eisenbarth, 2002); type 2 form of the disease, that accounts approximately 85% of cases and starts almost always in middle- and late-adulthood, is characterised by resistance to insulin action on glucose uptake in peripheral tissues, impaired insulin action to inhibit hepatic glucose production or dysregulated insulin secretion (American Diabetes Association, 2018). Type 2 diabetes is a polygenic metabolic disorder, but its onset could depend also on environmental factors such as diet, physical activity and age (Hu et al., 2001). Even though there is a marked geographical variation in diabetes prevalence, it is considered one of the largest global public health concerns because is a leading cause of mortality and reduced life expectancy. As reported by World Health Organization, the prevalence of diabetes has exponentially grown in the past decades increasing from 108 million in 1980 to 425 million in 2017 (World Health Organization, 2016) and it is expected to be 629 million by 2045 (International Diabetes Federation, 2017) (Fig. 1).

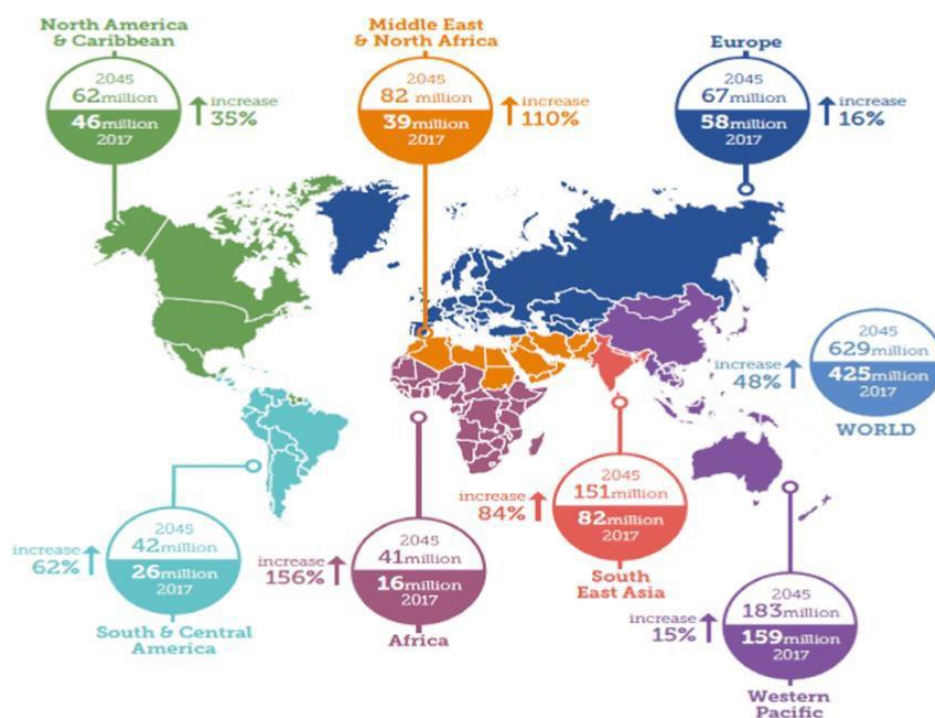


Figure 1 – Number of people with diabetes worldwide and per region in 2017 and the expected increase by 2045. Source: International Diabetes Federation.

The exponential growth is more marked in developing countries, especially in areas where populations are rapidly adopting typical Western lifestyle that includes physical inactivity and diets rich in red and processed meat and sugar-sweetened beverages but low in fruit and vegetables and where obesity is particularly common (Forouhi and Wareham, 2014).

Several clinical studies and meta-analysis have demonstrated that systemic insulin resistance is one of the most frequent consequences of obesity that represents a significant risk factor for developing type 2 diabetes (Centers for Disease Control and Prevention, 2004; Kahn et al., 2006). The accumulation of energy due to excessive calorie intake leads initially to fat accumulation in the subcutaneous tissue and then to other tissue compartments including liver, pancreas, muscles, perivascular and pericardium (Sattar and Gill, 2014). White adipose tissue is no longer considered an inert storage organ but rather an active endocrine biological structure producing and releasing plenty of cytokines, hormones and other factors called adipokines which have potential immunomodulatory effect (Fantuzzi, 2005). Because of obesity-induced adipose tissue expansion, adipocytes increase the production of inflammatory mediators and chemoattractant molecules such as MCP-1 that can promote the development of systemic pro-inflammatory status by recruiting into adipose tissue macrophages and other immune cells. Macrophages and T-lymphocytes residing in the adipose tissue are also a source of pro-inflammatory factors such as TNF- α , IL-1, IL-6, CRP, iNOS and MIF that have local effects on adipocytes and circulate in the periphery affecting the liver and skeletal muscle insulin sensitivity (Burhans et al., 2018; Nicholson et al., 2018). The association between inflammation and insulin resistance has been proposed for the first time by Hotamisligil and colleagues who demonstrated that the pro-inflammatory cytokine TNF- α is the principal mediator of insulin resistance (Hotamisligil et al., 1993). In mouse and rat models of obesity, the expression of TNF- α was induced locally within adipose tissue as well as systemically in the plasma. The neutralization of TNF- α activity with recombinant TNF- α receptor-immunoglobulin G chimeric protein resulted in the restoration of insulin sensitivity, suggesting a direct role for TNF- α in the development of insulin resistance. Since several studies have clearly shown a strong relationship between inflammation and type 2 diabetes pathogenesis, even if, to date, the treatment with TNF- α antagonists in the human has not reproduced the results observed in the mice (Ofei et al., 1996), additional clinical trials could be relevant to block TNF- α signalling, either alone or in conjunction with other cytokine-blocking approaches.

Insulin resistance gives rise to a hyperglycaemic state that is a major risk factor for the onset of long-term diabetic complications. Increasing evidence indicates that hyperglycaemia is the initiating cause of the tissue damage occurring in diabetes, contributing through several

mechanisms to both microvascular complications including retinopathy, neuropathy and nephropathy and cardiovascular diseases which in turn negatively impact the prognosis of patients with diabetes (Gleissner et al., 2007). However, tissue damages induced by hyperglycaemic conditions are variable and depend on the rate of glucose uptake by cells from extracellular fluids. It occurs by carrier-mediated facilitated diffusion through specific glucose transporters which are ubiquitously expressed in plasma membrane of cells (Mueckler, 1990). X-ray crystallography analysis of GLUT1, the first identified GLUT transporter, revealed a protein structure of 12 transmembrane α -helices organized in a membrane channel for the substrate transport (Deng et al., 2014). The study of glucose transporters has led to the discovery of a family of 14 structurally related glucose transporters with tissue specific expression and different transcriptional and post-transcriptional regulation (Kahn and Flier, 1990). All these transporters have in common the ability to transport glucose but differ from each other in terms of their relative transport efficiencies and kinetics. Most of them are high-affinity, low-capacity transporters with K_D constants ranging from 0.3 mM to 6 mM (Manolescu et al., 2007).

Many studies focused on the characterisation and regulation of glucose transport in those tissues where the modulation of glucose transport activity may be related to the development of diabetic complications. Most cells can reduce the transport of glucose inside the cell when they are exposed to hyperglycaemia in order to maintain intracellular glucose concentration constant. In fact, Kaiser and colleagues demonstrated in vascular smooth muscle cells the presence of an effective autoregulatory mechanism of the glucose transport activity that occurs through a change in the cellular content of GLUT1 protein (Kaiser et al., 1993). These results are in agreement with those described in fibroblasts, adipocytes, cultured brain cells and skeletal muscle cells that responded in a similar manner as vascular smooth muscle cells to changes in glucose levels, decreasing their transport activity by 1.5 to 2-fold when medium glucose concentration was increased up to 22 mM (Alpert et al., 2002; Klip et al., 1994). Although it is still unclear whether the cellular mechanism involved in this autoregulatory process consists in translocation of transporters between the internal membranes and the plasma membrane or in a change in their intrinsic activity, the adaptive mechanism operating in these cell types plays the important physiological role of protecting cells from prolonged exposure to high concentrations of glucose. In contrast, a typical characteristic of cells that can be damaged by hyperglycaemia, like endothelial cells and mesangial cells, is their lack of downregulation of glucose transport when extracellular glucose is elevated, leading to high glucose levels inside the cell (Clyne, 2021; Szablewski, 2017). A study performed by Tumova and colleagues indicated that the endothelial

cell uptake of glucose was rapid and was predominantly mediated by GLUT-1 transporter. The modulation of its function under hyperglycaemic conditions was relatively modest, suggesting that concerning glucose uptake and its transport across the plasmamembrane endothelial cells are unresponsive to increases in glucose concentration (Tumova et al., 2016).

These experimental evidences are particularly relevant because suggest that what causes hyperglycaemia-induced complications are mostly associated with intracellular mechanisms. Brownlee and colleagues discovered that in different cell types a relevant consequence of hyperglycaemia is the increase in reactive oxygen species (ROS) (Brownlee, 2001; Son, 2012). This was also confirmed by Yano and co-workers who, in a study conducted on cultured bovine aortic endothelial cells, observed an increase in intracellular ROS production after 24 hours of exposure to high glucose levels (Yano et al., 2004). In another study, it was also reported that the incubation of rat mesangial cells with 30 mM D-glucose caused an increase in ROS production within 15 minutes that could be prevented by inhibiting glucose transport or by treating cells with nonmetabolizing analogues of glucose (Ha and Lee, 2000). These results suggested that glucose uptake and its subsequent metabolism are required for high glucose-induced ROS generation in cell types that are unable to maintain their intracellular glucose concentration under hyperglycaemic conditions. In fact, in a hyperglycaemic environment there is more glucose that is oxidized through glycolysis and Krebs cycle and, consequently, more electron donors NADH and FADH₂ are pushed into the electron transport chain. As a result, the voltage gradient across the mitochondrial membrane increases until electron transfer inside complex III is blocked causing the electrons to back up to coenzyme Q that donates electrons to molecular oxygen, thereby generating superoxide anion (O^{-•}) (Rolo and Palmeira, 2006) (Fig. 2).

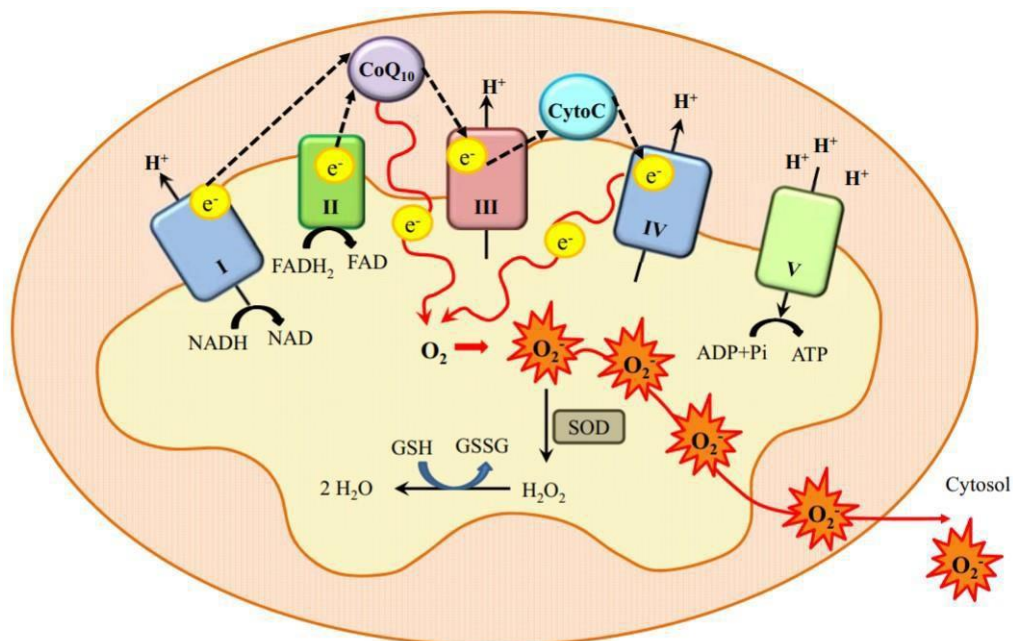


Figure 2 – The electron transportation chain and the generation of ROS in mitochondria. The electrons from NADH and FADH₂ are firstly transported to Complex I and II, then to coenzyme Q and to cytochrome C in the complex III. Finally, through complex IV they are transferred to O₂ producing H₂O. In this process, all the complexes pump protons out of mitochondrial matrix to form a gradient of protons between intermembrane space and mitochondrial matrix. The energy of the proton gradient drives ATP synthase to generate ATP. Hyperglycaemia can induce the blockage of the normal electron transportation and O₂ can accept the electrons increasing the production of reactive oxygen species (Fiorentino et al., 2013).

Furthermore, high glucose concentrations may promote ROS accumulation by increasing NADPH oxidase activity as well as upregulating the expression of its subunits like p22^{phox} and p47^{phox} (Lee et al., 2020). In fact, this enzyme drives the production of ROS by transferring electrons from NADPH to molecular oxygen. Elevated ROS levels finally lead to oxidative stress, a biological state that may be defined as an alteration in the balance between oxidant production and impaired action of the antioxidant systems.

2. Oxidative stress and reactive aldehydes: 4-hydroxy-2-nonenal

4-Hydroxy-2-nonenal (4-HNE) is one of the main products of lipid peroxidation, a process under which oxidants such as free radicals induce lipid oxidative damage, particularly of polyunsaturated fatty acids (PUFAs) which are demonstrated to be the most sensitive to oxidative modification. Among the different aldehydes that can be generated as secondary products during lipid peroxidation, 4-HNE is the most relevant because it is considered a very reactive and toxic molecule that is produced in relatively large amounts. In fact, since its discovery in 60s, 4-HNE has been extensively studied because of its high reactivity towards proteins and nucleic acids leading to the formation of cytotoxic and genotoxic adducts that are involved in the etiology and progression of several pathologies, such as diabetes, atherosclerosis, cancer and ageing (Leitinger, 2003; Nair et al., 2007; Zimniak, 2008). 4-HNE is also considered a signalling molecule being able to modulate several cellular processes, under both physiological and pathological conditions. In fact, many studies report the involvement of 4-HNE in the regulation of several stress-sensitive transcription factors such as nuclear factor erythroid 2-related factor 2 (Nrf2), activating protein-1 (AP-1), NF-κB and peroxisome proliferator-activated receptors (PPAR), in cell proliferation, cell survival, autophagy, senescence, apoptosis and necrosis (Dodson et al., 2017; Muzio et al., 2021; Sunjic et al., 2021).

2.1 4-HNE formation

4-HNE is an α , β -unsaturated aldehyde generated from the oxidation of ω -6 PUFAs, such as arachidonic acid and linoleic acid (Esterbauer et al., 1991). Under oxidative stress conditions lipid peroxidation is triggered mainly by ROS, especially hydroxyl ($\text{HO}\cdot$) and hydroperoxyl ($\text{HO}\cdot_2$) radicals. The hydroxyl radical ($\text{HO}\cdot$), in particular, is the chemically most reactive species of activated oxygen and, in biological systems, it is assumed to be formed through redox cycling by the Fenton reaction, where free iron (Fe^{2+}) reacts with hydrogen peroxide (H_2O_2), and the Haber-Weiss reaction, which results in the production of Fe^{2+} when superoxide reacts with ferric iron (Fe^{3+}). Indeed, the hydroperoxyl radical ($\text{HO}\cdot_2$) generates H_2O_2 which can react with redox active metals to further produce $\text{HO}\cdot$ through Fenton or Haber-Weiss reaction (Fig. 3). ROS have an important role in the chemistry of lipid peroxidation, since, in a not-specifically manner, they attack biomolecules located near their site of generation, thus initiating the oxidative chain reaction of polyunsaturated phospholipids (Ayala et al., 2014).

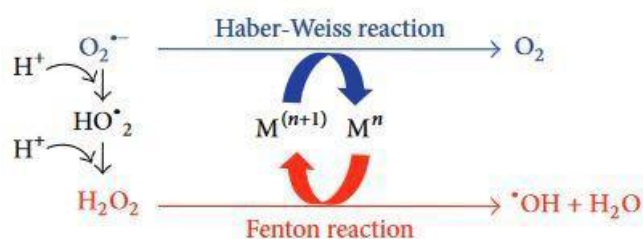


Figure 3 – Fenton and Haber-Weiss reaction. Reduced form of transition-metals (M^n) reacts through the Fenton reaction with hydrogen peroxide (H_2O_2), leading to the generation of $\cdot\text{OH}$. Superoxide radical ($\text{O}_2^{\bullet-}$) can also react with oxidized form of transition metals ($\text{M}^{(n+1)}$) in the Haber-Weiss reaction leading to the production of M^n , which then again affects redox cycling (Ayala et al., 2014).

The process of lipid peroxidation triggered by free radicals consists in three steps: initiation, propagation and termination (Yin et al., 2011). In the initiation step, hydroxyl radical abstracts the allylic hydrogen from the methylene group of the fatty acid aliphatic chain, forming the carbon-centered lipid radical ($\text{L}\cdot$). The process is followed by the stabilization of the carbon radical through a rearrangement of the molecule to form a conjugated diene. In the propagation phase, the lipid radical ($\text{L}\cdot$) rapidly reacts with oxygen to generate a lipid peroxy radical ($\text{LOO}\cdot$), that, in turn, reacts with another lipid molecule for the abstraction of a hydrogen atom forming a new $\text{L}\cdot$, which continues the chain reaction, and lipid hydroperoxide (LOOH). The last reaction consists in the donation of a hydrogen atom from antioxidants, such as vitamin

E, to the lipid peroxy radical species, resulting in the formation of nonradical products. Once lipid peroxidation initiation is triggered, a propagation of chain reactions will take place until termination products are released (Ayala et al., 2014) (Fig. 4).

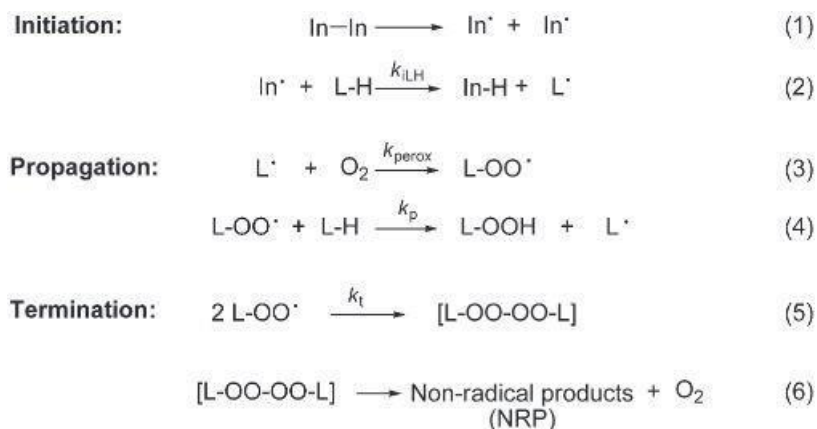


Figure 4 – Reactions in the free radical chain oxidation mechanism. In: initiator; L: lipid. One of the most potent initiator of the lipid peroxidation process is the hydroxyl radical (OH•) (Yin et al., 2011).

The main primary products of lipid peroxidation are lipid hydroperoxides, which are generated during the propagation step. These compounds might undergo a molecular breakdown to yield a broad array of smaller fragments, three to nine carbons in length, including aldehydes, such as 2-alkenals and 4-hydroxy-2-alkenals. Among them, 4-HNE, as previously reported, is the major aldehyde formed during lipid peroxidation of ω-6 polyunsaturated fatty acids, such as linoleic acid and arachidonic acid. In particular, as shown in figure 5, linoleic acid in plants can be oxidized to 9-hydroperoxyoctadecadienoate (9(S)-HPODE) by plant lipoxygenase and then a hydroperoxide lyase cleaves the hydroperoxide generating two aldehydes. One of them, the 3Z-nonanal, is readily oxidized through a non-enzymatic pathway to 4-hydroperoxy-2E-nonanal (4-HPNE) which represents the direct precursor of 4-HNE (Schneider et al., 2001). Even though the analogous of the enzyme hydroperoxide lyase has not found in animals, similar pathways were proposed to account for the formation of 4-HNE starting from two different intermediate metabolites: 9(S)-HPODE- or 13(S)- HPODE (Schneider et al., 2001) (Fig. 5). Following the abstraction of an allylic hydrogen and the addition of an oxygen molecule, a peroxy radical intermediate is produced which attacks the conjugated double bonds of another hydroperoxide, forming the corresponding dihydroperoxide derivative. This product is highly unstable, thus, after rearrangement and cleavage, it produces 9-oxononanoic acid and 4-HPNE. 4-HPNE might be reduced to form 4-HNE or dehydrated to generate 4-oxo-2-nonenal (4-ONE) (Liu et al., 2011) (Fig. 6).

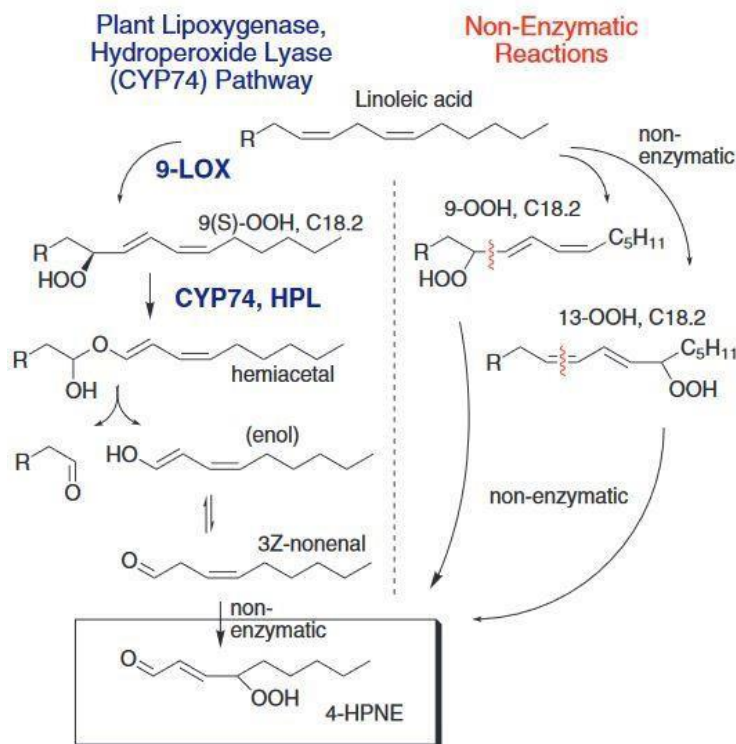


Figure 5 – Enzymatic and non-enzymatic pathways to 4-HPNE. In the plant lipoxygenase hydroperoxide lyase pathway, the 9-hydroperoxide of linoleic acid is cleaved to 3Z-nonenal via rearrangement into an unstable hemiacetal. Non-enzymatic oxygenation of 3Z-nonenal gives 4-HPNE. Indeed, autoxidation studies indicate that both the 9- and the 13-hydroperoxide of linoleic acid are precursors of 4-HPNE (Schneider et al., 2008).

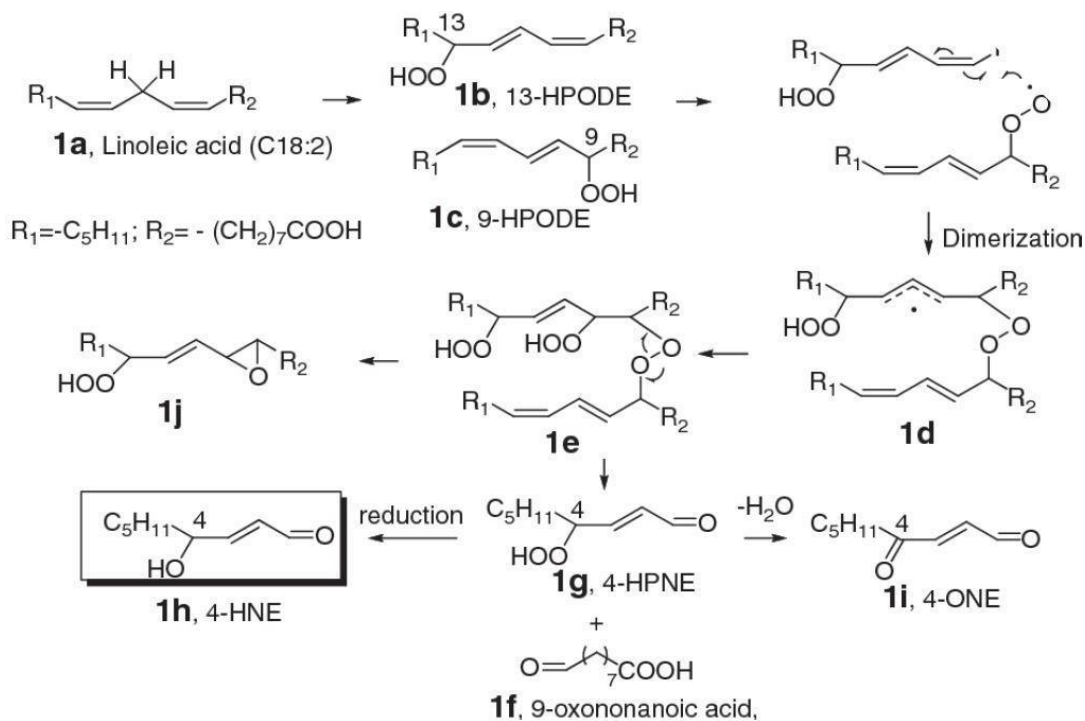


Figure 6 – Formation of 4-HNE from linoleic acid oxidation (Liu et al., 2011).

2.2 4-HNE structure and reactivity

4-HNE is considered one of the most reactive lipid peroxidation end products that is involved in cytotoxic processes associated with oxidative stress in different tissues (Poli and Schaur, 2000; Parola et al., 1999). Compared to free radicals, 4-HNE is relatively stable and can diffuse within the cell passing among subcellular compartments and attack target biomolecules far from the initial generation sites including proteins, DNA and phospholipids, generating a variety of intra- and intermolecular covalent adducts (Uchida, 2003). Furthermore, considering the high intracellular levels of glutathione (GSH), 4-HNE can react with this molecule forming the 3-glutathionyl-4-hydroxynonanal (GS-HNE) adduct (Gueraud, 2017).

4-HNE contains three functional groups which in many cases act in concert and help to explain its high reactivity: carbonyl group on carbon 1, a double-bond between carbon 2 and 3, and a hydroxyl group on carbon 4 (Fig. 7).

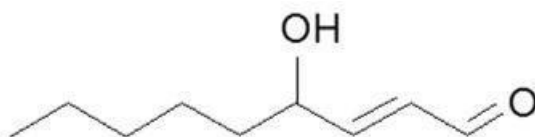


Figure 7 – Chemical structure of 4-HNE (Gueraud, 2017).

The conjugated system of a carbon to carbon double bond, the carbonyl group and the hydroxyl group at carbon 4 provide a partial positive charge to carbon 3. As a consequence, 4-HNE is considered as “soft electrophile” with the carbon 3 as the electrophilic center of the molecule that is susceptible to nucleophilic attack by cellular nucleophilic groups present in biomolecules, especially thiol and amino groups, in a reaction known as Michael addition. The adduct acquires a rotatory freedom at the C2-C3 bond and, as a consequence, 4-HNE can undergo a secondary reaction which occurs between the hydroxyl group on carbon 4 and the carbonyl group on carbon 1 leading to the formation of an intramolecular hemi-acetal (Schaur, 2003) (Fig. 8).

Furthermore, the 4-HNE carbonyl moiety can bind covalently to primary amines, such as the ϵ -amino group of lysine residues in proteins, forming a Schiff base that can undergo cyclisation generating a very stable pyrrole compound (Fig. 8).

As previously described, there is a competitive reaction of lysine residues for carbon 3 and

carbon 1 of 4-HNE on both carbon 3 and carbon 1 but, since the latter reaction is rather slow, reversible Michael adduct generation prevails (Luczaj et al., 2017). However, frequently these reactions occursimultaneously leading to the formation of protein cross-links (Fig. 9).

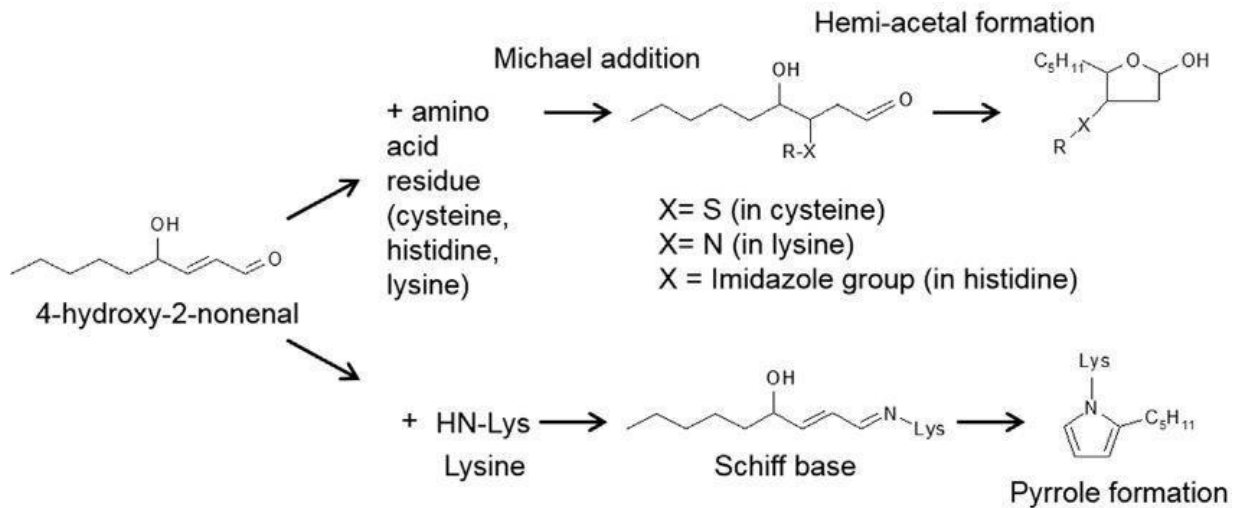


Figure 8 – Michael addition and Schiff base formation of 4-HNE on amino acids residues in proteins or peptides and further cyclisation (Gueraud, 2017).

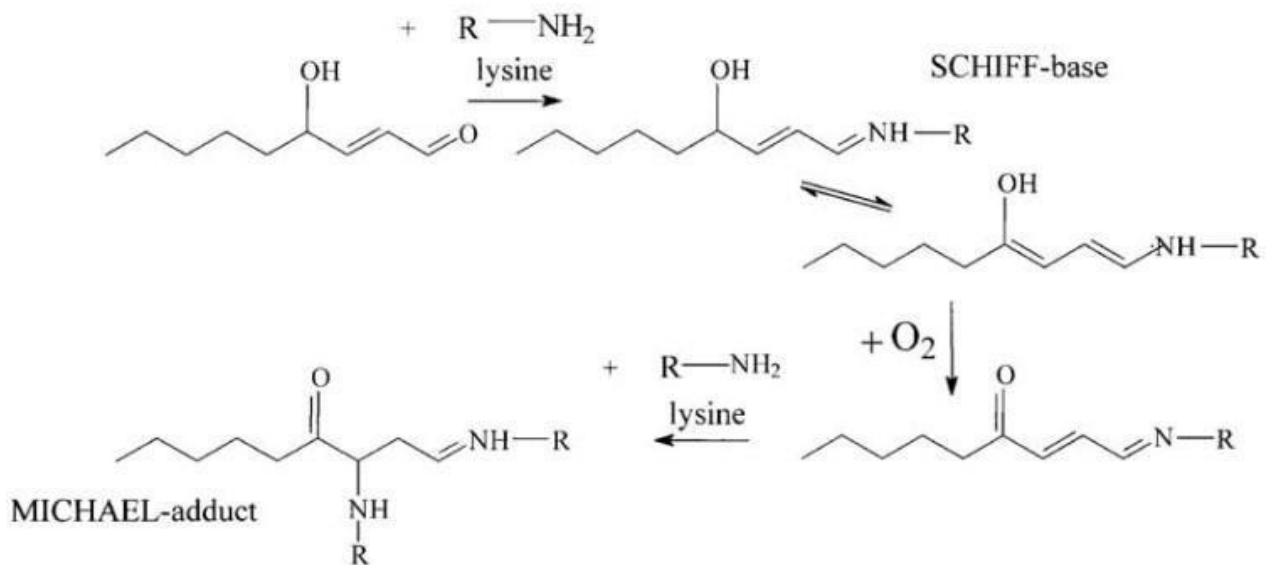


Figure 9 – Formation of lysine-derived protein cross-links (Schaur, 2003).

In addition, a noteworthy feature of 4-HNE consists in its chiral property due to the presence of a stereogenic center at carbon 4 so that it can exist as 4-(R)-HNE and 4-(S)-HNE (Fig. 10). The lipid peroxidation process leads to the formation of a racemic 50:50 mixture of the two 4-HNE enantiomers (Bringmann et al., 1994) but, according to several studies, 4-(R)-HNE and 4-(S)-

HNE seem to play a different biological role and to be detoxified through different metabolic pathways (Hiratsuka et al., 2000; Hiratsuka et al., 2001).

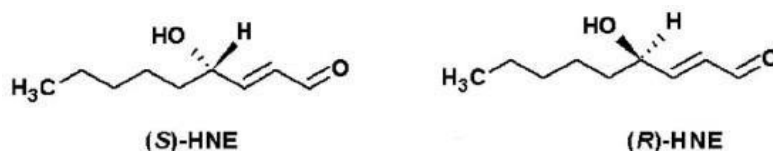


Figure 10 – 4-HNE enantiomers (Honzatko et al., 2005).

2.2.1 4-HNE-induced phospholipids modification

4-HNE is able to generate both Michael adducts and Schiff bases by reacting with amino phospholipids such as phosphatidylethanolamine (PE) and phosphatidylserine (PS). However, the adducts with phosphatidylethanolamine prevail, probably because of the low reactivity of phosphatidylserine with 4-HNE (Guichardant et al., 1998) and because it represents the least abundant phospholipid class in cellular membranes. The aldehyde-mediated phospholipids modification alters some structural properties of plasma membrane, affecting in particular its stability and fluidity and the phospholipids asymmetric distribution, whose maintenance is crucial for cellular life (Castegna et al., 2004).

2.2.2 4-HNE-induced DNA modification

The cytopathological and genotoxic effects of 4-HNE have been evidenced for the first time in cultured cell systems by Esterbauer and colleagues (Brambilla et al., 1986) who afterwards observed a significant increase in DNA fragmentation, sister-chromatid exchanges (SCE), micronuclei and chromosomal aberrations in primary hepatocytes culture exposed to different concentrations of 4- HNE (Eckl et al., 1993). This aldehyde is considered a highly mutagenic agent because of the formation of exocyclic adducts with DNA due to its reaction with the amino group of deoxyguanosine, followed by ring closure and subsequent Schiff base formation (Fig. 11). Another pathway responsible for the mutagenicity of 4-HNE involves its oxidation to the corresponding epoxide which is sufficiently stable that it is transported through compartments and eventually reacts with the deoxyguanosine moiety of DNA generating cyclic etheno adducts that have been shown to have important implications in carcinogenesis (Chen and Chung, 1996) (Fig. 12). The 4-HNE-derived adducts on DNA induce base substitutions, especially G → T transversions that are the predominant mutations, and in human cells they are shown to be repaired by the nucleotide excision repair (NER) pathway (Minko et al., 2009).

However, it is very likely that many proteins involved in DNA repair mechanisms may be modified by 4-HNE, resulting in detrimental effects on cellular DNA repair capacity that in turn may contribute to cytotoxicity and carcinogenicity of 4-HNE (Choudhury et al.,2013).

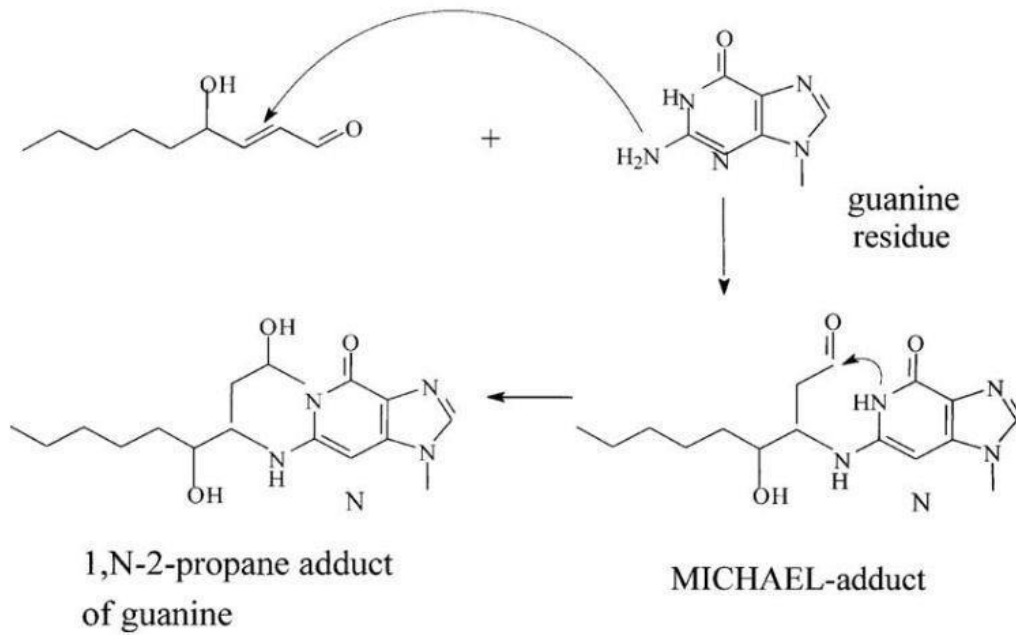


Figure 11 – Formation of a guanine adduct with DNA (Schaur, 2003).

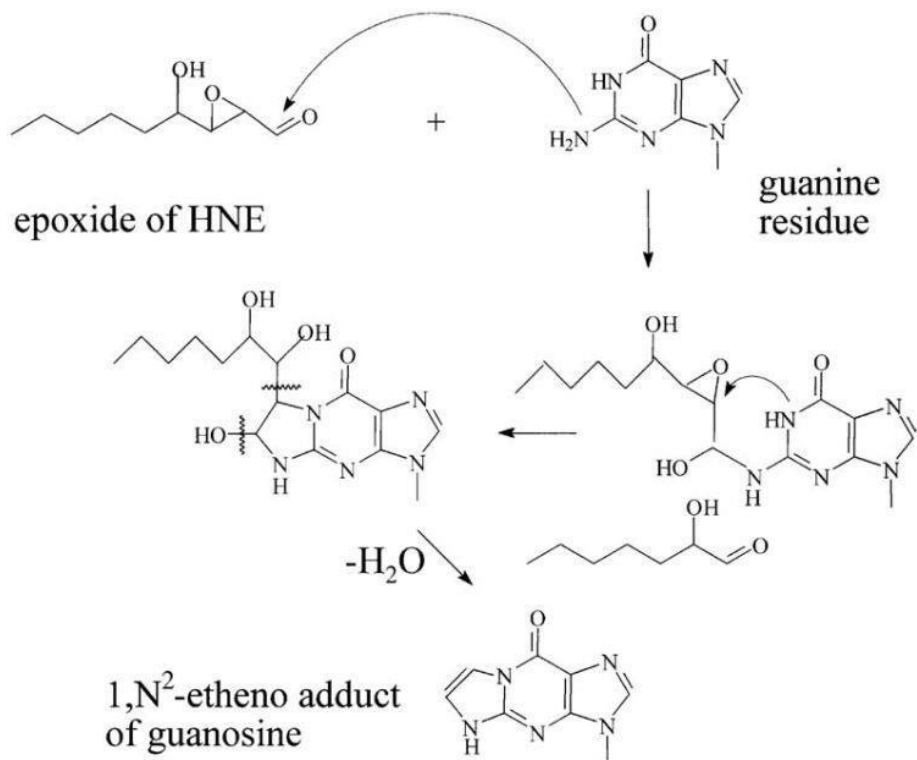


Figure 12 – Reaction of 4-HNE-epoxide with DNA (Schaur, 2003).

2.2.3 4-HNE-induced proteins modification

About 8% of the 4-HNE generated in the cell is bound to proteins forming in almost total cases Michael mostly with the thiol group of cysteine residues. The 4-HNE- induced protein modification has an impact both on the structure and, consequently, on the function of enzymes or proteins involved in several cellular processes (Gęgotek and Skrzydlewska, 2019).

As a consequence of 4-HNE modification, it is observed an increase in protein aggregates that are more susceptible to be removed by the proteasome (Poli et al., 2008). *In vitro* studies have demonstrated that the proteasome-dependent protein degradation plays a crucial role in preventing the accumulation of 4-HNE-protein adducts in the cell (Grune et al., 2003; Shringarpure et al., 2003). However, the efficiency of the degradation process under oxidative stress conditions depends on both 4-HNE levels and proteasome activity. In fact, high 4-HNE concentrations ($\geq 100 \mu\text{M}$) inhibit proteasome activity impairing cellular protein turnover so that 4-HNE modified proteins, no longer functional, accumulate in the cell altering its normal physiology (Grune and Davies, 2003; Okada et al., 1999). Under pathological conditions, a dramatic increase of 4-HNE-protein adducts levels occurs, contributing to the etiology and progression of neurodegenerative and metabolic disorders and cancer (Castro et al., 2017).

2.3 4-HNE metabolism

Since continuative oxidative stress conditions can lead to 4-HNE accumulation thereby compromising cell functions, the metabolic fate of 4-HNE has raised great attention. This is explained by the fact that, due to its high reactivity, 4-HNE undergoes a rapid biotransformation which regulates its cellular content, thus making the metabolic process an important factor to be considered for the modulation of its biological activity. 4-HNE detoxification occurs through a heterogeneous set of biotransformations, both enzymatic and non-enzymatic, yielding reversible and irreversible 4-HNE derivatives (Fig. 13). However, while the main enzymatic detoxification reactions of 4-HNE have been identified both in *in vitro* and animal models, the role played by non-enzymatic reactions in 4-HNE metabolism still needs to be elucidated.

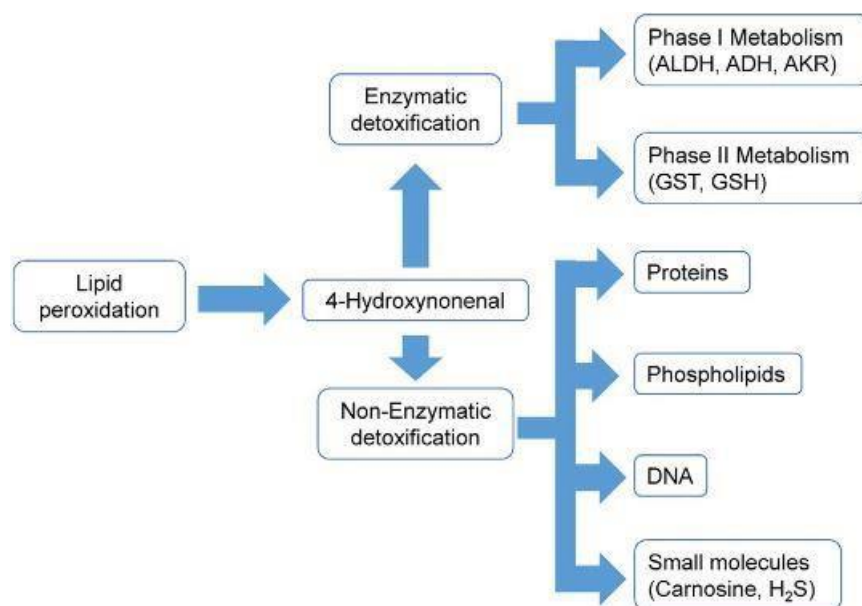


Figure 13 – Overview of main enzymatic and non-enzymatic detoxification pathways of 4-HNE (Mol et al., 2017).

2.3.1 Non-enzymatic detoxification

As described before, 4-HNE, due to its electrophilic properties, can spontaneously react with endogenous molecules containing nucleophilic sites such as proteins, nucleic acids and phospholipids. Even though biomolecules modification has been initially considered as toxic consequence of intracellular 4-HNE accumulation under oxidative stress conditions, several studies revealed that it can also have protective and modulatory effects that have reported to be obtained through two different mechanisms.

Highly oxidative conditions can irreversibly oxidize the thiol groups modifying consequently proteins' structure and function (Yang et al., 2015). However, considering the general reversibility of Michael adducts and that a vast majority of them is removed in intact cells, it has been suggested that 4-HNE-induced covalent modifications of thiol groups can protect proteins from irreversible inactivation, allowing their restoration when the oxidative stress disappears. In fact, several papers have revealed, using direct and indirect evidences, the ability of GSH to remove 4-HNE from 4-HNE- protein covalent adducts. Incubation of glutathione peroxidase with 4-HNE resulted in a loss of enzymatic activity in a concentration-dependent manner but this effect was almost completely prevented by adding 1 mM GSH to the incubation mixture 30 minutes after 4-HNE spiking (Bosch Morell et al., 1999).

A second protective mechanism involves some extracellular and cytosolic proteins, such as albumin and actin, that are highly reactive not only because of their abundance but also because they possess extremely reactive and accessible cysteine residues that can be richly modified by 4-HNE. When their concentration is largely higher than that of 4-HNE, albumin and actin have been identified as sacrificial substrates of 4-HNE being able to trap it almost completely with a minimal impact on their biological activity. The efficient quenching of these abundant proteins opens a question regarding their potential role as non-enzymatic detoxifying agents of 4-HNE (Dalle Donne et al., 2007; Aldini et al., 2006).

2.3.2 Enzymatic detoxification

The enzymatic metabolism of 4-HNE was investigated in well-differentiated rat hepatoma cell line MH₁C₁ by Ferro and co-workers at the end of the 1980s (Ferro et al., 1988) and then further characterised in both *in vitro* and *in vivo* models. Mammalian cells detoxify 4-HNE using a variety of redox enzymes (phase I metabolism) and/or through conjugation to GSH (phase II metabolism) (Fig. 14). In the first phase of 4-HNE enzymatic detoxification, the aldehyde is metabolized by several NAD(P)⁺- and NAD(P)H-dependent oxidoreductases (Fig. 14). Actually, different enzymes, such as aldehyde dehydrogenases (ALDH), can rapidly oxidize the 4-HNE carbonyl moiety generating 4-hydroxy-nonenoic acid (HNA). Different isoforms of ALDH have been described to catalyse this reaction, among which ALDH1A1, ALDH2 and ALDH3A1 are the most studied ones (Yoval Sánchez and Rodríguez Zavala, 2012). Many papers have been published on the protective role of ALDH enzymes towards 4-HNE cytotoxicity, thus underlying the relevance of such pathway in 4-HNE detoxification (Singh et al., 2013; Zhang et al., 2018). For instance, the overexpression or the activation of ALDH2 by several low-molecular-weight compounds resulted in an improved detoxification of 4-HNE and a consequent reduction of 4-HNE-protein adduct accumulation (Chen et al., 2008). Moreover, ALDH2 overexpression was shown also to prevent 4-HNE induced cell death in cultured primary hippocampal neurons (Bai and Mei, 2011). HNA is not the final metabolite after oxidation of 4-HNE, as it is able to undergo β -oxidation. This reaction is considered a very relevant step in 4-HNE detoxification, as demonstrated by Li and colleagues who observed that this pathway might be inhibited in ischemic rat heart, thus increasing both 4-HNE concentration and, as a consequence, the formation of 4-HNE-protein adducts, contributing to the onset of the pathology (Liet al., 2013).

Besides oxidation, the carbonyl group of 4-HNE can also be reduced to the corresponding

alcohol 1,4-dihydroxynonene (DHN) in reactions catalysed by alcohol dehydrogenase (ADH) or aldo-keto reductase (AKR) activities. ADHs are a family of NADH-dependent enzymes mainly located in the cytosol of hepatic cells whose principal function is breaking down alcohols. Although these enzymes have not been extensively studied in humans, there are some of them described to show activity towards aldehydes in rats (Boleda et al., 1993). On the other hand, the aldo-keto reductase superfamily is reported to have in humans at least 15 isozymes but only few are able to catalyse the reduction of 4-HNE and, among these, the most relevant are reported to be AKR1B10 and AKR1B1. The first one catalyses the NADPH-dependent reduction of 4-HNE and other reactive aldehydes such as acrolein, crotonaldehyde and trans-2-hexanal to their corresponding alcohols, but also the reduction of their glutathionyl conjugates, except for GS-HNE (Zhong et al., 2009). In contrast, AKR1B1 has been found to have more activity towards glutathionyl conjugates than towards free 4-HNE (Srivastava *et al.*, 1995). Unlike the oxidation of 4-HNE whose role has been deeply investigated relating to the onset of different pathologies, further studies need to be performed in order to discover protective roles of the 4-HNE reductive detoxification pathway.

The phase II metabolism refers to the conjugation of 4-HNE with glutathione to give 3-glutathionyl-4-hydroxynonanal (GS-HNE), due to Michael addition between the 4-HNE electrophilic carbon 3 and the GSH cysteine residue. Since the GSH Michael addition removes the C2-C3 double bond, GS-HNE exists for 95% as a cyclic hemiacetal, for the reaction between hydroxyl group on C4 and the carbonyl group on C1, and 5% as a free aldehyde (Schaur, 2003). Although 4-HNE conjugation with GSH could occur spontaneously, there are enzymes catalyzing this process which belong to the α class of glutathione-S-transferase family (GSTs) and, overall, play an important role in the detoxification of electrophiles (Schaur, 2003). Since GST was found to be inhibited by the accumulation of the resulting GS-HNE adduct, such conjugate needs to be further metabolized and excreted by cells in the extracellular environment. Thus, GS-HNE can be either reduced or oxidized through pathways that have been well described. The oxidative pathway consists in the adduct NAD⁺-dependent oxidation catalyzed by aldehyde dehydrogenase to 4-hydroxynonanoic acid–glutathione (GS-HNA), that can undergo dehydration reaction to form the corresponding cyclic lactone (GS-HNL) (Alary et al., 2003). Alternatively, NADPH-dependent aldo-keto reductases can reduce GS-HNE to 3-glutathionyl-1,4-dihydroxynonene (GS-DHN) (Srivastava et al., 1995). In addition, a new function for the carbonyl reductase 1 (CBR1) enzyme has been recently highlighted since it has been shown to be able to oxidize the hemiacetal form of GS-HNE to GS-HNL using NADP⁺ as cofactor and to reduce the free aldehyde to GS-DHN in a NADPH-dependent manner, as well.

Furthermore, CBR1 can convert GS-HNA to glutathionyl-4-ketononanoic acid (GS-ONA) (Moschini et al., 2015; Rotondo et al., 2016).

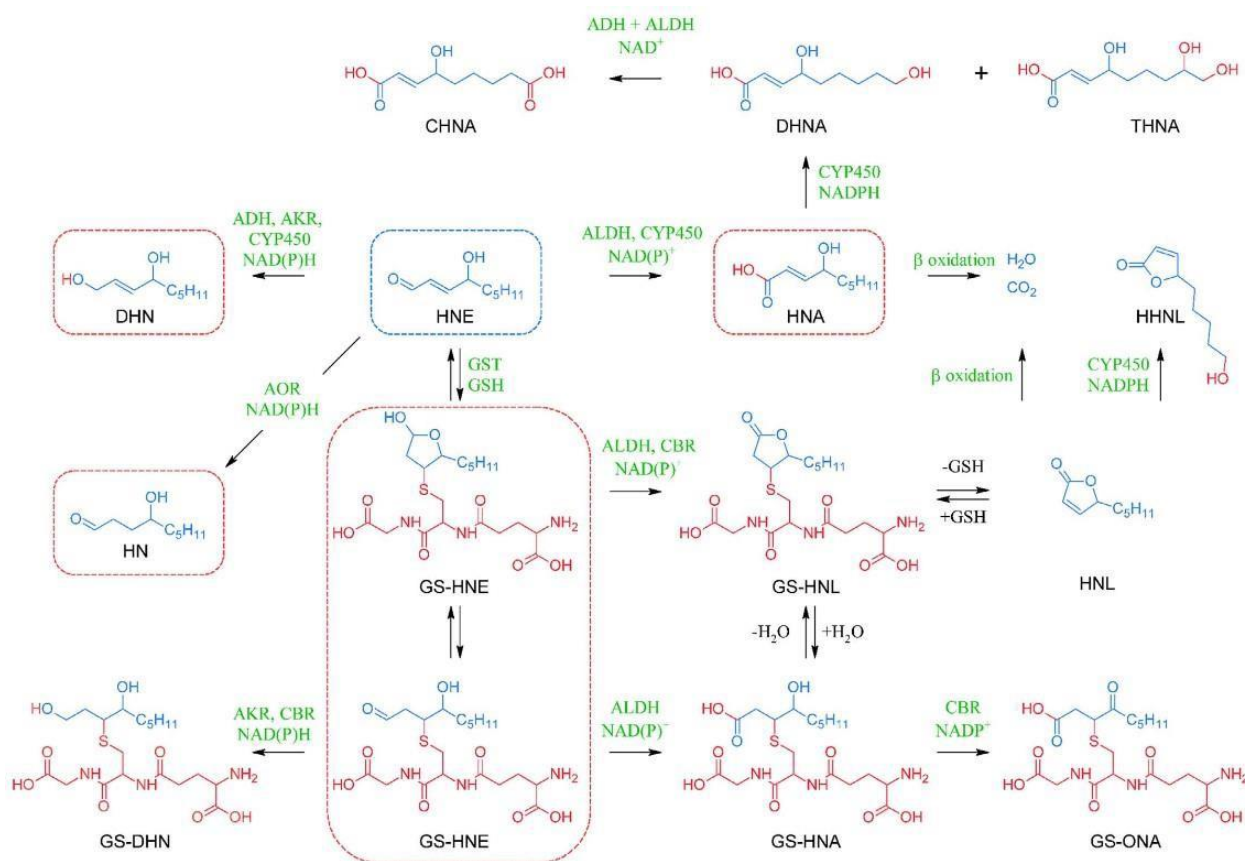


Figure 14 – Phase I and II of 4-HNE enzymatic detoxification. Blu structures represent original 4-HNE, whereas the red structures show the modifications (Mol et al., 2017).

GSH conjugates are not the final metabolites of 4-HNE disposal and, in the last part of 4-HNE detoxification, they are exported through the plasma membrane, finally converted to their mercapturic acid derivatives in the kidney and excreted into the urine (Petras et al., 1995). It has been reported that GS-HNE and its glutathionylated derivatives can be extruded by cells in a process that involves integral plasma membrane glycoproteins belonging to the ATP-dependent Multidrug Resistance Proteins (MRPs) transporter family. Although MRPs show a broad substrate specificity (Renes et al., 2000), MRP2 is the major responsible for the transport of glutathione conjugates and has been identified to be GS-HNE specific in rat hepatocytes. In fact, it was observed that hepatocytes from MRP2-deficient rats have a four-fold diminished ability to transport GS-HNE outside the cell compared to hepatocytes from wild-type rats (Reichard et al., 2003). The efflux of GS-HNE seems to be mediated also by RLIP76, another ATP-

dependent transporter that has been reported to be present in the human lens epithelial cells membrane, playing a crucial role in regulating the intracellular concentration of 4-HNE, in conjunction with GSTs. In fact, blocking the transport of GS-HNE by coating the cells with anti-RLIP76 IgG led to potentiation of the apoptotic effect of 4-HNE, thus confirming that the ATP-dependent transport of GS-HNE is essential for protecting cells against the deleterious effect of 4-HNE (Sharma et al., 2003).

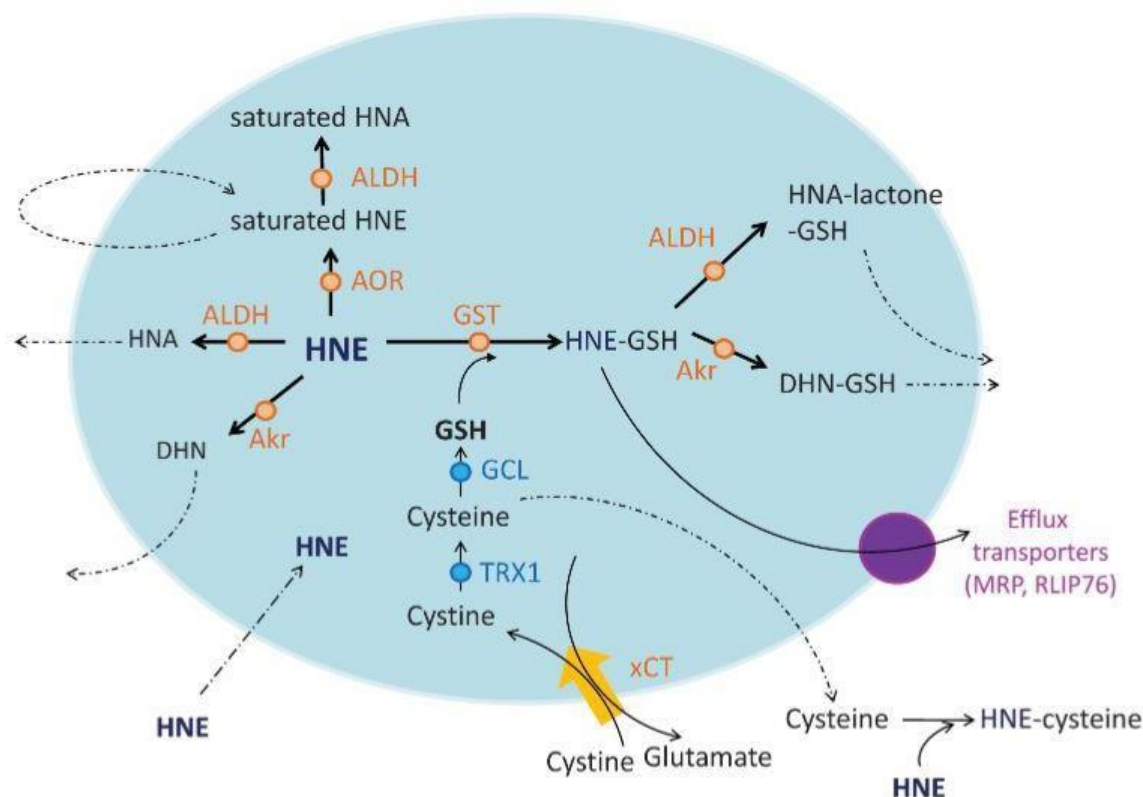


Figure 15 – Putative pathways involved in 4-HNE detoxification (Dalleau et al., 2013).

2.4 Enantioselectivity of 4-HNE metabolism

As described before, 4-HNE has C4 as chiral carbon and the two enantiomeric forms are naturally generated by the lipid peroxidation process as a racemic mixture of 4-(R)-HNE and 4-(S)-HNE (Bringmann et al., 1994). Although several studies have been performed to deeply understand 4-HNE reactivity and detoxification, only few have been performed in order to clarify a possible role of 4- HNE chirality in the aldehyde reactivity.

Uchida and colleagues observed a differential cellular distribution of 4-(R)-HNE- and 4-(S)-HNE- modified proteins using monoclonal antibodies directed toward each adduct in the renal cortex of rats exposed to oxidative tissue damage (Hashimoto et al., 2003). On the other hand, both

enantiomers of 4-HNE show high reactivity towards DNA but they generate four stereoisomeric 4-HNE- deoxyguanosine exocyclic adducts that are markedly different in their ability to induce mutations and in their efficiency to be repaired by NER proteins (Fernandes et al., 2003; Choudhury et al., 2004). In addition, in a study performed by Hiratsuka and co-workers it was reported that the (S)-enantiomer of 4-HNE, in respect to the (R)-enantiomer, could inactivate more readily at a lower concentration two rabbit muscle glycolytic enzymes, glyceraldehyde-3-phosphate dehydrogenase (GAPDH) and 3- phosphofructokinase (Hiratsuka et al., 2000).

Therefore, considering the relevant role that the enzymatic pathways play in 4-HNE detoxification, some authors focused their research also on the enantioselectivity of glutathione S-transferases. GSTs enantioselectivity has been studied by several authors in different animal models and cell types, obtaining however apparent inconsistent data. In fact, while some authors observed the GST 4-(S)- HNE-enantioselectivity in heart and liver, others reported that 4-HNE brain metabolism was not enantioselective (Sadhukhan et al., 2014), suggesting that GSTs selectivity could be organ dependent, likely because of the high GSTs polymorphism (Hayes et al., 2005). A study performed by Balogh and collaborators to examine the simultaneous metabolism of the individual 4-HNE enantiomers evidenced that hGSTA4-4, recognized as one of the predominant isoforms responsible for the conjugation of 4-HNE and GSH, shows a modest but significant preference for the biotransformation of 4-(S)-HNE even though it exhibits high catalytic efficiency for 4-(R)-HNE, as well. This result underlies that hGSTA4-4 plays a key role in the detoxification of both 4-HNE enantiomers providing protection from the harmful consequences of lipid peroxidation products that are generated as a racemate (Balogh et al., 2008). Further experiments have been carried out by these authors in order to examine also hGSTA4-4 product stereoselectivity and, eventually, to characterize the different GS- HNE diastereomers produced through LC/MS and NMR analysis. In fact, GS-HNE has an additional chiral center at the site of Michael addition generating, as a consequence, four GS-HNE diastereomers (Fig. 16).

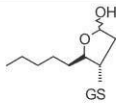
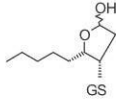
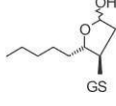
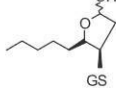
Structure	Stereochemistry
	3S,4R-GSHNE
	3S,4S-GSHNE
	3R,4S-GSHNE
	3R,4R-GSHNE

Figure 16 – Stereochemical configurations for the GS-HNE diastereomers (Balogh et al., 2008).

In particular, NMR analysis showed that, while in the spontaneous reaction all the GS-HNE diastereomers are produced, hGSTA4-4 conjugated GSH to 4-HNE in a stereoselective manner, generating only 3S,4R-GS-HNE and 3S,4S-GS-HNE (Balogh et al., 2008). The biological implications of hGSTA4-4 product stereoselectivity remain to be determined, even though some studies reported that the stereochemistry at the site of conjugation could significantly impact GS- HNE bioactivity, transport and further metabolism. In fact, the different distribution of the GS-HNE diastereomers observed in liver of RLIP76^{-/-} mice in respect to that in wild type mice liver, proved that the RLIP76 transporter exports GS-HNE with a marked stereospecificity, showing higher affinity for the GS-HNE diastereomers that are preferentially generated by hGSTA4-4 (Singhal et al., 2008). Finally, Guéraud and colleagues performed *in vitro* studies incubating rat liver cytosolic fractions with the 4-HNE glutathione conjugates originating from 4-(R)-HNE or 4-(S)-HNE in order to clarify their metabolic fate. Mass-spectrometry analysis of the main products of oxidative and reductive metabolism of GS-HNE revealed that 4S-GS-HNE was quantitatively more metabolized than 4R-GS- HNE through a retro-Michael reaction. However, when NADPH was added to the incubation mixture a significant increase in the amount only of 4R-GS-DHN was observed (Guéraud et al., 2005). These results suggest that various enzymes involved in the GS-HNE biotransformation show a marked substrate stereospecificity, as it has been recently reported for CBR1 and AKR1B1 that appear to contribute in a complementary manner to the removal of all GS-HNE diastereomers. In fact, AKR1B1 has shown to preferentially reduce the 3S,4R-GS-HNE diastereomer which, on the contrary, is the only one transformed at a markedly reduced rate by CBR1 in the NADP⁺-

dependent oxidative pathway probably because its reduced capacity to stably interact with the catalytic residues of CBR1, as demonstrated through molecular modelling studies (Rotondo et al., 2016; Balestri et al., 2019). However, further research into the potential stereochemical implications concerning the various diastereomers of GS-HNE and related metabolites will allow to elucidate the significance of chirality especially regarding their subsequent metabolism, transport and biological activity.

2.5 4-HNE in cell signalling processes

As reported before, due to its high reactivity, 4-HNE can undergo several reactions generating covalent adducts especially with proteins, nucleic acids and phospholipids, providing, as a consequence, the basis for the cell and tissue damage associated with the onset of several pathologies. 4-HNE is physiologically present in human blood and serum at concentrations lower than 1 μM (Esterbauer et al., 1991) contributing to many biological functions. In particular, 4-HNE might play modulatory roles by modifying proteins, including enzymes, receptors and transcription factors, that are variously involved in several cellular response pathways and gene expression regulation (Zhang and Forman, 2017). It is relevant underlying that 4-HNE effect as signalling molecule is closely dependent on cell type, the duration of exposure and its intracellular concentration (Zhang and Forman, 2017), so that cell response is strongly modulated by the ability of enzymatic detoxification systems to metabolize 4-HNE. For instance, this aldehyde plays an important role in cell survival and death (Chaudhary et al., 2010) (Fig. 17). In fact, it has been shown to induce dose- and time-dependent loss of cell viability along with an increase in apoptosis involving caspase-1, -3 and -8 activation in human lens epithelial cells (Choudhary et al., 2002). Furthermore, 4-HNE has been demonstrated to be involved in the regulation of various pro-inflammatory pathways mediated by NF- κ B and AP-1, whose activation leads to the expression of chemokines, cytokines and growth factors responsible for inflammatory response in several cell types.

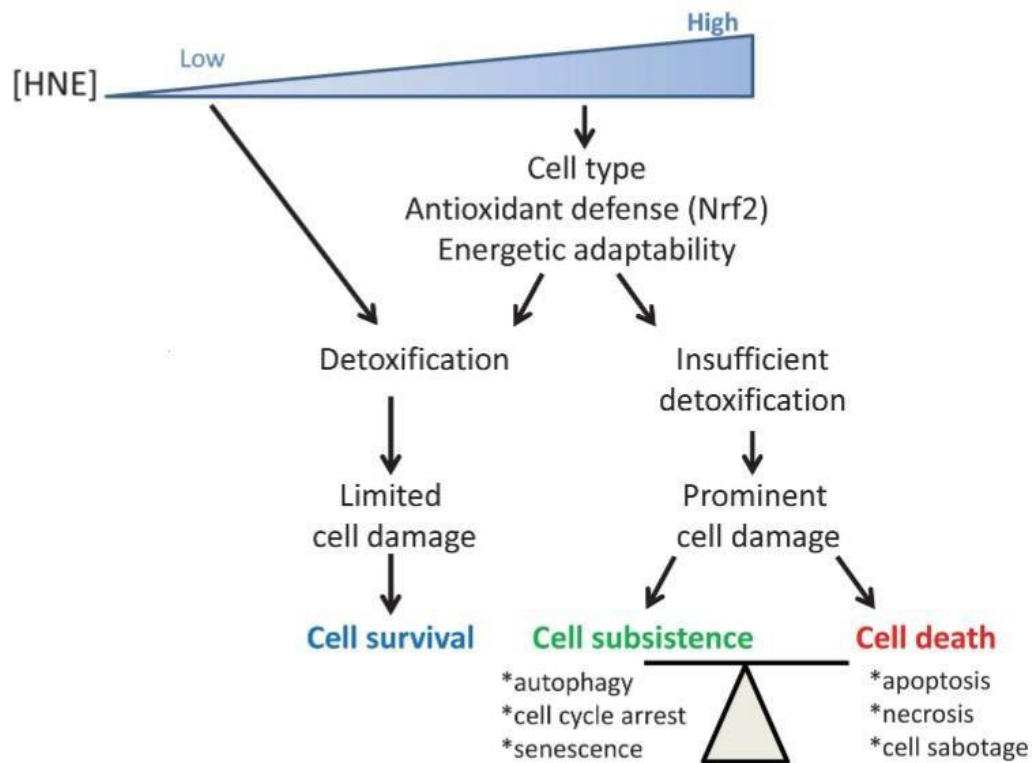


Figure 17 – Summary of cell fate upon 4-HNE exposure. When a cell is exposed to a low dose of 4-HNE, it can be removed by detoxification processes without affecting cell viability. Upon a high dose of 4-HNE, the response will depend on the capacity of the cell to metabolize 4-HNE by detoxification that is controlled by three parameters: the cell type, the antioxidant defense and the energetic adaptability. If the damage is important, the cells can only subsist by autophagy, senescence or cell cycle arrest. Otherwise, cell death is induced according to different pathways like apoptosis, necrosis or atypical cell death (Dalleau et al., 2013).

2.5.1 Pro-inflammatory effect of 4-HNE

Inflammation is generally defined as a response to environmental, intracellular and extracellular insults, including pathogens, DNA damage and metabolic stress, that is vital to health, but its dysregulation contributes to tissue damage. In fact, increasing reports have demonstrated the close association between inflammation and progression of various neurodegenerative diseases (Guzman-Martinez et al., 2019) and multiple age-related pathologies (Ferrucci and Fabbri, 2018). Although some different signalling pathways have been identified that directly communicate states of injury and infection, it is surprising that in each of them one common transcriptional activator, named NF- κ B, is involved in the enhancement of the inflammatory response (Liu et al., 2017). It is now known that NF- κ B pre-exists in the cytoplasm of most cells in an inactive form bound to the inhibitor I κ B α . Upon receipt of an appropriate signal, the I κ B kinases (IKK) phosphorylate I κ B α and, as a consequence, NF- κ B is released from I κ B and translocates to the nucleus where it can upregulate transcription of

specific genes (Zinatizadeh et al., 2020). Many papers reported the effect of 4-HNE in regulating NF- κ B-mediated inflammatory signalling pathways. In particular, it has been shown that 4-HNE can induce either activation or inhibition of NF- κ B depending both on its concentration and cellular model adopted (Fig. 18) even though the mechanisms are not clearly understood. For instance, exposing cultured rat cortical neurons to 10 μ M 4-HNE, Camandola and colleagues observed the inhibition of NF- κ B (Camandola et al., 1997) that, in contrast, in a different cell type (vascular smooth muscle cells) resulted activated by adding 1 μ M 4-HNE to the medium (Ruef et al., 2001). In addition, 1-10 μ M 4-HNE was not able to increase NF- κ B binding activity in both human promonocytic cells and hepatic stellate cells (Parola et al., 1998; Camandola et al., 1997).

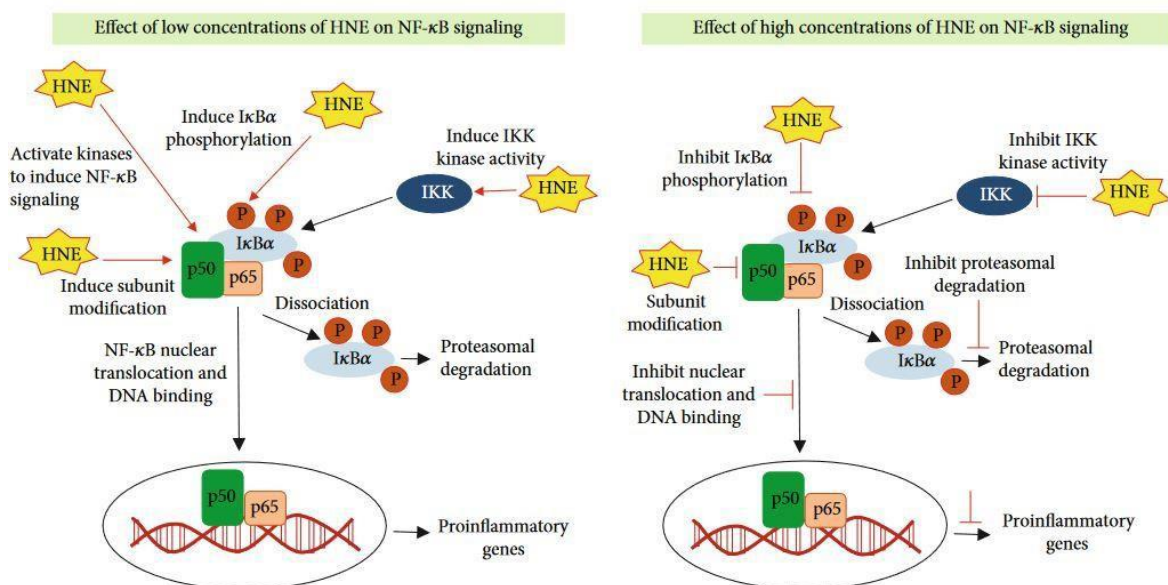


Figure 18 – Role of 4-HNE in NF- κ B-mediated pro-inflammatory signalling. 4-HNE exerts pleiotropic effects on NF- κ B: at low concentrations ($< 5 \mu$ M) it activates NF- κ B whereas at high concentrations ($> 5 \mu$ M) inhibits NF- κ B (Sonowal and Ramana, 2019).

Different studies have demonstrated that 4-HNE was able to form covalent adducts with IKK, directly regulating its activity. In fact, Ji and colleagues reported that 4-HNE could prevent I κ B α phosphorylation and subsequent degradation, reducing NF- κ B DNA binding activity and its transactivation, following treatment of Jurkat T cells with tetradecanoylphorbol acetate (TPA)/ionomycin (IM). In the same work, they demonstrated that 4-HNE induced the loss of IKK activity concomitant with the formation of higher molecular size forms of IKK which were detected by western blotting using antibodies against IKK or HNE-protein conjugates. Thus, 4-HNE might be assumed to be an endogenous inhibitor of NF- κ B that acts by modifying covalently IKK constituent proteins (Ji et al., 2001).

Furthermore, 4-HNE might modulate NF- κ B activity by interaction with upstream kinases or by

direct modification of NF- κ B subunits. In fact, almost all NF- κ B subunits contain a highly conserved cysteine residue in the N-terminal region of the Rel homology domain (RHD), which is identified as Cys-38 in human RelA (it will be further discussed in the following chapters). This residue can be oxidated or nitrosylated and these modifications are reported to inhibit RelA DNA binding compromising its ability to induce anti-apoptotic gene expression (Caviedes et al., 2021; Sen et al., 2012).

Finally, always concerning 4-HNE as signalling molecule, recent studies have shown that 4-HNE metabolizing enzymes including AKR1B1, ALDH1 and GSTs could regulate various pro-inflammatory pathways by generating 4-HNE metabolites such as GS-HNE and GS-DHN that can be further act as secondary signalling molecules. In fact, although 4-HNE metabolites are less electrophilic in respect to 4-HNE or not reactive at all, some of them show a biological activity which is even more pronounced than that of the parent compound. Ramana and co-workers demonstrated that PKC, NF- κ B, and AP-1 were stimulated after treatment of rat aortic smooth muscle cultures with 4-HNE, GS-HNE and GS-DHN, leading to cell growth. However, only the effect induced by 4-HNE and GS-HNE, but not by GS-DHN was abolished by inhibition or antisense ablation of AKR1B1 and the same anti-inflammatory effect was observed on the TNF- α -induced synthesis of prostaglandin E2 and activity of cyclooxygenase (COX) in human colon cancer cells (Tammali et al., 2007). Furthermore, the exposure to oxidative stress conditions of adipocytes resulted in the production of GS-HNE and GS-DHN that were able to induce a macrophage inflammatory response via intercellular cross-talk (Frohnert et al., 2013). Taken together, these findings provide evidence that GS-DHN is an important mediator of various pro-inflammatory signalling pathways in different cell type, suggesting that the inhibition of AKR1B1 and CBR1, the two enzymes that are reported to catalyse GS-HNE reduction, could represent an effective therapeutic strategy in order to modulate the inflammatory response.

3. Glycative stress and glucotoxicity: D-glucose

Glucose is the primary metabolic fuel of mammals and represents the major precursor for the synthesis of other carbohydrates which are fundamental for cellular survival, such as neurotransmitters in the brain (aspartate, glutamate, and γ -aminobutyric acid) and ribose for nucleotides synthesis (Nakrani, Wineland and Anjum, 2021). In humans, the range of normal blood glucose concentration is 70-110 mg/dl and is tightly regulated by maintaining the balance between the sources of glucose in blood (diet, glycogenolysis, gluconeogenesis) and its removal (glycolysis, glycogenesis, lipogenesis, uronic acid pathway) through hormonal regulation. However, alterations in glucose homeostasis can result in hyperglycaemia condition that occurs when the blood glucose level is more than 180 mg/dl after taking a meal (Szablewski, 2014). Persistent hyperglycaemia has

several devastating effects on different cell types. In fact, numerous studies reported that high concentrations of glucose can be deleterious to cell viability, triggering multiple changes in metabolism which, eventually, can induce pro-apoptotic pathways (Giri et al., 2018) (Fig. 19). Moreover, hyperglycaemia has also been shown to be one of the factors contributing to inflammation in several cell types, enhancing TNF- α and other cytokines expression as well as p38, ERK and IKK α /IKK β phosphorylation (Panahi et al., 2018). Indeed, human lens epithelial cells, whose susceptibility to oxidative stress and 4-HNE-induced apoptosis has been previously considered (Choudhary et al., 2010), proved to be particularly sensitive to elevated glucose levels with the development of inflammation and secondary diabetes complications, such as diabetic cataract (Chang and Petrash, 2018).

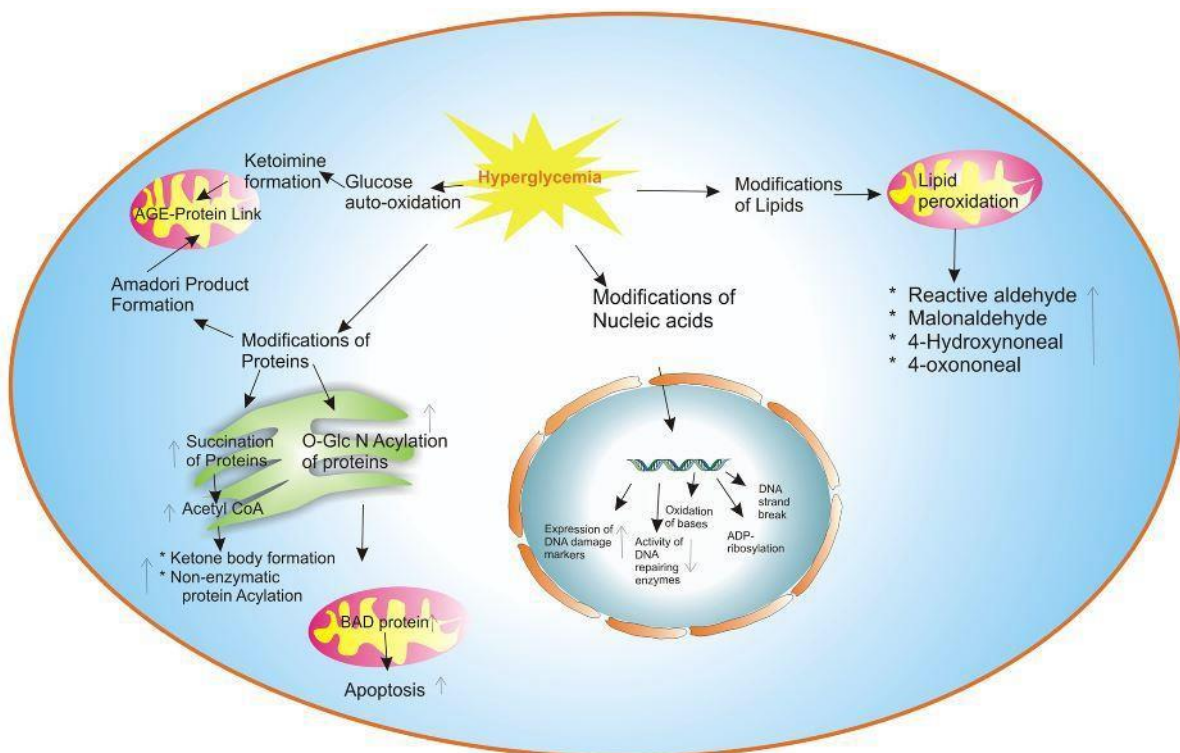


Figure 19 – Deleterious complications due to prolonged hyperglycaemia in cells (Giri et al., 2018).

The mechanisms that are involved in cytotoxicity associated with high glucose levels are the increased flux of glucose through the polyol pathway, the activation of protein kinase C (PKC) isoforms, the increased intracellular formation of advanced glycation end products (AGEs) and the expression of the receptor for advanced glycation end products (RAGEs). All these mechanisms of hyperglycaemia-induced damage, overall, contribute to increase oxidative stress in cells (Volpe et al., 2018; Yan, 2018).

3.1 The polyol pathway

The polyol pathway is composed of two reactions (Fig. 20). In the first one, which is the rate-limiting step, D-glucose is reduced to sorbitol by aldose reductase (AKR1B1), using NADPH as a cofactor, whereas in the second reaction NAD⁺-dependent sorbitol dehydrogenase (SDH) catalyses the oxidation of sorbitol to D-fructose (Niimi et al., 2021). Given the extremely low affinity that aldose reductase shows for D-glucose, under normoglycaemic conditions less than 3% of glucose is reduced by aldose reductase. However, during hyperglycaemia large amount of the glucose molecule is channelled into the polyol pathway, resulting in an enhanced formation of sorbitol and excessive consumption of NADPH (Srivastava et al., 2005).

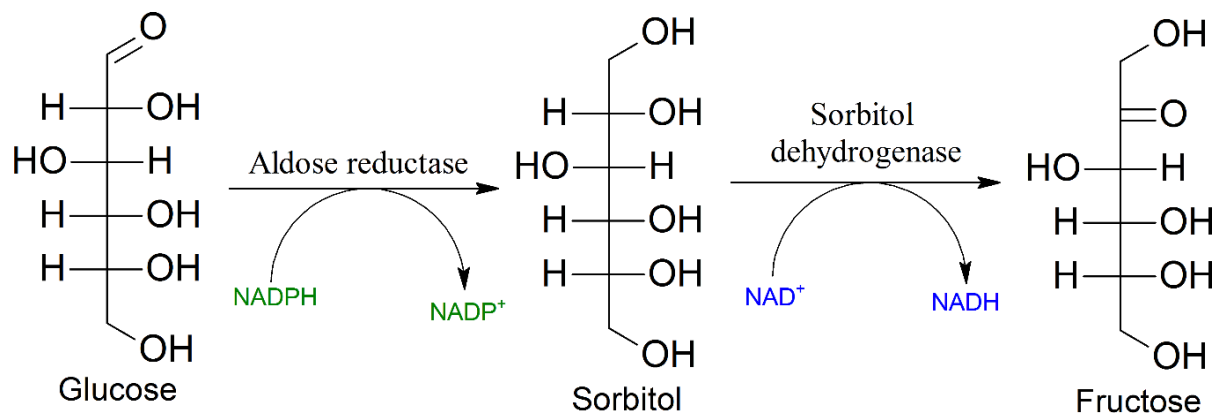


Figure 20 – The polyol pathway is a two-step metabolic pathway (Brownlee, 2005).

The impairment of redox balance due to the depletion of NADPH represents a significant consequence of the polyol pathway activation. In fact, since NADPH is a cofactor required by the antioxidant enzymes glutathione reductase and glutathione peroxidase to regenerate GSH, the decreased ratio NADPH/NADP⁺ alters the cytoplasmic redox status by substantially decreasing GSH levels (Srivastava et al, 2005; Lee and Chung, 1999). Thus, the limitation of NADPH and consequently the reduction of ROS scavenging enzymes activity are crucial for enhancing intracellular oxidative stress, indicated as the main source of long-term diabetic complications, with the concomitant increase in the level of lipid peroxidation products. These considerations have been confirmed by the observation that antioxidants could provide a good protection against 50 mM glucose-induced cataractogenesis in rat lenses (Ansari et al., 1994; Srivastava e Ansari, 1988). Likewise, aldose reductase gene knockdown has been shown to slow down the development and progression of diabetic complications, confirming the detrimental role of this enzyme (Reddy et al., 2011).

Additionally, hyperactivation of the polyol pathway is associated with the increase in levels of sorbitol, a polyhydroxylated alcohol with strongly hydrophilic properties that, for this reason, does not diffuse readily through cell membranes and accumulates intracellularly, altering cell osmotic

balance. Accumulation of sugar alcohols causes water retention and swelling in the lens, all events that lead to cataractogenesis in diabetic patients (Steinmetz et al., 1973). Furthermore, the consumption of NAD^+ by sorbitol dehydrogenase causes the aberrant shift of the ratio NADH/NAD^+ compromising cellular capacity of utilizing oxygen and giving rise to a metabolic condition defined as pseudohypoxia (Williamson et al., 1993). In fact, under pseudohypoxic conditions, even though partial pressure oxygen is normal, NADH accumulation may impact the activity of numerous cytoplasmic and mitochondrial enzymes that use NAD^+ as cofactor and are inhibited by NADH affecting many metabolic pathways such as the glycolytic pathway, pyruvate dehydrogenase complex, Krebs cycle and the electron transport chain and resulting in accumulation of glyceraldehyde-3-phosphate and its prior metabolites that have to be disposed by alternative glucose metabolic pathways (Fig. 21). All these alternative pathways lead to ROS production, thus aggravating cellular oxidative stress. Therefore, the NADH/NAD^+ redox imbalance initially causes reductive stress but gradually leads to oxidative stress and culminates in cell death and tissue dysfunction (Song et al., 2019).

Finally, the high amount of fructose produced by the polyol pathway is rapidly metabolized by fructokinase, leading to depletion of intracellular phosphate and ATP, which contributes to generate local oxidative stress and inflammation (Johnson et al., 2014).

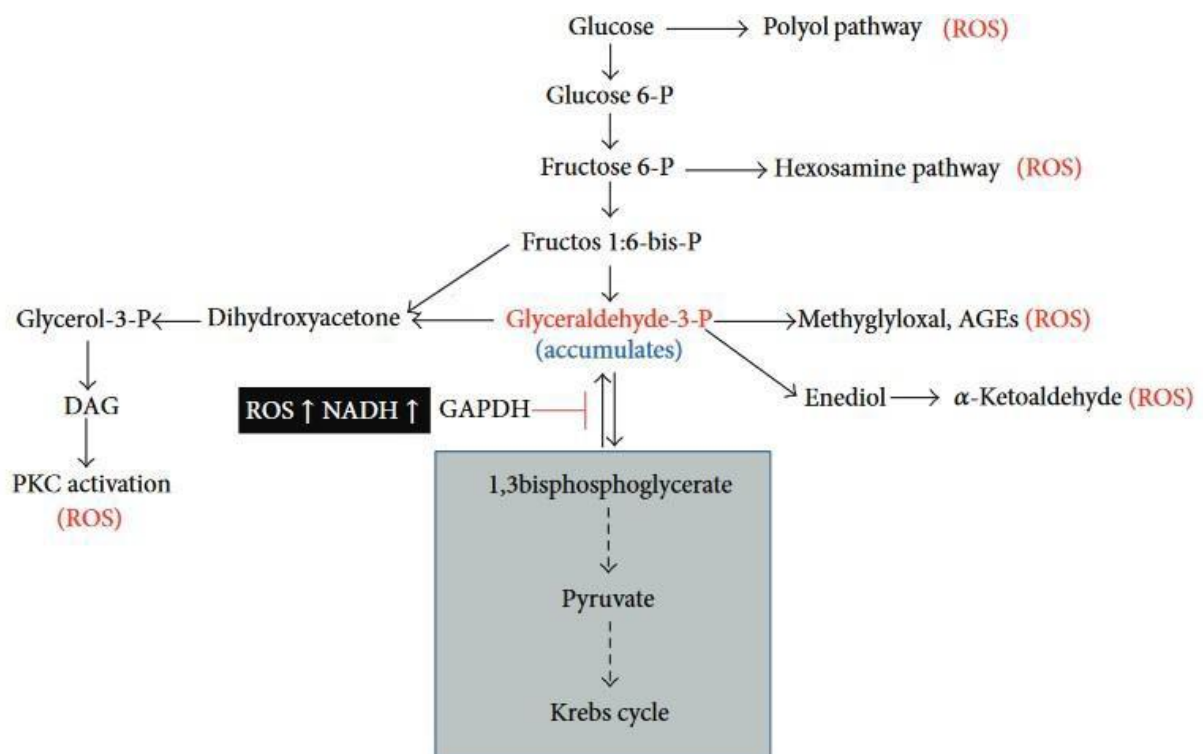


Figure 21 – The branch-off pathways that are activated when glyceraldehyde-3-phosphate dehydrogenases is inhibited by NADH accumulation. These alternative pathways are linked to ROS

production, thus further exacerbating oxidative stress (Yan, 2014).

4. Oxidative and glycative stress: inflammatory response

Different studies, which were focused on diabetes pathology, reported an interconnection in cells between oxidative and glycative stress (Li et al., 2018; Cianfruglia et al., 2020; Fiorentino et al., 2013). As described before, hyperglycaemia promotes oxidative stress by supporting metabolic pathways, such as glycolysis, Krebs cycle, NADPH oxidase and PKC pathways, that indirectly lead to ROS overproduction. The excess of free radical formation can provoke lipid peroxidation, resulting in the generation of toxic by-products such as reactive aldehydes, including 4-HNE (Ito et al., 2019). In addition, high glucose concentrations cause dysfunction of antioxidant systems due to enzymatic glycation, reduction of the activity of the glutathione peroxidase/glutathione reductase system and perturbation of NADPH/NADP⁺ and NAD⁺/NADH ratio (Yaribeygi et al., 2019). Glucose auto-oxidation leads to the formation of glyoxals, transformation of the Amadori product deoxyglucosone, and fragmentation of glyceraldehyde-3-phosphate and dihydroxyacetone phosphate to methylglyoxal (Vlassara et al., 1992); these compounds react with free amino groups of intracellular and extracellular proteins, forming AGEs whose binding to RAGE receptors induces the generation of intracellular ROS and the subsequent activation of the redox sensitive transcription factor NF- κ B (Ohtsu et al., 2017). NF- κ B plays a crucial role in cellular processes including immune and inflammatory response, cellular adhesion, differentiation, proliferation, autophagy, senescence and apoptosis (Verzella et al., 2020) regulating the expression of a variety of genes associated with inflammation, including interleukin-6 (IL-6), tumor necrosis factor- α (TNF- α), intracellular adhesion molecule-I (ICAM-I). NF- κ B is also responsible for inducible cyclooxygenase-2 (COX-2) expression (Liu et al., 2017).

4.1 NF- κ B (nuclear factor kappa-light-chain-enhancer of activated B cells)

NF- κ B is an eucaryotic transcription factor described for the first time in 1986 as a nuclear factor necessary for immunoglobulin kappa light chain transcription in B cells (thereby coining the abbreviation NF- κ B) (Sen and Baltimore, 1986). It was originally thought that NF- κ B was not produced in other cells because it could not be detected by a gel shift assay using the Ig κ DNA binding site. However, subsequent studies reported that NF- κ B pre-exists in the cytoplasm of most cells in an inactive form bound to the inhibitor I κ B that masks NF- κ B DNA binding ability

(Baldwin, 1996). Upon cellular stimulation with an appropriate signal, NF- κ B is released from I κ B and translocates to the nucleus where it can upregulate transcription of specific genes, acting as an inducible transcription factor (Ghosh and Karin, 2002). Since its discovery, NF- κ B responsive sites, known as κ B sites, have been characterized in the promoters and enhancers of numerous genes, making NF- κ B an important component in the inducible expression of many proteins, including cytokines, acute phase response protein and cell adhesion molecules. In addition, NF- κ B is active in the nucleus of mature B cells, plasma cells, macrophages and some neurons. It was suggested also that the constitutive activation of NF- κ B probably allows some cells to maintain a differentiated phenotype that is defined by the production of cell-type specific proteins. NF- κ B family members are represented by five different members: Rel (c-Rel), RelA (p65), RelB, NF- κ B1 (p105), and NF- κ B2 (p100) (Fig. 22). Each member contains an N-terminal 300 amino acid conserved region known as the rel homology domain (RHD) that contains a nuclear localization sequence and is responsible for DNA-binding, dimerization and interaction with proteins belonging to the inhibitory I κ B family members (Ghosh et al., 1995; Muller et al., 1995). NF- κ B1 and NF- κ B2 are synthesized as proforms, p105 and p100, which are then proteolytically processed to p50 and p52 respectively (Caamaño and Hunter, 2002). All five members of NF- κ B family act as homo- or heterodimers. Each combination of rel proteins, in addition to showing specificity for DNA binding sites, has its own transactivating potential (Wong et al., 2011). In fact, p50 and p52 homodimers act as repressors, while those dimers containing either RelA or c-Rel are transcriptional activators; RelB shows to benefit from a regulatory flexibility that allows it to be both an activator (Ryseck et al., 1992) and a repressor (Ruben et al., 1992), depending on the DNA sequence it binds to and the heterodimers it forms. The inability of p50 and p52 to act alone as activators is probably due to lack of a variable C-terminal domain which is present in the sequence of the activating rel proteins and is most likely responsible for transactivation of NF- κ B responsive genes. Furthermore, NF- κ B subunits also contain sites for phosphorylation and other post-translational modifications that are relevant for activation and crosstalk with other signalling pathways.

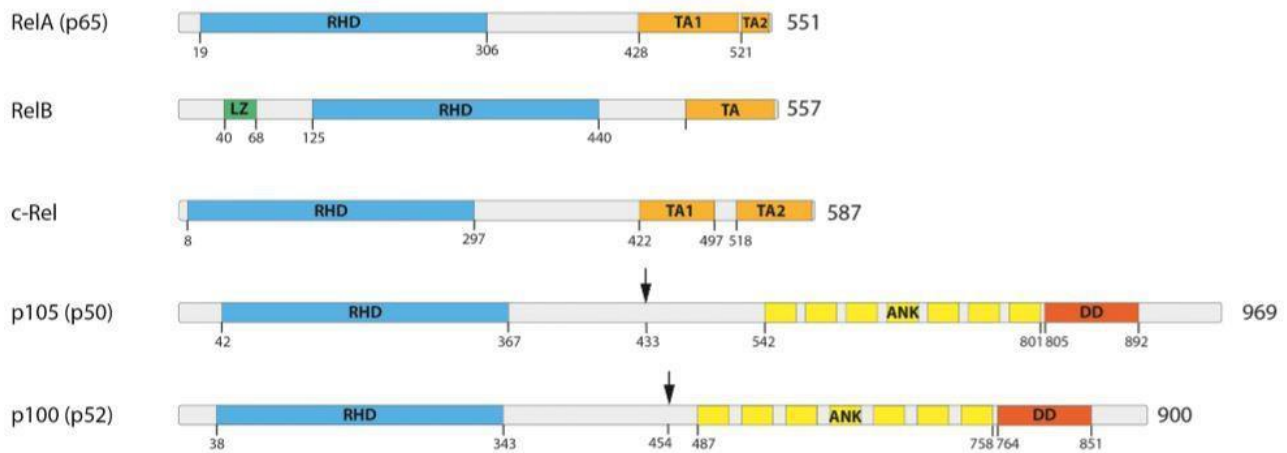


Figure 22 – The five members of the NF- κ B family of proteins (Hoesel and Schmid, 2013).

I κ B protein family includes I κ B α , I κ B β , I κ B ϵ , I κ B γ , and Bcl-3 (Fig. 23). All of these inhibitors contain multiple regions of homology known as ankyrin-repeat motifs through which they interact with the DNA-binding domains (RHDs) of NF- κ B transcription factors, masking their nuclear localization sequence and, thus, transcriptionally inactivate them. The specific interaction between ankyrin-repeats and rel-homology domains appears to be a crucial, evolutionarily conserved feature of the regulation of NF- κ B proteins. Each I κ B differs in the number of these repeat motifs, and this number seems to influence the specificity of the interaction between I κ B and the NF- κ B dimer (Ghosh et al., 1998). The best characterized I κ B is I κ B α , mainly because it was the first member of this family to be cloned. It is a 37 kDa protein that, like I κ B β , contains an N-terminal domain that is phosphorylated in response to signals, a central ankyrin repeat domain and a C-terminal PEST domain which is involved in the basal turnover of the protein (Malek et al., 2003). The peculiar characteristic of I κ B α is its ability to regulate rapid but transient induction of NF- κ B activity under physiological conditions through an autoregulatory feedback loop. In fact, given the presence of κ B sites in the I κ B α promoter, the activation of NF- κ B causes the upregulation of I κ B α which serves to shut off the signal (Verma et al., 1995).

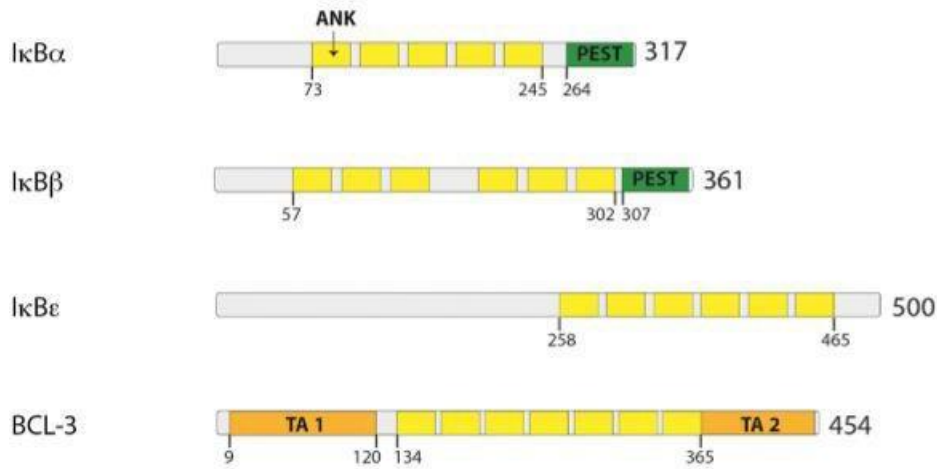


Figure 23 – The IκB protein family consists of four members (Hoesel and Schmid, 2013).

NF-κB is active when released from the IκB molecules, a condition that is achieved through the degradation of these inhibitors in a multi-step process that is initiated by site-directed ubiquitination of target proteins. Then, the degradation of such modified proteins is carried out by the multicatalytic ATP-dependent proteasome complex. The first evidence that inducible degradation of IκBα might be dependent on ubiquitination was provided by using inhibitors of the proteasome. In fact, treatment of cells with these inhibitors blocked the IκBα degradation after stimulation with TNF-α (Colleran et al., 2011). Subsequently, it was reported that IκBα undergoes proteasome-mediated degradation after phosphorylation. IκB phosphorylation is catalysed by an enzyme complex containing IκB kinases (IKK1/IKKα and IKK2/IKKβ) and one non-catalytic regulatory subunit (NF-κB Essential Modulator, NEMO or IKKγ) (Hayden and Ghosh, 2008). The IKK complex can interact with upstream signaling molecules or kinases and are activated by several mechanisms, such as phosphorylation of activation loop serines (Ser-177 and Ser-181) of IKK2 by upstream kinases (Delhase et al., 1999) or via proximity-induced self-activation of IKK-dimers by mutual transphosphorylation (Schmid and Birbach, 2008).

There are at least two distinct pathways involved in the activation of NF-κB family both leading to the translocation of NF-κB dimers from the cytoplasm to the nucleus (Mercurio et al., 1993): the classical or canonical pathway and the alternative or noncanonical pathway (Fig. 24).

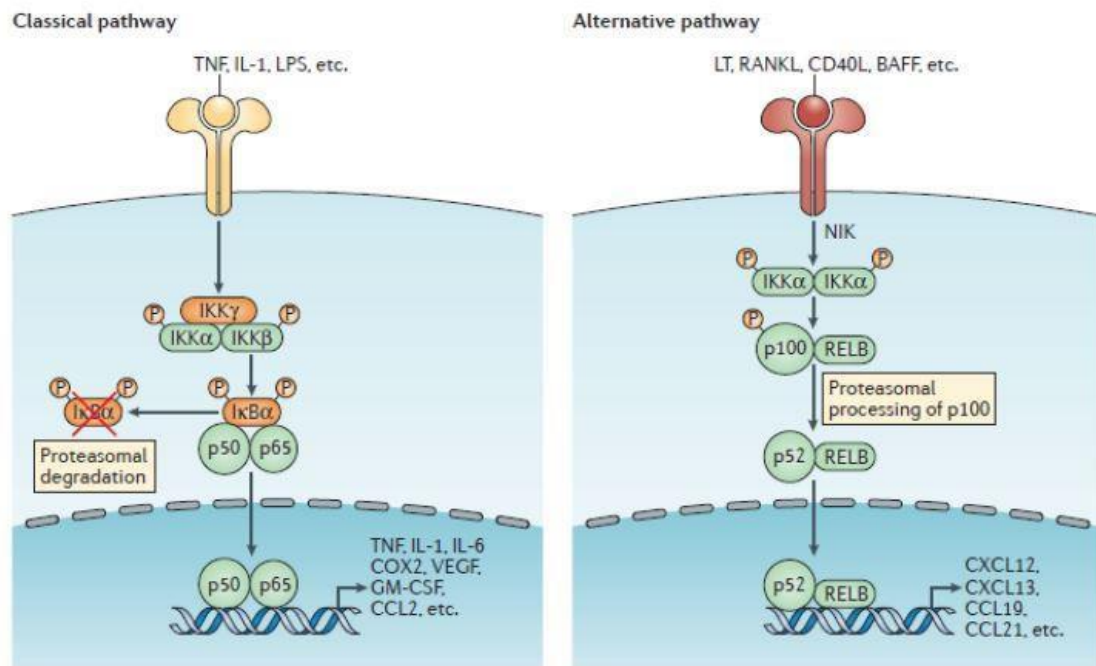


Figure 24 – Classical and alternative NF- κ B-activating pathways (Taniguchi and Karin, 2013).

The classical NF- κ B-activating pathway is triggered in response to microbial products like lipopolysaccharides (LPS) and pathogen-associated molecular patterns (PAMPs), stress, proinflammatory cytokines like tumor necrosis factor α (TNF- α) and interleukin-1 β (IL-1 β) (Perkins and Gilmore, 2006; Hoesel and Schmid, 2013). It depends on the phosphorylation of I κ B-kinase IKK (IKK β , IKK α and IKK γ) and the phosphorylation and ubiquitination of I κ B. In particular, IKK complex catalyses the phosphorylation of Ser-32 and Ser-36 of subunit I κ B α , which is followed by polyubiquitination at Lys-21 and Lys-22 of I κ B α and subsequent degradation by the 26S proteasome. Therefore, NF- κ B dimers are released from the inhibitor and can translocate to the nucleus and activate transcription of target genes. The canonical pathway activates NF- κ B dimers comprising RelA, c-Rel, RelB, and p50 (Chen, 2005; Gilmore, 2006).

The noncanonical pathway is activated by ligands, such as lymphotoxin β (LT β), B cells-activating factor, receptor activator of nuclear factor kappa-B ligand (RANKL) and cluster of differentiation 40 ligand (CD40L), that bind to a subset of tumor necrosis factor (TNF) receptors (Sun, 2017). Upon stimulation, TNF receptor-associated factor 2 recruits a complex containing cellular inhibitor of apoptosis 1 and 2, leading to TRAF3 proteolysis and activation of the NF- κ B-inducing kinase (NIK). This kinase activates IKK α homodimers, that phosphorylate at the two C-terminal sites, on serine residues Ser-866 and Ser-870, the proform of p100 (NF-

κ B2), in order to trigger p100 for the formation of p52 (Senftleben, 2001). This event consists of polyubiquitination and proteasomal degradation only of p100 inhibitory C-terminal half (Xiao et al., 2001). Subsequently, the N-terminal portion of NF- κ B, namely the p52 polypeptide containing the Rel homology domain, is released. This mature protein form can finally associate with RelB, forming p52–RelB dimers, and undergo nuclear translocation (Dejardin et al., 2002). Since degradation of I κ Bs and nuclear translocation of the NF- κ B dimers alone are not sufficient in inducing a maximal NF- κ B response, emerging evidence suggests that NF- κ B undergoes a variety of post-translational modifications that play a key role in determining the strength and the duration of NF- κ B nuclear activity as well as its transcriptional output, adding another important level of complexity to the transcriptional regulation of NF- κ B (Perkins, 2006). The first modification of RelA (p65) to be thoroughly studied was phosphorylation.

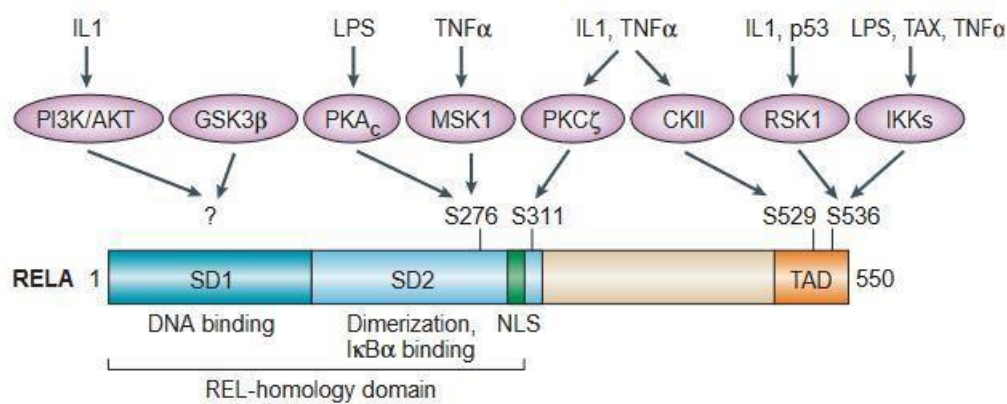


Figure 25 – Post-translational phosphorylation of RelA (Chen and Greene, 2004).

RelA can be phosphorylated both in the cytoplasm and in the nucleus in response to a variety of stimuli at phosphorylation sites including seven serines and three threonines that are located within the N-terminal RHD and the C-terminal transcriptional activation domains. Phosphorylation of these sites results in either increased or decreased levels of transcription depending on the sites of phosphorylation. For instance, either TNF- α or lipopolysaccharide (LPS) induces RelA phosphorylation at serine 276, located in the RHD domain for the activation of PKA_c (the catalytic subunit of protein kinase A) in the cytoplasm and MSK-1 (mitogen- and stress activated protein kinase-1) in the nucleus (Zhong et al., 1997; Vermeulen et al., 2003), leading, as a consequence, to the enhance of the binding of RelA itself with the coactivator CREB-binding protein (CBP) and its paralog p300. This could be explained by conformational changes in NF- κ B, induced by the

phosphorylation of Ser-276 that appears to enhance the binding of RelA to its coactivators. The main effect of CREB and of its paralog p300 is to form a bridge between NF- κ B and the components of the cellular transcriptional machinery, enhancing the RelA transcriptional activity. Ser-276 phosphorylation makes also this complex more effective at displacing histone deacetylase complexes (HDACs) which are frequently bound to NF- κ B dependent enhancers of target genes in unstimulated cells (Zhong et al., 2002). In contrast, the unphosphorylated RelA conformation might promote its association with co-repressors suppressing not only a subset of NF- κ B target genes but also non-NF- κ B-regulated genes through an epigenetic mechanism (Dong et al., 2008). Besides Ser-276, Ser- 529 and Ser-536 of RelA, located in the TAD domain, can be phosphorylated as well, thus facilitating the assembly with other members of the basic transcriptional machinery, such as TFIIB or TATA-binding protein (Schmitz et al., 1995).

Another important post-translational modification of RelA that has been extensively studied is acetylation. It seems to be restricted to the nucleus accordingly to the mainly nuclear localization of relevant histone acetyltransferases that have been implicated as the effectors of RelA acetylation both *in vivo* and *in vitro* (Chen et al., 2001), by adding acetyl groups to lysine residues. Reversible acetylation of RelA regulates many functions of NF- κ B, including DNA binding activity, transcriptional activity and its ability to associate with I κ B α . RelA contains three lysine residues (lysines 218, 221 and 310) whose modification is involved in different biological responses (Chen et al., 2002). In fact, acetylation at lysine 221 enhances the DNA binding of NF- κ B and, in addition to acetylation at lysine 218, impairs its association with I κ B α probably because it induces conformational changes on RelA. Acetylation of lysine 310 is required for full transcriptional activity of RelA even if it does not seem to affect its binding to DNA or I κ B α assembly. In addition to the conformational change, acetylation might create a docking site for the recruitment of some NF- κ B transcription cofactors as demonstrated by Chen and colleagues who observed that acetylated lysine 310 could be recognized by transcriptional co-activators that phosphorylate RNA polymerase II inducing the transcription of a subset of NF- κ B target genes (Chen et al., 2002). Finally, it is likely that lysine acetylation could reduce NF- κ B DNA binding activity by neutralizing the positively charges of lysine residues, weakening their interaction with the negatively charged DNA, as it was observed for lysine 122 and lysine 123. For these residues, in fact, it was evidenced the interaction with DNA in the crystal structure of the RelA/p50 heterodimer bound to a κ B-enhancer (Chen et al., 1998).

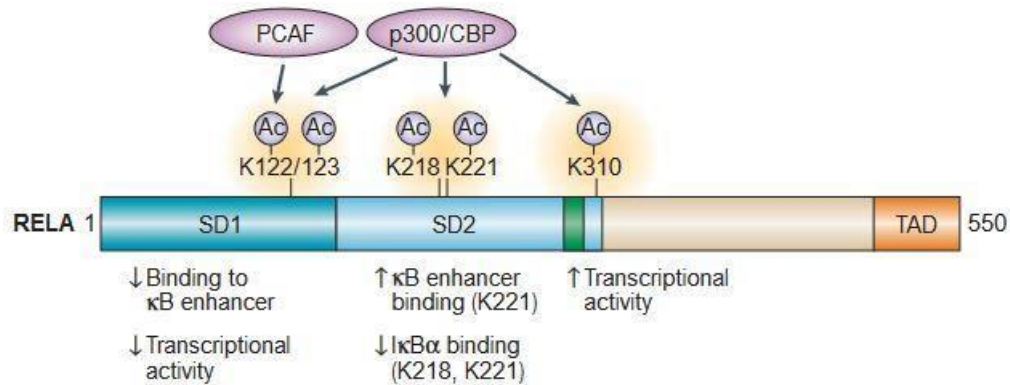


Figure 26 – Post-translational acetylation of RelA (Chen and Greene, 2004).

Along with acetylation of RelA subunit, its counterpart deacetylation, mediated by both histone acetyltransferases and histone deacetylases, plays a crucial role in NF- κ B pathway modulation, as well. There are studies providing evidence that SIRT1, a NAD⁺-dependent protein deacetylase, is responsible for NF- κ B signaling suppression through deacetylation of p65, thus leading to the reduction of the inflammatory responses mediated by this transcription factor (Yeung et al., 2004; Yang *et al.*, 2012). In fact, SIRT1 can physically interact with RelA and inhibits transcription by deacetylating the lysine 310 of this subunit having profound effects on modulating cell survival in response to TNF- α signalling in non-small-cell lung cancer (NSCLC) cell lines treated with resveratrol, a small-molecule agonist of sirtuin activity (Yeung et al., 2004).

Once in the nucleus, NF- κ B interacts with promoter of the gene targets to enhance their transcription. Nowadays the expression of over 400 different genes has been identified to be controlled by NF- κ B binding sequences. These include inflammatory cytokines such as TNF- α , IL-1, IL-6, and chemokines, adhesion molecules, viral proteins, telomerase, angiogenesis factors like VEGF, anti-apoptotic proteins, cell cycle-regulatory genes and inflammatory enzymes such as 5-lipoxygenase (5-LOX) and cyclooxygenase-2 (COX-2) (Serasanambati and Chilakapati, 2016).

4.2 COX-2 (*cyclooxygenase-2*)

Cyclooxygenases, also known as prostaglandin endoperoxide synthases, are key enzymes required to convert arachidonic acid, released by secretory or cytoplasmic phospholipase A₂ from cell membrane upon mitogen or mechanical stimuli to prostaglandins that are shown to be important lipid signalling molecules (Smith et al., 1996). Two different enzymes have been identified, namely COX-1 and COX-2, that are among the most studied and best understood mammalian oxygenases. Human COX-1 and COX-2 are homodimers of 576 and 581 amino acids, respectively. Both enzymes are

glycoproteins containing three high mannose oligosaccharides, one of which is essential to facilitate protein folding. In addition, another oligosaccharide, present only in COX-2 isoform, regulates its degradation. Each subunit of the dimer has three distinct domains: the N-terminal β -sheet domain referred to as EGF domain because of its similarity to other epidermal growth factor-like protein structure, the membrane binding domain that is composed of four α -helices and anchors the protein to the plasma membrane and the C-terminal catalytic domain which contains both the cyclooxygenase active site and the peroxidase active site with the heme prosthetic group (Garavito et al., 2002). Therefore, the COX enzymes possess two distinct enzymatic activities, being able to act both as peroxidase and as cyclooxygenase, each associated with an independent active site. These enzymes catalyse, in a first bis-oxygenase reaction, the conversion of the arachidonic acid to prostaglandin G₂ (PGG₂) using two molecules of O₂ and then the reduction of the 15-hydroperoxyl group of this molecule to the corresponding alcohol by the addition of two electrons in a peroxidase catalysed reaction forming the PGH₂ (Fig. 27) (Smith et al., 2000).

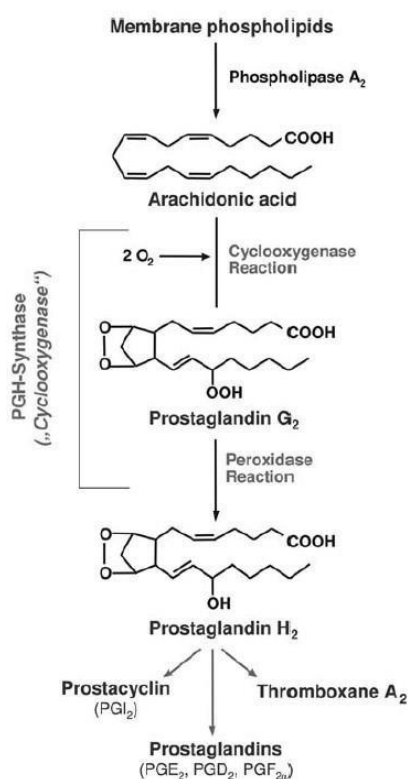


Figure 27 – Biochemical function of COX enzymes. Cyclooxygenases are bifunctional enzymes with fatty acid cyclooxygenase activity catalysing the conversion of arachidonic acid to PGG₂ and prostaglandin hydroperoxidase activity catalysing the conversion of PGG₂ to PGH₂ (Smith et al., 2000).

Although COX-1 and COX-2 show the 60% identity in sequence, have similar tertiary structure and carry out essentially the same catalytic reaction, their function appear to be consistent with the

tissue expression pattern as demonstrated through analysis conducted with selective inhibitors of the two enzymes (Masferrer et al., 1994). In fact, COX-1 is widely distributed and constitutively expressed in most tissues providing prostaglandins that are required for homeostatic functions, while COX-2 is expressed in response to a variety of inflammatory and proliferative stimuli playing a key role in prostaglandin formation during pathophysiologic states such as inflammation and tumorigenesis (Tanabe and Tohnai, 2002).

Transcriptional regulation of COX-1 gene, known as *Ptgs-1*, has been examined in endothelial cells, which express constitutively high levels of the enzyme. The *Ptgs-1* gene has a TATA-less GC-rich promoter containing multiple start sites for transcription. Furthermore, gel shift assays have demonstrated the presence in the *Ptgs-1* promoter of two Sp1 *cis*-regulatory elements that bind the *trans*-activating Sp1 protein and maintain the basal level of transcription (Xu et al., 1997). In fact, mutagenesis experiments have proven that mutation of both Sp1 binding sites significantly reduced the promoter activity to 29% in respect to that of the wild type. On the other hand, COX-2 is an inducible enzyme encoded by *Ptgs-2* gene whose expression is regulated by many consensus *cis*- elements in the 5'-flanking region including NF-IL6 motif, cAMP response element-binding protein (CREB) and CCAAT/enhancer-binding protein (C/EBP) boxes and a regulatory site for NF- κ B (Fig.28) (Appleby et al., 1994).

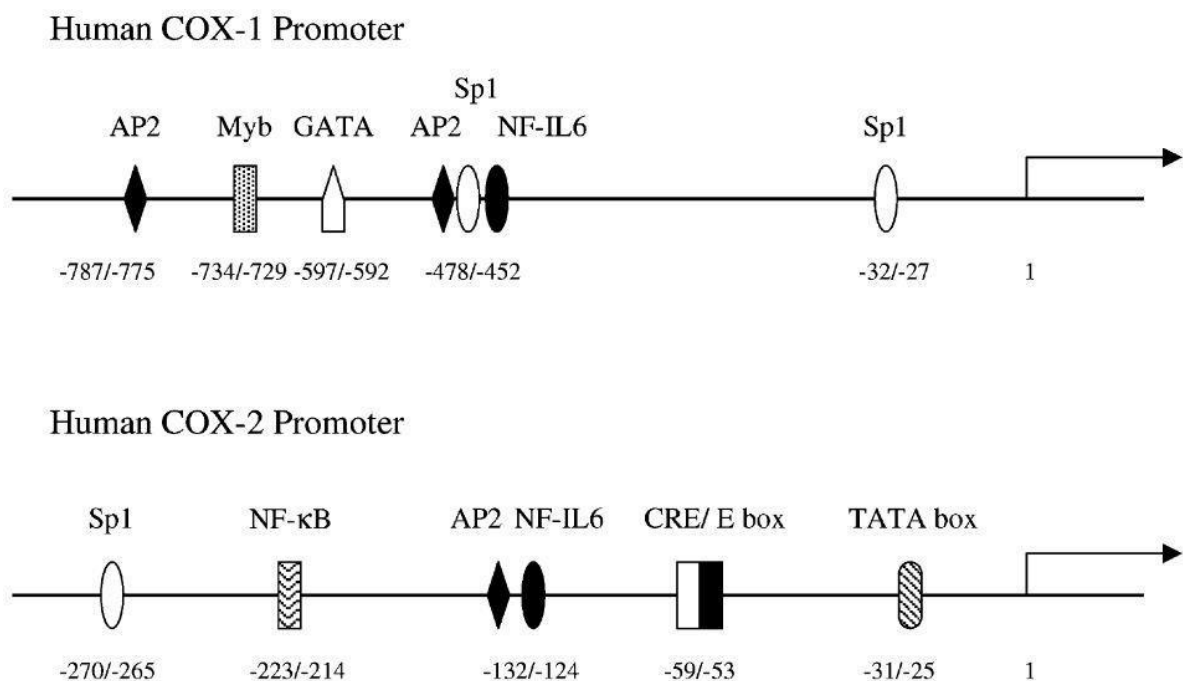


Figure 28 – Regulatory elements in the human COX-1 and COX-2 promoters (Tanabe and Tohnai, 2002).

In fact, as previously reported, NF- κ B signalling is involved in COX-2 expression stimulated by TNF-

α , hypoxia, LPS and IL-1 β in several cell types. Some experiments have shown that treatment with antisense oligonucleotides for p65, decoy oligonucleotides containing the NF- κ B binding motifs and inhibitors of the I κ B kinase resulted in inhibition of COX-2 expression, suggesting that NF- κ B activation is required for induction by pro-inflammatory stimuli (Lim et al., 2001). Furthermore, transfection of cultured mouse osteoblastic MC3T3-E1 cell line with a reporter gene construct containing mutated COX-2 promoter sequence has proven that mutations in the NF- κ B *cis*-regulatory sites attenuated transcriptional activation of the COX-2 promoter after stimulation with TNF- α (Yamamoto et al., 1995). Interestingly, recent evidence has indicated that NF- κ B in turn can be affected by COX-2 activity leading to a positive or negative feedback control mechanism dependent on whether COX2 and its effector prostaglandins up-regulate or down-regulate NF- κ B function. In fact, according to a study performed by Poligone and Baldwin, the inhibition of COX-2 could enhance the ability of TNF- α to induce NF- κ B activation in HT-29 human colon epithelial cells while the constitutive expression of COX-2 negatively regulated NF- κ B activation, as it was observed in colorectal cells transfected with a COX-2 expression vector so that TNF- α did not promote nuclear translocation of NF- κ B (Poligone and Baldwin, 2001). Furthermore, it was reported that this negative effect could be due to prostaglandins that might function both as positive as well as negative regulators of NF- κ B. In particular, PGA₁, PGA₂ and PGJ₂ were all able to suppress the activation of NF- κ B directly inhibiting IKK (Straus et al., 2000) while, on the contrary, PGE₂ activates the transcriptional activation domain of p65 in order to regulate NF- κ B activity (Fig. 29).

In addition, NF- κ B regulatory effect on COX-2 gene expression under hyperglycaemic conditions was demonstrated in cultured human mesangial cells (HMCs) that are considered one of the most typical targets of diabetic complications. In fact, Kiritoshi and colleagues observed that incubation of HMCs with 30 mM glucose significantly increased mitochondrial membrane potential, intracellular ROS production, COX-2 protein expression and PGE₂ synthesis. By using wild type/mutant constructs of reporter gene assays they showed that the two NF- κ B binding motifs located in the promoter of COX-2 gene had a synergistic effect on the hyperglycaemia-induced COX-2 expression as mutation of either one of them had a partial inhibitory effect whereas mutation of both sites resulted in complete inhibition (Kiritoshi et al., 2003). Furthermore, the hypothesis that diabetic conditions could induce COX-2 expression via NF- κ B activation was tested in THP-1 monocytic cells by Shanmugam and co-workers through promoter deletion analysis and use of pharmacological and genetic inhibitors of NF- κ B (Shanmugam et al., 2004).

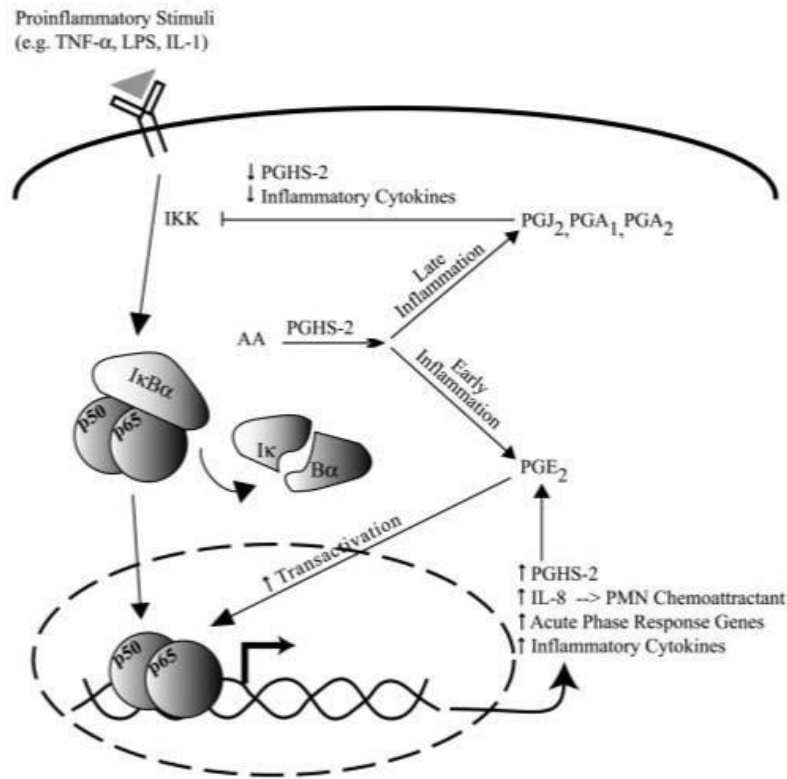


Figure 29 – Role of prostaglandins in regulating NF-κB activity. Several pro-inflammatory stimuli trigger signalling cascades that increase NF-κB nuclear levels leading to the induction of COX-2 expression. The enzyme catalyses the conversion of arachidonic acid into various prostaglandins, among which PGE₂ is initially the most abundant. It increases the transactivation function of NF-κB enhancing the expression of NF-κB-dependent inflammatory genes. Eventually a shift occurs in which PGE₂ becomes less abundant while other prostaglandins, including PGA₁, PGA₂ and PGJ₂ are increased and inhibit NF-κB activity through IKK inhibition. This negative feedback loop leads to reduced COX-2 gene expression due to a decreased NF-κB activity (Poligone and Baldwin, 2001).

Among the inducers that have been identified to be involved in the up-regulation of COX-2 expression one of the most relevant is 4-HNE. A first demonstration of a link between COX-2 and 4-HNE was provided by experiments performed by Kumagai and collaborators who conducted a screen of the effect exerted by oxidized fatty acids on COX-2 induction in rat liver epithelial RL34 and mouse macrophage RAW264.7 cell lines and showed that 4-HNE, but not other α , β -unsaturated aldehydes, was able to stimulate COX-2 expression (Kumagai et al., 2004). However, the 4-HNE-induced signalling mechanism responsible for COX-2 expression resulted to be NF-κB independent since no significant change in the IκB and NF-κB levels was observed after treatment with 4-HNE. Instead of the NF-κB pathway, 4-HNE triggered a rapid and significant phosphorylation of p38 mitogen-activated protein kinase (MAPK) activating the p38 MAPK pathway that leads to the up-regulation of COX-2 through the stabilization of its mRNA. On the other hand, an

alternative mechanism by which 4-HNE induces COX-2 gene expression was proposed. In fact, it was found that COX-2 levels were inversely correlated with the levels of p53, a transcription factor that regulates the response to several stimuli, as demonstrated by the increase of both mRNA and protein levels of COX-2 observed after the down-regulation of p53 with antisense oligonucleotides. Immunoprecipitation experiments showed that in cells under physiological conditions p53 is bound to Sp1 in a heterocomplex that negatively regulates its transcriptional activity. 4-HNE was reported to promote the dissociation of p53-Sp1 complex and the concomitant nuclear translocation of Sp1 inducing COX-2 gene expression (Fig. 30) (Uchida, 2017) but only in the presence of serum in cell culture medium. In particular, Kanayama and colleagues identified the modified LDLs such as oxidized LDLs as active serum component essential for the induction of COX-2 by 4-HNE demonstrating the existence of a link between the oxidative modification of LDLs and the activation of the inflammatory response. In fact, 4-HNE and oxidized LDLs appeared to cooperatively induce COX-2 expression in macrophages through a mechanism involving the 4-HNE-induced up-regulation of the scavenger receptor CD36 which, in turn, promotes COX-2 expression by the modified LDLs (Kanayama et al., 2007). A study performed by Ishii and co-workers provided the first evidence that 4-HNE, thanks to its ability to readily enter cells and react with proteins, is one of the most effective activators of the redox sensitive transcription factor Nrf2 that is involved in the up-regulation of CD36 under oxidative stress conditions (Ishii et al., 2004). However, the association of the CD36/oxidized LDLs pathway with the transcription factors p53 and Sp1 in the 4-HNE-mediated induction of COX-2 expression still needs to be clarify.

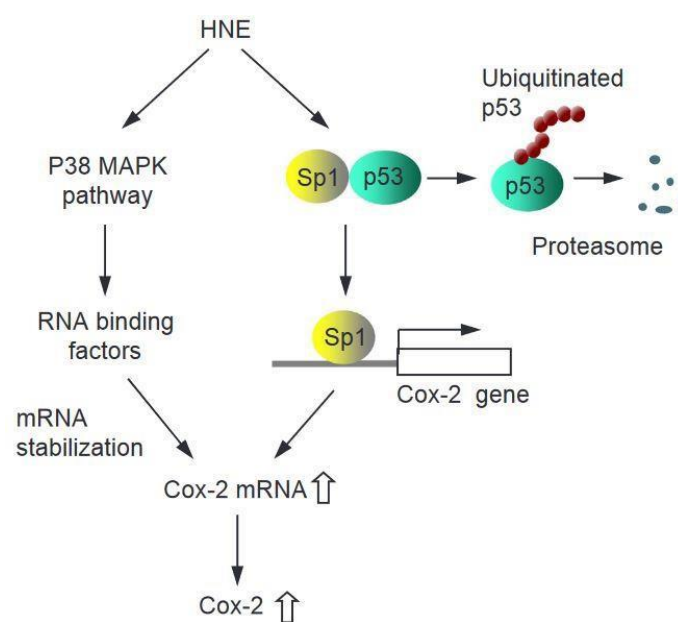


Figure 30 – A proposed mechanism pf 4-HNE-mediated induction of COX-2 gene expression (Uchida, 2017).

5. Oxidative and glycative stress: role of two NADPH-dependent enzymes

As previously discussed, increased oxidative stress observed in type 2 diabetes is thought to play an important role in the pathogenesis of diabetic complications. ROS-induced cellular damage occurs in biological systems because of an inadequate detoxification of free radicals that results in accumulation of oxidized nucleic acids, proteins and lipids. The induction of oxidative stress in diabetes is dependent on multiple mechanisms that are all associated with high glucose levels. In this situation, two NADPH-dependent enzymes, aldose reductase (AKR1B1) and carbonyl reductase (CBR1) appear to play a key role since they proved to be involved in detoxification processes of either endogenous or exogenous toxic molecules produced under oxidative stress (Singh et al., 2013) and, for this reason, represent a defence mechanism against cellular apoptosis and tissue degeneration, typical of age-related diseases. AKR1B1 is also reported to play a role in inflammation due to its catalytic activity on GS-HNE producing GS-DHN and contributing to trigger a pro-inflammatory signalling that mediates the NF- κ B activation (Srivastava and Ramana, 2009). Consequently, since AKR1B1, but CBR1 as well, that has also been reported to be able to reduce GS-HNE (Rotondo et al., 2016), could be involved in modulating GS-DHN levels. For this reason, the inhibition of both these enzymes could significantly confer protection against inflammation-induced tissue damage. Additionally, given the mechanistic role of AKR1B1 in the onset and progression of diabetes and its complications due to increased glucose flux through the polyol pathway under hyperglycaemic conditions, it is considered a potential therapeutic target to prevent tissue injury associated with prolonged hyperglycaemia such as cardiomyopathy, neuropathy, nephropathy and retinopathy.

5.1 Aldose reductase (AKR1B1)

Aldose reductase (AKR1B1; EC 1.1.1.21) is a monomeric NADPH-dependent cytosolic enzyme belonging to the superfamily of aldo-keto reductases (AKRs) (Ramana, 2011) that was first identified as a protein with glucose reducing activity in 1956 by Hers (Hers, 1956). The aldose reductase gene is found on human chromosome 7 locus q35 and is distributed over about 18 kb containing 10 exons that code a 316 amino acids protein (Graham et al., 1991). Since AKR1B1 and other members of the AKRs superfamily show high amino acid sequence identity, they share also a common three-dimensional structure adopting an identical (α/β)₈-barrel fold, as

determined by X-ray crystallography (Wilson et al., 1992). In AKR1B1 this regular structure is interrupted by a large loop between β -strand 4 and α -helix 4 and by another one between β -strand 7 and α -helix 7. After α -helix 8 there is an extra α -helix followed by the C-terminal loop (Fig. 31). At the base of the barrel there is a highly conserved catalytic tetrad (Tyr 55, Asp 50, Lys 84, His 117) belonging to the AKR active site that is equally conserved both structurally and in sequence. Thus, it has been indicated that three loops on the C-terminal side of the AKR structure are crucial for discriminating between different substrates. Furthermore, the multiple sequence alignment of members of AKRs superfamily has revealed the presence in all proteins of a highly conserved nicotinamide-cofactor-binding pocket (Jez et al., 1997). In fact, the AKRs catalyse the reduction of a wide range of substrates involving hydride transfer from NAD(P)H to the substrate acceptor carbonyl group generating the corresponding alcohol.

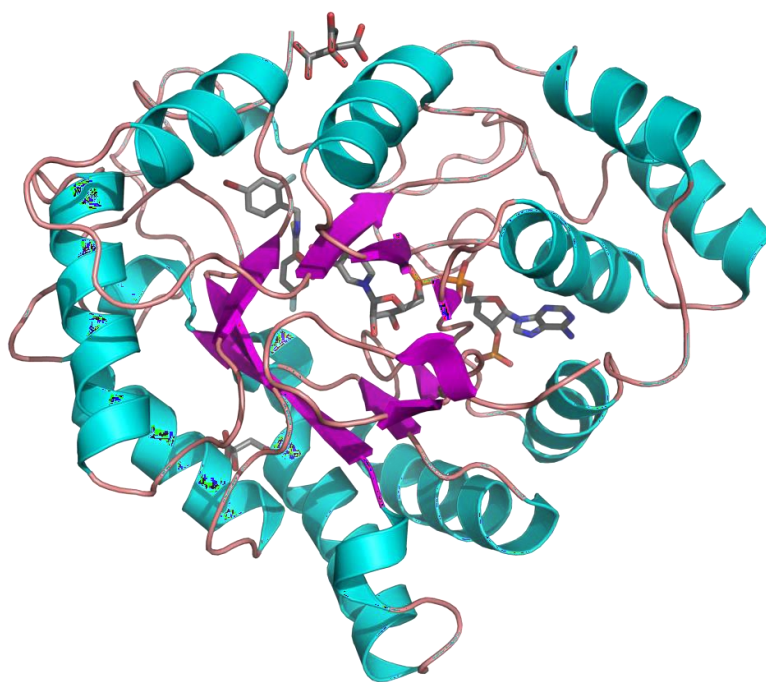


Figure 31 – Crystal structure of AKR1B1 (Source: Protein Data Bank).

According to structural studies and X-ray analyses of aldose reductase crystals, substrate-binding domain is characterized by the presence of highly plastic and hydrophobic residues (Borhani et al., 1992) that make the enzyme able to reduce both aldehydes and keto groups of aromatic and aliphatic molecules, suggesting that AKR1B1 exhibits a broad substrate specificity (Vander Jagt et al., 1995). Furthermore, these studies indicate that the high hydrophobicity of the AKR1B1 catalytic site, in addition to the lack of the ionic residues typical of polyol-

binding proteins, precludes efficient carbohydrate reduction, thus explaining the poor affinity that the isolated enzyme shows for glucose (K_M of 50–100 mM) and suggesting that hydrophobic aldehydes are likely to be the preferred substrates. In the early 2000s, several studies reported that AKR1B1, in addition to reducing glucose, also efficiently reduces medium- to long-chain (C-6 to C-18) aldehydes generally generated during lipid peroxidation, such as 4-HNE, and their glutathione conjugates (Srivastava et al., 1995; VanderJagt et al., 1995). Collectively, these evidences show that AKR1B1 may represent an important metabolic route for the detoxification of lipid-derived aldehydes that are reported to be involved in the pathogenesis of several diseases such as diabetes, aging, ischemia, and cancer. This conclusion is supported by the observation that AKR1B1 catalyses the reduction of 4-HNE with a catalytic efficiency that is four orders of magnitude higher than that for glucose (Vander Jagt et al., 1995). Furthermore, the significant overexpression of AKR1B1 observed after the exposure of VSMCs to 4-HNE (Rittner et al., 1999) confirms the role of this enzyme in the metabolism of toxic lipid-derived aldehydes that is closely associated with its capability to reduce the adduct GS-HNE, as well. In fact, molecular modelling studies and site-directed mutagenesis experiments have revealed that AKR1B1 catalytic site forms a specific glutathione-binding domain that selectively interacts with the glutathione backbone of glutathione-aldehyde conjugates and, for the range of aldehydes tested by Dixit and co-workers, the glutathione conjugates resulted to be better substrates than the corresponding free aldehydes (Fig. 32) (Dixit et al., 2000).

Substrate	m/z	K_m μM	k_{cat} min^{-1}	k_{cat}/K_m $min^{-1} \mu M^{-1}$
Propanal		5120 ± 320	28.1 ± 1.7	0.005 ± 0.0003
GS-propanal	364.4	13.2 ± 1	87.9 ± 8.7	6.8 ± 0.7
Hexanal		8.4 ± 1	23.4 ± 0.8	2.9 ± 0.1
GS-hexanal	406.3	7.2 ± 1	74.0 ± 6.6	10.6 ± 1.0
Nonanal		25.1 ± 7	36.9 ± 4.6	1.5 ± 0.2
GS-nonanal	448.3	9.3 ± 7	66.0 ± 8.9	7.3 ± 0.9
<i>trans</i> -4-Decenal		44 ± 1	34.2 ± 4.5	0.8 ± 0.1
GS- <i>trans</i> -4-decenal	460.4	4.2 ± 1	55.4 ± 9.9	13.8 ± 2.3

Figure 32 – Kinetic parameters of aldehydes and corresponding glutathione conjugates as AKR1B1 substrates (Dixit et al., 2000).

One possible explanation for the enhanced AKR1B1 catalytic efficiency towards glutathione

conjugates could be that these substrates are larger in size, thus providing more opportunity for hydrophobic interactions with the active site. However, since the catalytic efficiency of the enzyme towards free aldehydes did not increase in proportion to the chain length, it was suggested that the AKR1B1 higher efficiency with glutathione conjugates was due to the specific recognition of the glutathione backbone at the active site. Therefore, these results indicate that glutathiolation of lipid-derived aldehydes may be an effective mechanism for enhancing the efficiency of toxic aldehydes metabolism. In fact, the incubation of human lens epithelial cells (HLECs) or rat lens with 15 μM 4-HNE, followed by high performance liquid chromatography (HPLC) analysis, demonstrated that one of the major metabolic transformations of 4-HNE in ocular tissues involves conjugation with glutathione to generate GS-HNE that is subsequently reduced to GS-DHN by AKR1B1 (Choudhary et al., 2003). Reduction of GS-HNE to GS-DHN could therefore be a major detoxification reaction to prevent the propagation of 4-HNE-induced oxidative damage (Esterbauer et al., 1975). However, it has also to be considered that GS-DHN is reported to be, as it was described before, a cellular signalling mediator resulting in protein kinase C (PKC), NF- κ B and AP-1 activation and leading to cell growth or apoptosis in different cell types (Fig. 33) (Ramana et al., 2006). Consequently, pharmacological inhibition of AKR1B1 might limit the effects associated with inflammatory or proliferating responses (Ramana et al., 2006).

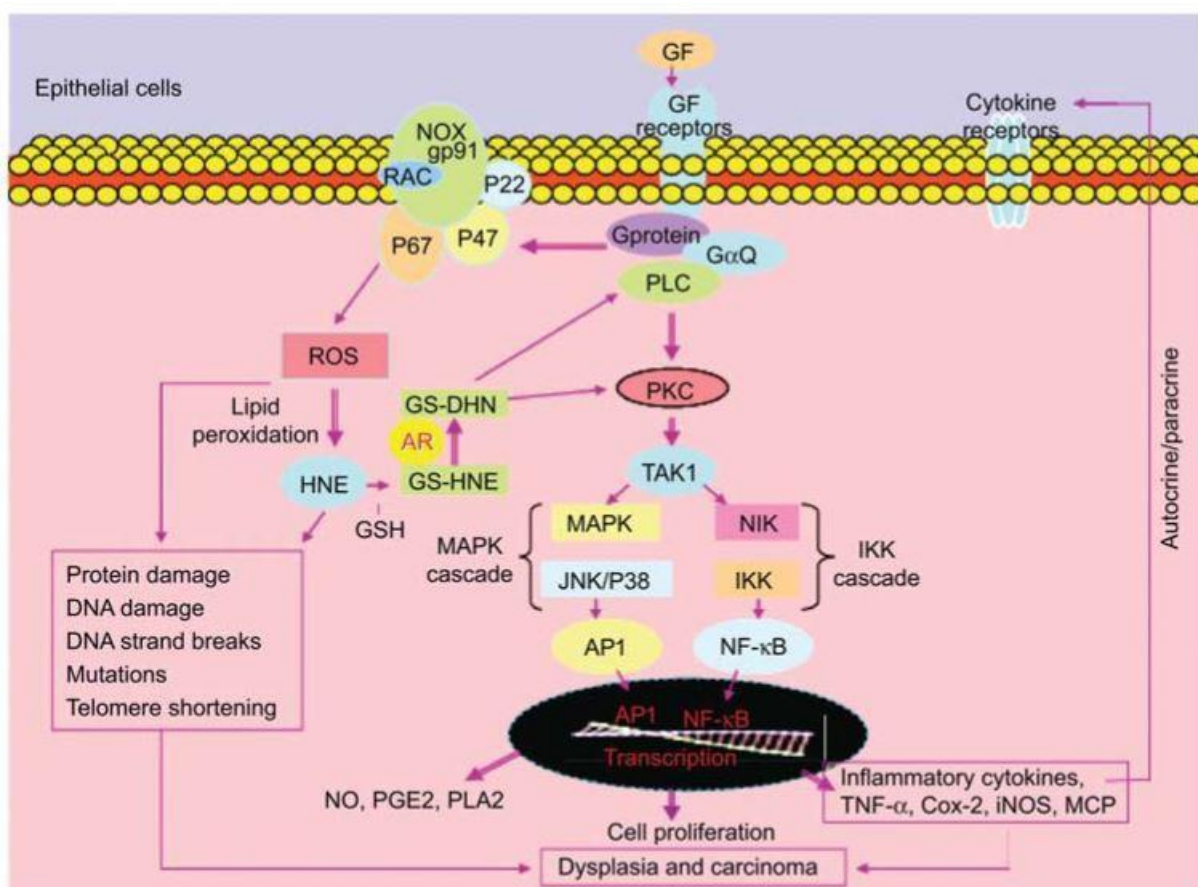


Figure 33 - AKR1B1 mediates growth factor-induced inflammatory and proliferating signalling (Ramana, 2011).

5.2 Carbonyl reductase (CBR1)

Carbonyl reductase 1 (CBR1; EC 1.1.1.184) belongs to the short chain dehydrogenases/reductases (SDR) superfamily (Wermuth, 1992), one of the largest enzyme superfamilies. Despite low sequence identities between different forms (15-30%), specific sequence motifs are detectable, reflecting highly conserved three-dimensional architecture that display a highly similar α/β folding pattern with a Rossmann fold secondary structure in the N-terminal part of the enzyme consisting of a central β - sheet flanked on either side by α -helices (Fig. 34) (Ghosh et al., 1991). Sequence comparisons, site-directed mutagenesis and crystallographic analysis have revealed that most of the highly conserved secondary structure elements are a GlyXXXGlyXGly motif in the N-terminal part and a triad of Ser, Tyr and Lys residues in the center part of the peptide chain that appear to be involved in cofactor binding and catalysis, respectively. On the other hand, the least sequence homology is found in the C-terminal portion of the enzyme, suggesting that it may be involved in substrate specificity (Jornvall et al., 1995).

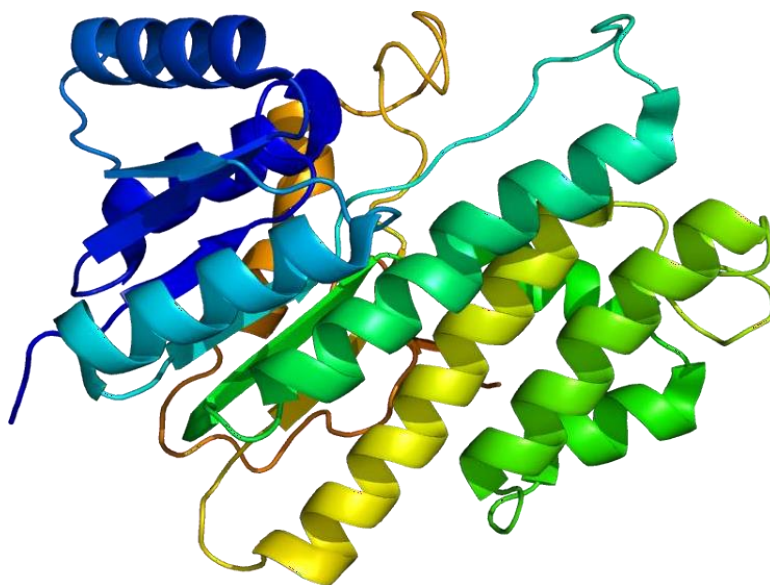


Figure 34 – Crystal structure of human CBR1 (Source: Protein Data Bank).

In the human genome, three SDR genes have been identified; CBR1, CBR3 and CBR4 but the well-known isoform is CBR1 (Matsunaga et al., 2006). CBR1 has been first isolated in 1973

from human brain and was initially designated as aldehyde reductase. Later, it was named carbonyl reductase by Wermuth who characterized its enzymatic properties observing that it reduces a wide spectrum of biologically and pharmacologically active carbonyl compounds (Wermuth, 1981). The carbonyl reductase gene is mapped to band 21q22.12 and consists of 3142 basis, comprising three exons and two introns. Its structure is characteristic of many housekeeping genes, lacking a CAAT and TATA box and containing a GC-rich island extending into the first exon (Lemieux et al., 1993). It codes for a monomeric cytosolic enzyme which consists of 277 amino acids and has a molecular weight of 30,375 Da. CBR1 was detected by immunohistochemical staining in different tissues, however, the highest enzyme levels were observed in the ones that are in close contact with exogenous compounds such as liver, the epithelia of the gastrointestinal tract and the epidermis (Wirth and Wermuth, 1992), suggesting that CBR1 might play a crucial role in the detoxification of xenobiotics. The main substrates of CBR1 are reported to be prostaglandins, steroids, biogenic amines and quinones derived from polycyclic aromatic hydrocarbons as well as a variety of xenobiotics containing carbonyl groups such as the anti-cancer anthracycline doxorubicin and the vitamin K2 precursor menadione (Ahmed et al., 1978). More recently, CBR1 has been linked to the detoxification of reactive aldehydes such as 4-oxonon-2-enal (4-ONE) that is believed to be involved in oxidative stress-related neurodegenerative disorders given its high reactivity towards DNA and proteins, in particular nucleophile residues such as cysteine, histidine and lysine (Doorn and Petersen, 2003). CBR1 catalyzes reductive reactions at several functional groups of 4-ONE to form multiple products. The ketone-reducing activity was found to predominate, since 4-HNE represents about 70% of the total product, even though CBR1 is proved to mediate hydride transfer to the carbon double bond of 4-ONE, generating 4-oxononanal (4-ONA). Importantly, 4-ONE is able to form an adduct with glutathione (GS-ONE) which is, in turn, a substrate for both CBR1 and AKR1B1, suggesting that these enzymes play an equally important role in detoxification of toxic aldehydes generated as a consequence of radical-mediated lipid peroxidation (Fig. 35) (Doorn et al., 2003).

Interestingly, CBR1 contains five cysteine residues close to the active site, none of which is conserved within the family (Tinguely and Wermuth, 1999), that appeared to be necessary for substrate binding. Tinguely and Wermuth conducted experiments of site directed mutagenesis observing that Cys-227, is involved in the correct substrate orientation of carbonyl substrates, even though it does not seem to be relevant for some GSH-conjugated substrates. In fact, they reported that CBR1 activity was dramatically reduced for the mutant enzyme using menadione as

substrate, whereas it was maintained almost similar to the activity of the wild-type enzyme when, as substrate, it was used its conjugated with GSH.

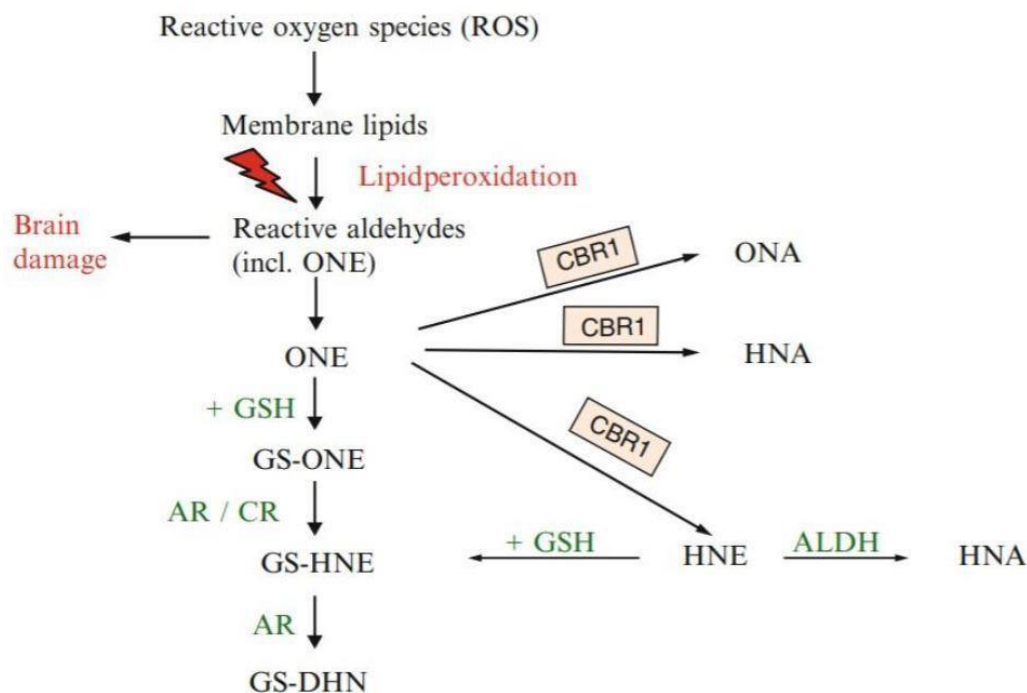


Figure 35 – Scheme of reduction of the lipid peroxidation product 4-ONE by CBR1 and AKR1B1 (Guest and Grant, 2016).

The ability of CBR1 to reduce glutathione adducts is also reported by Wermuth who observed that GSH conjugates of otherwise poorly recognized substrates such as PGA_1 were readily reduced by CBR1 at low concentrations (Wermuth, 1981). Therefore, it was hypothesized that cellular GSH adducts might be particularly relevant as CBR1 substrates, having an impact on biological processes in the human body. In fact, Bateman and colleagues demonstrated through X-ray co-crystal structure analysis of CBR1 in complex with GSH that the enzyme has a glutathione binding site which lies within its catalytic pocket (Bateman et al., 2008) where GSH-substrate adducts and mixed disulfides can bind, thus modulating the enzymatic activity. In agreement with this observation, Moschini and co-workers have recently reported that CBR1 was unable to reduce a number of alkanals and alkenals but, in contrast, it showed strong affinity for GS-propanal, GS-hexanal and GS-nonanal, suggesting that the insertion of a glutathionyl moiety made these molecules very good reducible substrates for the enzyme. In addition, the same authors demonstrated that the enzyme, besides catalyzing efficiently the reduction of

glutathionylated alkanals, like GS-HNE to GS-DHN, can also act as a NADP⁺-dependent dehydrogenase, by oxidizing with a specificity constant of $12.3 \times 10^3 \text{ mM}^{-1} \text{ min}^{-1}$ the hydroxyl group of GS-HNE in its hemiacetal form, giving the 3-glutathionylnonanoic- δ -lactone (GSHNA-lactone) (Moschini et al., 2015). This result highlights the relevance of CBR1 in the detoxification pathways of cytotoxic lipid peroxidation derivatives, especially at the high NADP⁺/NADPH ratios present under oxidative stress conditions. In this context, CBR1 seems to play a dual role in 4-HNE detoxification and recovery of cell reducing power. The ability of CBR1 to act bidirectionally on GS-HNE was demonstrated through a mass spectrometry approach by monitoring the redox process in reaction mixtures containing CBR1, GSHNE and NADPH. Indeed, it was observed that both GSHNA-lactone and GS-DHN accumulated with the concomitant disappearance of GS-HNE, suggesting that both the reductive and oxidative transformation of GS-HNE occurred simultaneously (Fig. 36) (Rotondo et al., 2016). Due to this CBR1 dual catalytic activity on GS-HNE, the enzyme might play a dual role, both in terms of 4-HNE detoxification and, through the production of GS-DHN, in terms of involvement into the inflammatory signalling. However, since these results have only been shown *in vitro*, more studies are necessary to evaluate CBR1 activity *in vivo*.

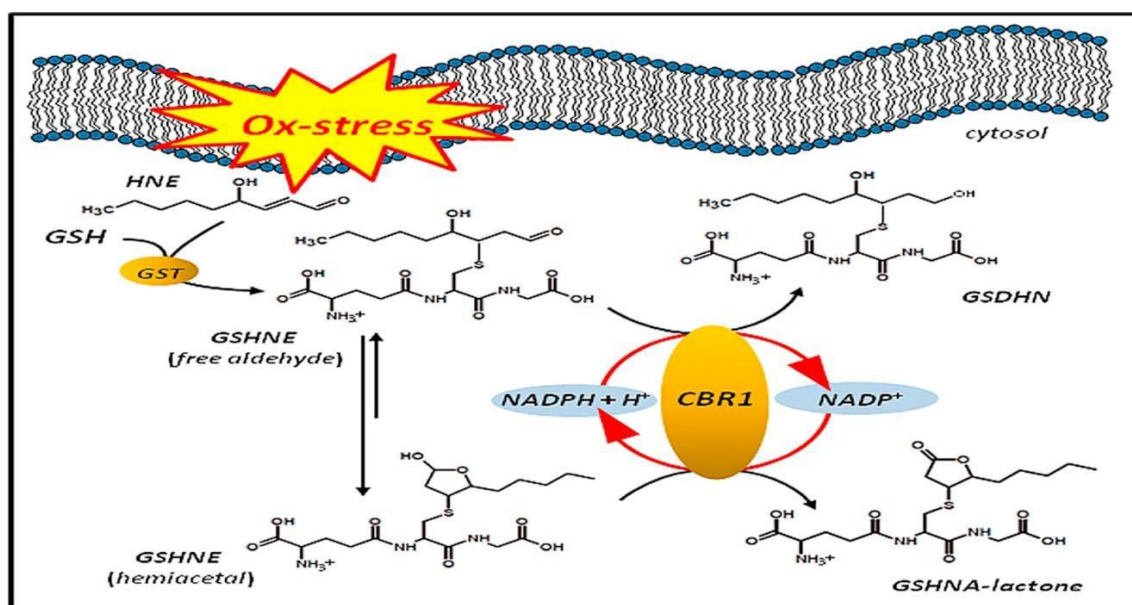


Figure 36 - CBR1 dual activity towards the GS-HNE adduct (Rotondo et al., 2016).

AIM OF THE THESIS

The aim of this thesis is investigating, in a cultured human lens epithelial cell line (HLE-B3), the pro-inflammatory effect of two endogenous stimuli, 4-HNE and D-glucose, by evaluating both the activation of the transcription factor NF- κ B and cyclooxygenase-2 (COX-2) expression. This is particularly relevant because the inflammatory signalling pathways induced by these molecules are closely interlinked by aldose reductase (AKR1B1) activity that appears to play a key role as signalling mediator. For this reason, the involvement of this enzyme in 4-HNE- and D-glucose-induced inflammatory response is assessed by using two well-known inhibitors of AKR1B1, sorbinil and rutin, with the aim of creating a reliable *in vitro* cell model system on which testing the anti-inflammatory action of AKR1B1 inhibitors and their effectiveness in preventing diabetic complications associated with inflammation.

MATERIALS AND METHODS

1. Materials

Instruments	Company
Thermoblock 780, water jacketed CO2 incubator	THERMO
Class II biological safety cabinet	HERAEUS
Chemical fume hood	BICASA
EL808 Ultra Microplate Reader	BIO-TEK INSTRUMENTS INC.
pH Meter	DENVER INSTRUMENT COMPANY
Cryovials Falcon tubes 15 ml, 50 ml 24-well plate 96-well plate 35 mm culture dish 25 cm ² flask (T25) 75 cm ² flask(T75) 10 cm Petri dish 2 ml, 5ml, 10 ml, 25 ml serological pipettes Scrapers Plastic cuvettes 0.2 µm syringe filter	SARSTEDT
Primo® microcentrifuge tubes 1.5 ml	EUROCLONE
Smart R17 refrigerated microcentrifuge	HANIL SCIENCE INDUSTRIAL
Vacuum filtration device	MILLIPORE
Libra S80 Double Beam Spectrophotometer	BIOCHROM
FLUOstar® Omega Plate Reader	BMG LABTECH
Mini-PROTEAN® Tetra Cell Casting Stand & Clamp kit Electrophoresis chamber PowerPac Basic Power Supply Trans-blot Turbo System Trans-blot Turbo Mini 0.2 µm PVDF transfer packs ChemiDoc imaging system	BIORAD

Chemicals	Company
TGX Stain-Free FastCast acrylamide kit Bradford reagent Prestained protein standards Bromophenol blue	BIORAD
MEM Fetal bovine serum (FBS)L-glutamine Gentamycin Penicillin/Streptomycin Crystal violet	EUROCLONE
Phenylmethylsulfonyl fluoride (PMSF)	CALBIOCHEM

Cell Lysis Buffer Primary anti-COX-2 antibody Anti-rabbit IgG HRP-linked antibody Nonfat dry milk	CELL SIGNALLING TECHNOLOGY
Immobilon Western Chemiluminescent HRP Substrate	MILLIPORE
HLE-B3 cell line	ATCC
TNF- α	R&D Systems
Hygromycin	PanReac AppliChem ITW Reagents
D-glucose Glycine	VWR Chemicals BDH®
E.coli XL-1	AGILENT
Sodium bicarbonate	CARLO ERBA
Sodium dodecyl sulfate	APPLICHEM
Ethylenediaminetetraacetic acid (EDTA)	JUORO
Potassium chloride (KCl) Sodium chloride (NaCl) Hydrochloric acid (HCl) Sodium hydroxide (NaOH) Potassium dihydrogenphosphate (KH ₂ PO ₄) Acetic acid Ammonium sulphate Sodium phosphate monobasic	J.T.BAKER
L-idose NADPH	CARBOSYNTH
Calcium chloride	MERK MILLIPORE

3-(4,5-Dimethylthiazol-2-yl)-2,5-diphenyltetrazolium bromide
(MTT)1,4-Dithiothreitol (DTT)
Rutin
1-Methyl-2-phenylindole
2-Mercaptoethanol
DMEM (D5030)
L-Glutathione reduced
Glycerol
Iron(III) chloride
Trypsin/EDTA
Isopropyl alcohol
Methanesulfonic acid
Sodium citrate
Ethanol
Methanol
Acetonitrile
Sorbiniol
Phenol red sodium salt
Bovine serum albumin
(BSA)Human serum
albumin (HSA)HEPES
Tetrasodium pyrophosphate
($\text{Na}_4\text{O}_7\text{P}_2$)Sodium fluoride (NaF)
5,5'-dithiobis-2-nitrobenzoic acid (DTNB)

SIGMA ALDRICH CO.

Sodium orthovanadate (Na ₃ VO ₄) β-glycerophosphate TEMED Ammonium persulfate (NH ₄) ₂ S ₂ O ₈ Tween-20 Tris	
Bio-Glo™ Luciferase Assay reagent Passive Lysis Buffer FuGENE® HD Transfection Reagent pGL4.32[luc2P/NF-κB-RE/Hygro] vector QuantiLum® Recombinant Luciferase	PROMEGA

2. Methods

2.1 Cell culture

The human lens epithelial B3 cell line (HLE-B3) was obtained from American Type Culture Collection (ATCC, Rockville, MD, USA). They are cultured in 75 cm² tissue culture flasks in 15 ml of Minimal Essential Medium (MEM) supplemented with 20% (v/v) fetal bovine serum (FBS), 2 mM L-glutamine and 1% (v/v) penicillin/streptomycin (complete medium) at 37°C in a humidified chamber with 5% CO₂. The population-doubling time of exponentially growing cells is 48 hours, and they can be maintained in culture for over 76 population doublings with no decrease in their proliferative capability. As cells reach about 60-70% confluence, they must be subcultured in order to prevent the culture dying. To subculture the cells the spent medium is removed, and the cell monolayer is washed twice with 3 ml of PBS (0.8% (w/v) NaCl, 0.02% (w/v) KCl, 0.02% (w/v) KH₂PO₄, 0.06% (w/v) Na₂PO₄) and with 1 ml of trypsin/EDTA solution. Then, cells are detached by maintaining them for 2 minutes at room temperature with 1 ml of trypsin/EDTA solution. Afterwards, 5 ml of complete medium are added to inactivate trypsin activity and the 6 ml total volume harvested is transferred into two distinct T75 flasks. This procedure is performed four times in two weeks maximum, in order to reach the number of cells required to conduct the experiments.

2.2 HLE-B3 cells preparation for the experimental procedures

HLE-B3 cells are trypsinized, counted in a Bürker chambre using the optical microscope in order to seed a constant density of 20,000 cells/cm² in 10 cm dishes and incubated for 72 hours in complete medium. If not otherwise specified, the medium is then replaced with MEM

supplemented with 0.5% (v/v) FBS, 1% (v/v) L-glutamine and 50 µg/ml gentamycin. After 24 hours, HLE-B3 cells are exposed to the treatments that will be discussed in the following paragraphs.

2.3 Incubation of HLE-B3 cells under three different experimental conditions

Before proceeding with 4-HNE treatment, HLE-B3 cells are incubated under three different experimental conditions to determine the most appropriate one to highlight the aldehyde-induced inflammatory response in this cell line: MEM containing 0.5% (v/v) FBS, 2 mM L-glutamine and 50 µg/ml gentamycin (condition **A**), serum-free MEM supplemented with 2 mM L-glutamine and 50 µg/ml gentamycin (condition **B**) and Krebs-Hanseleit bicarbonate buffer solution (1.2 mM KH₂PO₄, 11 mM glucose, 2.4 mM MgSO₄, 4.7 mM KCl, 118 mM NaCl, 1.25 mM CaCl₂, 25 mM NaHCO₃) supplemented with 2 mM L-glutamine (condition **C**). Under these experimental conditions cell viability, the rate of 4-HNE removal from the culture medium and the pro-inflammatory effect of 4-HNE are assessed after different incubation times, as it will be described in the Results section.

2.4 Pro-inflammatory treatment of HLE-B3 cells

2.4.1 4-HNE treatment

HLE-B3 cells are treated with fixed concentration of 4-HNE for different times of incubation in serum-free MEM supplemented with 2 mM L-glutamine and 50 µg/ml gentamycin, as described in the Results section, after which they are harvested through different techniques depending on the analysis that have to be performed. Cells incubated under the same conditions in the absence of 4-HNE are used as control. Furthermore, the effect of DMSO solution of sorbinil and rutin, two inhibitors of NADPH-dependent reductase activities, on the inflammatory response induced by 4-HNE is evaluated by pre-incubating HLE-B3 cells with either 100 µM sorbinil or 100 µM rutin for 1 hour before replacing the medium and starting the 4-HNE treatment. Another condition tested consists in the addition of 100 µM sorbinil to the incubation medium along with 4-HNE. In all the experiments performed to assess the inhibitors' effect, control is represented by HLE-B3 cells incubated with 0.1% (v/v) DMSO in the presence of 4-HNE.

2.4.2 Hyperglycaemia treatment

HLE-B3 cells are treated with different final concentrations of D-glucose for different incubation times, as it will be reported in the Results section. Cells incubated under euglycaemic conditions are used as control.

2.5 4-HNE preparation and quantification

Diethyl acetal of 4-HNE is synthesized by Prof. Bellina's team from the department of Chemistry of the University of Pisa and stored in hexane at -80°C until use. Free aldehyde is obtained after the complete evaporation of hexane by means of nitrogen gas flux at room temperature and consequent acid hydrolysis (pH 3) of the diethyl acetal by resuspending 4-HNE in 1 mM HCl and maintaining the solution under agitation for 1 hour at 4°C . The concentration of 4-HNE is determined spectrophotometrically by measuring the absorbance at 224 nm using extinction coefficient of $13.75\text{mM}^{-1}\text{cm}^{-1}$.

2.6 Spectrophotometric GSH quantification

The spectrophotometric quantification of GSH is performed following Ellman's method (Ellman, 1959). The assay consists in a colorimetric reaction due to the reduction of DTNB by GSH to yield a mixed disulfide and highly chromogenic TNB with extinction coefficient of $13.6\text{mM}^{-1}\text{cm}^{-1}$ at 412 nm (Fig. 37). The reaction mixture (0,7 ml final volume) contains 90 mM pH 7.4 sodium phosphate buffer, 0.25 mM EDTA and 0.5 mM DTNB with 0.1% (w/v) sodium citrate.

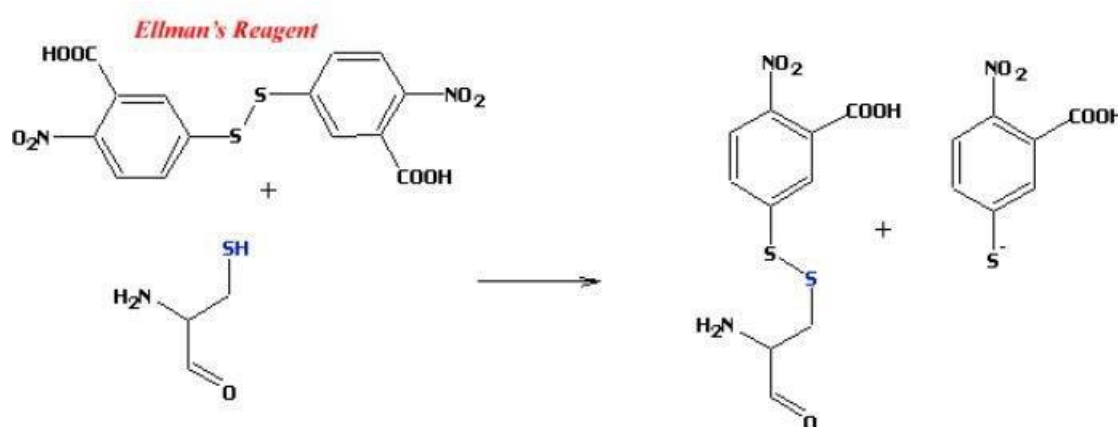


Figure 37 – Reaction of Ellman's reagent with thiols. DTNB reacts with sulphydryl groups of GSH forming mixed disulfides and TNB, a coloured product whose absorption spectrum shows a peak at 412 nm.

2.7 GS-HNE preparation and quantification

The GS-HNE adduct is prepared by incubating 1 mM 4-HNE and 1.5 mM GSH in 50 mM pH 7.4 sodium phosphate buffer, at 37 °C for 1 hour followed by an overnight incubation at 4 °C. The reaction is monitored by measuring the absorbance at 224 nm ($\epsilon_{224} = 13.75 \text{ mM}^{-1} \text{ cm}^{-1}$) and the concentration of the GS-HNE adduct is determined by the difference between the initial concentration of 4-HNE in the reaction mixture and its residual concentration present at the end of incubation time. Since under this condition the reaction yield is not more than 90%, generally the GS-HNE solution obtained has a concentration of 0.9 mM.

2.8 4-HNE determination in the incubation medium

The rate of 4-HNE removal from cell culture media is calculated by measuring the residual concentration of the aldehyde in the incubation medium by a colorimetric assay. This method is based on the measurement of absorbance at 586 nm of a stable chromophore generated by the reaction of 4-HNE with two molecules of 1-methyl-2-phenylindole under acidic conditions. In particular, aliquots of 133 μl incubation medium are taken out at predetermined times and added to 650 μl of a solution of 10 mM 1-methyl-2-phenylindole in a mixture of acetonitrile/methanol (3:1) and 150 μl of concentrated methanesulfonic acid containing 34 μM Fe(III). The absorbance is measured upon incubation of the reaction mixture (1 ml final volume) at 45°C for 30 min (Gerard-Monnier et al., 1998). The concentration of 4-HNE is determined referring to a calibration curve made with different concentrations of a standard 4-HNE solution prepared in 1 mM HCl (Fig. 38).

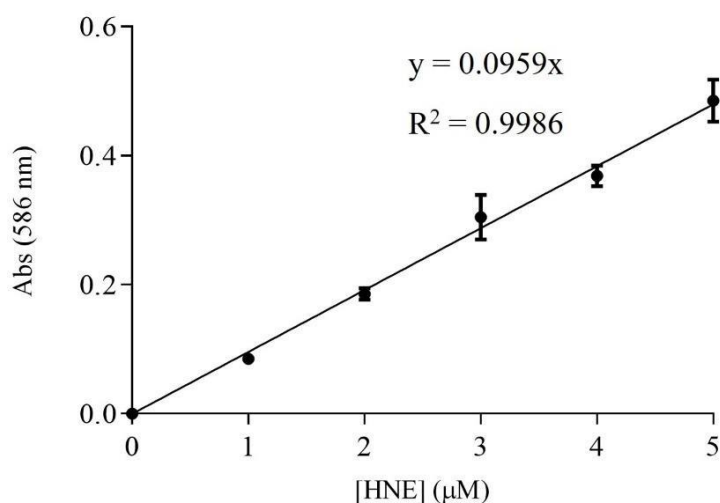


Figure 38 – Calibration curve for 4-HNE determination. The absorbance values at 586 nm are plotted as functions of 4-HNE concentration. Values are expressed as mean \pm SD of at least three independent measurements.

2.9 *D-glucose preparation*

D-glucose is solubilized in PBS at a concentration of 716 mM and sterilized by filtration through 0.2 μ m sterile filters, before any treatments with cells.

2.10 *DMEM (Dulbecco's Modified Eagle's Medium) preparation*

For 1 L of medium, 8.3 g of DMEM (D5030), 3.7 g of sodium bicarbonate (NaHCO₃) and 0.0159 g of phenol red sodium salt are solubilized in ultra-pure water (milliQ). Then, the solution is sterilized by filtration through 0.2 μ m sterile filters under class II biological safety cabinet and stored at 4 °C, until further use.

2.11 *Cell viability assays*

Cytotoxicity assays are performed in order to determine if the pro-inflammatory stimuli tested (4- HNE and hyperglycaemia) eventually lead to cell death. HLE-B3 cells are seeded at a density of 20,000 cells/cm² and incubated in 24-well plates in complete medium for 72 hours. The medium is then removed and substituted with MEM supplemented with 0.5% (v/v) FBS, 2 mM L-glutamine and 50 μ g/ml gentamycin. After 24 hours, HLE-B3 cells are exposed to the treatments that will be discussed in the Results section and cell viability is then assessed by both MTT and crystal violet assays.

2.11.1 *MTT assay*

MTT cell viability assay is a colorimetric assay introduced by Mosmann in 1983 (Mosmann, 1983). It is based on the reduction of the tetrazolium salt MTT (3-(4,5-dimethylthiazol-2-yl)-2,5- diphenyltetrazolium bromide) to insoluble formazane crystals, that have a dark purple blue colour, as a result of dehydrogenase activities (mainly found in mitochondria) (Fig. 39). Cell metabolic activity of NAD(P)H-dependent cellular oxidoreductase is proportional to the number of viable cells present. HLE-B3 cells are incubated with MTT solution (0.5 mg/ml in PBS) for 30 minutes at 37 °C, in a humidified 5% CO₂ atmosphere. Then, the formazane crystals are dissolved by the addition of 0.04 N HCl in isopropanol, thus resulting in a coloured solution whose absorbance is finally quantified by measuring at the wavelength of 563 nm through a

microplate reader.

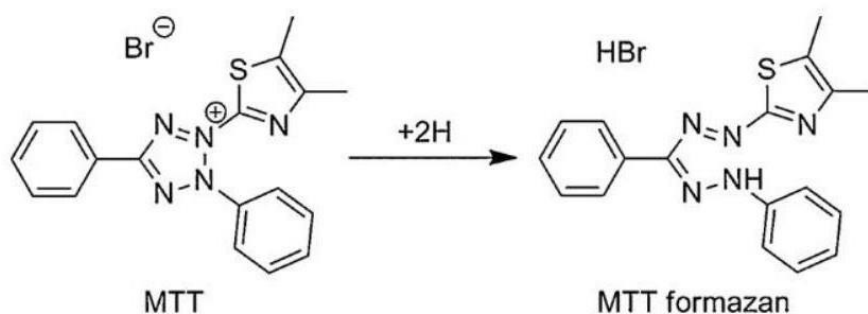


Figure 379 – MTT reduction to its corresponding formazan crystal catalyzed by NAD(P)H-dependent mitochondrial dehydrogenase (Grela et al., 2018).

2.11.2 Crystal violet assay

Crystal violet staining is a quantitative colorimetric assay for evaluating the number of adherent cells by using a dye, crystal violet, that binds to DNA (Feoktistova et al., 2016). The incubation medium is removed from the wells and HLE-B3 cells are rinsed twice with 1 ml PBS. Then 200 μ l of 0.5% (w/v) crystal violet staining solution (0.5 g per 100 ml of methanol) are added to each well and the plate is incubated for 15 minutes at room temperature under gentle agitation. The plate is washed with tap water four times and subsequently air-dried at room temperature for 24 hours. After adding 600 μ l of 10% (v/v) acetic acid to each well, the plate is incubated under agitation for 10 minutes at room temperature in order to solubilize the crystal violet dye. The amount of the crystal violet staining in each well is directly proportional to the number of cells attached to the plate and can be quantified by measuring the absorbance at 596 nm through a microplate reader.

2.12 HLE-B3 crude extracts preparation for HPCE analysis and enzymatic assays

In order to obtain crude extracts on which to perform enzymatic activities and capillary electrophoresis (HPCE) analysis, cells, after medium removal, are rinsed twice with PBS containing 1 mM PMSF, harvested with a scraper and immediately stored at -80°C until further use. Crude extracts are obtained through three cycles of freezing and thawing followed by a 10,000 \times g centrifugation at 4°C for 30 minutes. The supernatant is then retrieved, thus forming the crude extract.

2.13 Sample preparation for HPCE analysis

Intracellular glutathione and GS-HNE content is measured in cell crude extracts obtained as previously described (Paragraph 2.12). Crude extracts are subjected to acidification by the addition of 0.03 N HCl and then to ultrafiltration, using 3000 kDa filters, by centrifugation at 14,000 x g for 1 hour at 4°C. To measure the concentration of total glutathione, crude extracts are incubated with the reducing agent dithiothreitol (DTT) at a final concentration of 5 mM for 2 hours at room temperature before acidification and subsequent ultrafiltration. The concentration of glutathione and GS-HNE present in the samples is determined according to a calibration curve made with standard GSH and GS-HNE solutions, whose concentration is previously verified through spectrophotometric measurements (paragraph 2.6 and paragraph 2.7) (Fig. 40 and Fig. 41), and expressed in terms of nanomoles normalized to micrograms of protein.

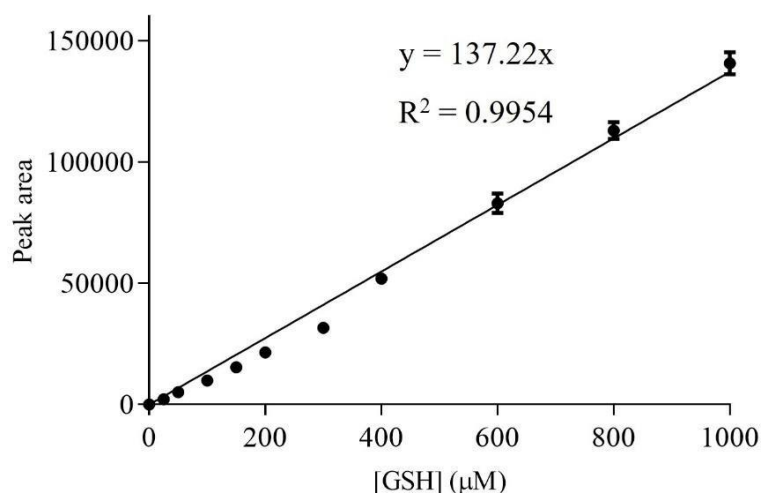


Figure 380 – Calibration curve for GSH determination. Peak area is plotted as a function of GSH concentration. Capillary electrophoresis is performed as described in the Paragraph 2.14 and electropherogram is monitored at 214 nm. Values are expressed as mean \pm SD of at least three independent measurements.

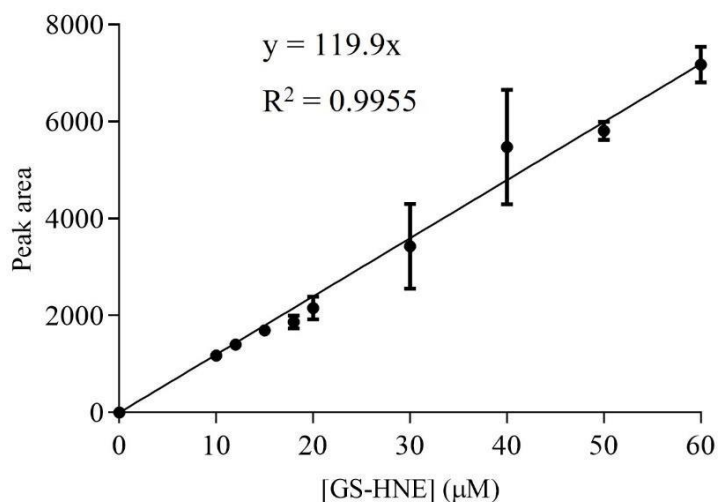


Figure 41 – Calibration curve for GS-HNE determination. Peak area is plotted as a function of GS-HNE concentration. Capillary electrophoresis is performed as described in the Paragraph 2.14 and electropherogram is monitored at 214 nm. Values are expressed as mean \pm SD of at least three independent measurements.

2.14 High performance capillary electrophoresis (HPCE)

High performance capillary electrophoresis (HPCE) is performed to measure intracellular glutathione and GS-HNE content in HLE-B3 cells. The HPCE technique used is based on the operating mode of free-zone capillary electrophoresis of *Beckman P/ACE system MDQ*, where samples are injected into the capillary filled with buffer and their separation primarily occurs depending on differences in charge density. A coated fused-silica capillary column, whose measurements are 50 cm and 74 μ m for length and inner diameter, respectively, is employed. Before usage, the capillary is thoroughly rinsed. In fact, 5-minute 0.1 M NaOH and 2-minute distilled H₂O washes are usually performed under 20 ψ constant pressure. Then, the capillary is equilibrated with 100 mM pH 8.5 Tris borate buffer, for 5 minutes, under 25 ψ constant pressure. Subsequently, the sample is injected into the capillary in 6 seconds, under 1 ψ constant pressure. Sample separation occurs in 10 minutes, applying a constant voltage of 30 kV. The electropherogram regarding the electrophoresis separation is monitored at 214 nm.

2.15 NADPH-dependent enzymatic activities assay

In order to evaluate the inhibitory effect of sorbinil and rutin on the NADPH-dependent reductase activities, reaction mixtures containing 0.82 M sodium phosphate buffer pH 6.8, 0.18 mM NADPH, 0.5 mM EDTA, 0.4 M ammonium sulphate, the crude extract sample, and different concentrations of the inhibitor are incubated for 4 minutes at 37°C before adding 8 mM L-idose as a substrate. The enzymatic activity is then determined by spectrophotometer following the decrease in absorbance at 340 nm due to the oxidation of NADPH ($\epsilon_{340} = 6.22 \text{ mM}^{-1} \text{ cm}^{-1}$) at 37°C within a 4-minute interval. Dose-inhibition curves are determined through non-linear regression analysis using the GraphPad Prism 7.0 software.

2.16 HLE-B3 cell lysates preparation for Western blotting analysis

Cellular extracts for Western blotting analysis are prepared by removing the incubation medium from the dish, rinsing cells twice with 3 ml PBS supplemented with inhibitors of proteases and phosphatases, namely NaF (10 mM), Na₄O₇P₂ (10 mM), Na₃VO₄ (2 mM), β -glycerophosphate (33 mM) and PMSF (1 mM) and lysing them by incubation for 5 minutes on ice with 400 μ l of

a lysis solution, consisting in Lysis Buffer (Cell Signaling) diluted to 1X in ultra-pure water with protease and phosphatase inhibitors (NaF (10 mM), Na₄O₇P₂ (10 mM), Na₃VO₄ (2 mM), β-glycerophosphate(33 mM), PMSF (1 mM)). Cell lysates are harvested with a scraper and transferred in Eppendorf tubes, which are again kept on ice for 10 minutes. Finally, the samples are centrifugated for 10 minutes at 14,000 x g at 4° C; the supernatant is retrieved, aliquoted and stored at -80 °C until use.

2.17 Protein quantification

The protein concentration is quantified according to Bradford colorimetric assay (Bradford, 1976) which is based on the use of Coomassie brilliant blue, a dye able to bind to primarily basic (especially arginine) and aromatic amino acid residues in a quantitative manner, resulting in its colour variation from red to blue. When the dye binds to proteins it has a maximum absorption at 595 nm. The increase of absorbance at 595 nm is proportional to the amount of bound dye, and consequently to the concentration of protein present in the sample. Mixtures (final volume 1 ml) containing 800 μl of ultra-pure water, in which the sample is diluted, and 200 μl of the Coomassie dye are vortexed and maintained for 15 minutes at room temperature. Finally, for each sample, the absorbance reading at 595 nm is performed. A calibration curve is created using varying quantities of bovine serum albumin (BSA) in order to determine protein concentration in the samples (Fig. 42).

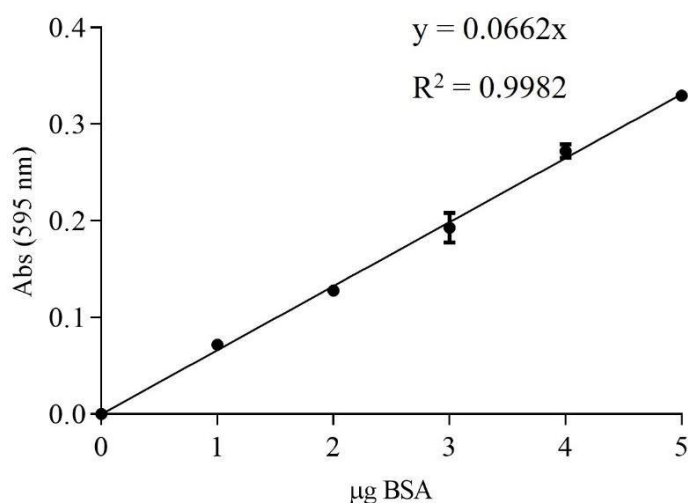


Figure 42 - Calibration curve for Bradford protein assay. The absorbance at 595 nm is plotted as functions of standard BSA quantities, expressed as micrograms of protein. Values are reported as mean ± SD for at least three measurements.

2.18 Western blotting

Protein samples undergo polyacrylamide gel electrophoresis (PAGE) using 12% denaturing SDS/polyacrylamide gels, whose thickness is 0.75 mm, according to the method introduced by Laemmli (Laemmli, 1970). The *TGX Stain-Free Fast Cast Acrylamide Kit* by Biorad is used to prepare both the resolving and the stacking gels containing a proprietary trihalo compound that is able to bind covalently the tryptophan residues in the proteins. This compound makes proteins fluorescent directly in the gel, after a short photoactivation consisting in gel exposition to UV light for 5 minutes. Protein denaturation is promoted by adding to each sample Sample Loading Buffer (250 mM Tris-HCl, pH 6.8 with 10% (w/v) SDS, 30% (v/v) glycerol, 0.05% (w/v) bromophenol blue salt) and 0.7 M β -mercaptoethanol and by heating the mixture at 70°C for 10 minutes. The amount of proteins loaded is 25 μ g. Protein separation occurs under constant voltage (200 V) in a running buffer at pH 8.8 containing 25 mM Tris, 192 mM glycine and 1% SDS. Once electrophoresis is over, the resolving gel is thoroughly washed with ultra-pure water and then exposed to UV light for 5 minutes in Chemidoc camera (Bio-Rad), to allow its activation. The result of this process is an image where all proteins in the gel can be visualized (Fig. 43).

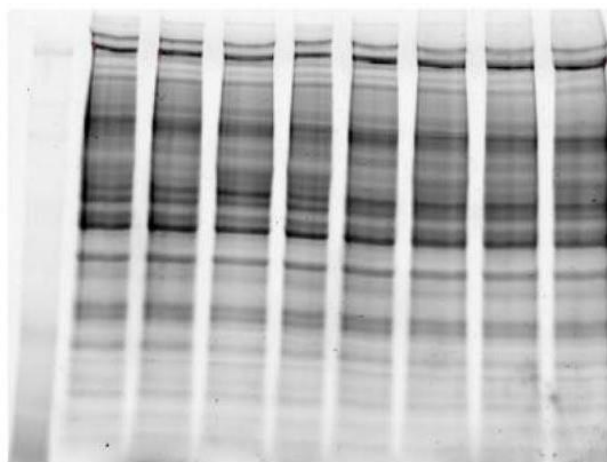


Figure 43 – Example of Biorad Stain free technology acquisition of gel.

Then, separated proteins are transferred from the gel to a 0.2 μ m PVDF membrane using *precast Trans-Blot Turbo Transfer Pack Midi* kit (Biorad). This procedure is carried out in 6 minutes, under constant current of 1.3 A and fixed voltage maximum of 25 V through the Trans-Blot Turbo Transfer System by Biorad. Thanks to the Stain Free method, the proper transfer of

proteins to the membrane for all lanes is verified (Fig. 44).

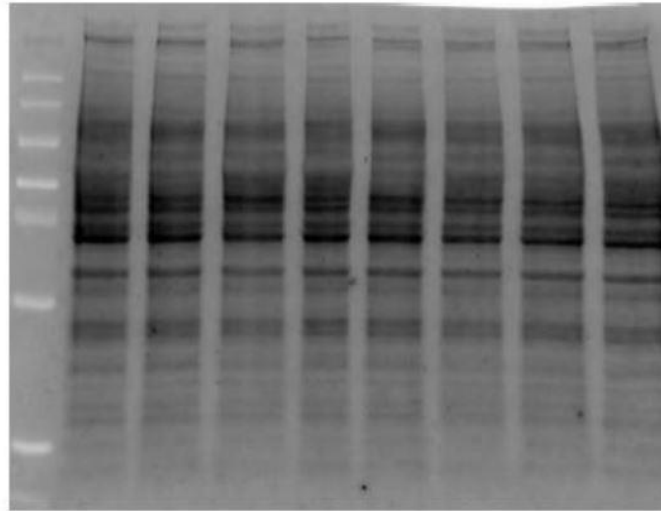


Figure 44 – Example of Biorad Stain free technology acquisition of membrane.

Subsequently, the membrane undergoes three-5minute washes with TBST (50 mM pH 7.5 Tris-HCl; 150 mM NaCl with 0.1% (v/v) Tween[®] 20 detergent). Then, it is blocked with 5% (w/v) milk powder in TBST for 1 hour at room temperature to prevent the non-specific binding of the primary antibody. After washing the membrane for 5 minutes with TBST three times, it is incubated overnight at 4°C with the primary antibody specific for COX-2 diluted 1:1000 in 5% (w/v) milk powder in TBST. The next day, the primary antibody is removed, the membrane is washed three times with TBST for 5 minutes and incubated with HRP-linked secondary antibody anti-rabbit diluted 1:1000 in 5% (w/v) milk powder in TBST for 1 h at room temperature. Afterwards, the membrane undergoes three- 5minute washes with TBST followed by two-5minute washes with TBS 1X. Immunoreactive bands are then detected using the *ImmobilonTM Western Chemiluminescent HRP* substrate consisting in luminol that is oxidized by horseradish peroxidase in the presence of hydrogen peroxide, thus generating energy released in the form of light. The ChemiDoc charge-coupled device captures this luminescent signal providing images that are acquired in a time interval between 30 and 600 seconds. Eventually, densitometry measurements were calculated using the Bio-Rad Image Lab software. The band intensity of COX-2 is normalized to total protein that can be measured directly on the image previously acquired through the *Stain free* technology. Western blotting data are reported in terms of fold change that is calculated by dividing the normalized signal intensity of the COX-2 band in each sample by the normalized intensity of the COX-2 band in the t_0 sample obtained

by cells that were harvested before starting treatment. The resulting ratios are used to compare relative COX-2 protein levels between treated and control samples.

2.19 Evaluation of NF- κ B activation through a stably transfected HLE-B3 cell line

The activation of the transcription factor NF- κ B in response to different pro-inflammatory stimuli is investigated through a specific cell model system, consisting of HLE-B3 cells stably transfected with pGL4.32[luc2P/NF- κ B-RE/Hygro] plasmid (HLE-B3_F cells) (Fig. 45). This vector contains the hygromycin resistance gene and five copies of the NF- κ B response element (NF- κ B-RE), which, consequently to NF- κ B binding, regulates the transcription of *luc2P* reporter gene encoding the luciferase of *Photinus pyralis*. In addition, in order to perform selection and amplification in XL-1 *E.coli* line, the plasmid contains ampicillin resistance gene.

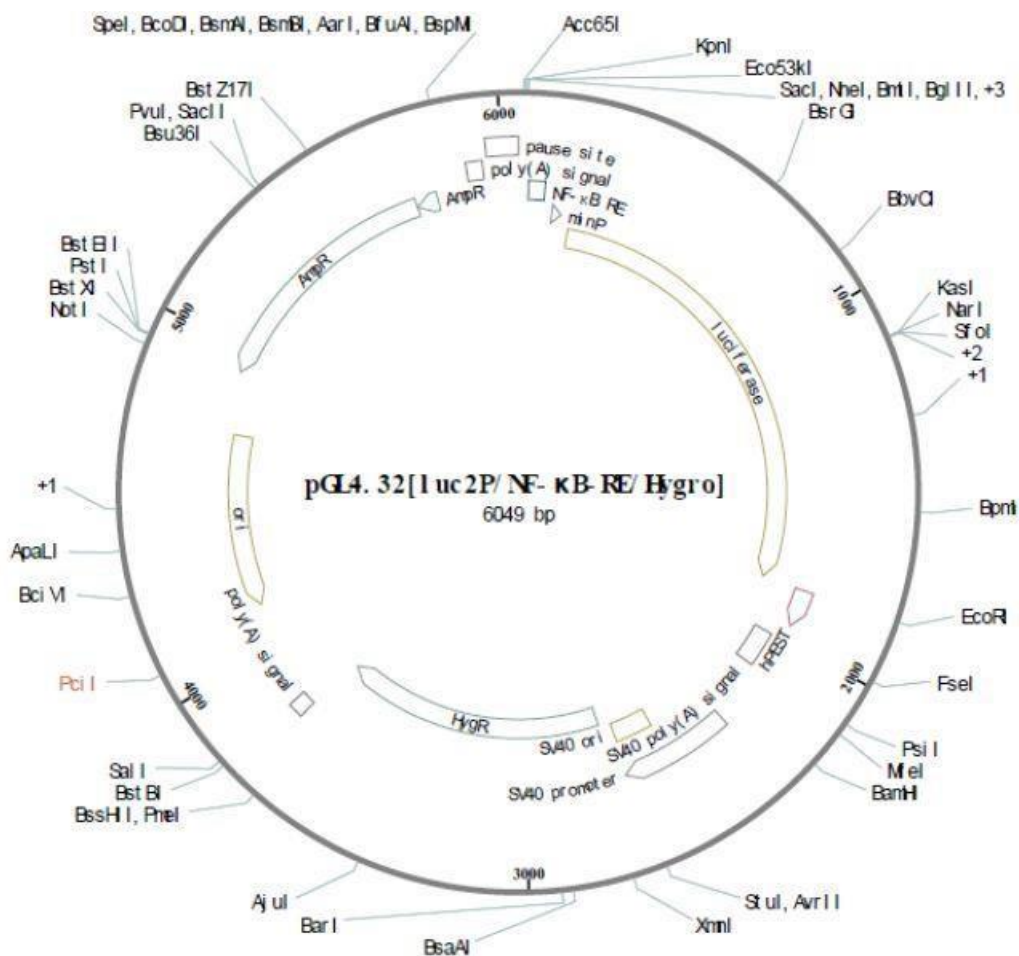


Figure 45 – pGL4.32[luc2P/ NF- κ B-RE/Hygro] plasmid map. The plasmid contains 5 copies of NF- κ B responsive element (NF- κ B-RE), ampicillin resistance gene and hygromycin resistance gene for mammalian

cell selection.

2.20 Empty control vector preparation

The pGL4.32[*luc2P*/NF- κ B-RE/Hygro] vector is incubated with specific restriction enzymes in order to remove the *Firefly* luciferase gene from the plasmid. The digested vector is loaded on an 0.8% agarose gel, prepared in 0.04 M tris acetate buffer supplemented with 1mM EDTA (TAE Buffer), and then run at 90 V using as a running buffer the TAE Buffer with 2 mg/ml ethidium bromide. The band in the agarose gel containing the empty plasmid is extracted using the QIAEX II® Gel Extraction Kit. The obtained linear plasmid is then ligated using the T4 DNA ligase and the T4 DNA Ligase buffer. This empty vector is used for the transfection of control cells to verify the absence of any luminescent signal in cells treated with pro-inflammatory stimuli and incubated under the same experimental conditions as HLE-B3_F cells.

2.21 Amplification of *pFireflyLuc2P* and empty vector in *XL-1* cells

E. coli XL-1 cells are thawed on ice and then separately incubated with 50 ng of *pFireflyLuc2P* and empty plasmid, respectively. Afterwards, cells are left on ice for 1 hour, then incubated at 42°C for 1 minute and finally for 5 minutes on ice. 300 μ l of Luria-Bertani (LB) medium (10 g/l tryptone, 5 g/l yeast extract and 10 g/l NaCl) are added, followed by incubation of cells at 37°C for 1 hour. After spinning cells down quickly, 200 μ l of LB are removed and the cells are gently resuspended in the residual LB medium. 50 μ l and 100 μ l of the cell suspension are transferred into plates containing 15 ml of LB supplemented with 100 μ g/ml ampicillin and 15 g/l agar and incubated overnight at 37°C. Isolated colonies are collected and added to 10 ml of LB containing 100 μ g/ml ampicillin. The tubes are left overnight at 37°C under agitation. Then 850 μ l of cell culture are supplemented with 150 μ l of glycerol to create a glycerol stock of transformed cells and stored at -80°C. The residual suspension is centrifuged at 5000 \times g at 4°C. The pellet is used to purify the plasmids using the miniprep kit EuroGOLD Plasmid Miniprep Kit I. The final concentration of the plasmids is evaluated using the absorbance at 260 nm, taking into account that a 50 μ g DNA/ml solution has an absorbance of 1.0 at 260 nm. The ratio of Abs₂₆₀/Abs₂₈₀ is measured; values higher than 1.8 indicates plasmids purity > 90%.

2.22 Stable transfection of *HLE-B3* cell line

3×10^5 HLE-B3 cells are plated in 35 mm dishes in complete medium (2 ml) and incubated for 24 hours at 37°C in a humidified 5% CO₂ atmosphere. The next day, the medium is removed and two washes with 1 ml MEM containing 10% FBS, 1% penicillin/streptomycin and 1% glutamine are performed, leaving the cells in 1 ml of the same medium. The cells are then transfected using the FuGENE® HD Transfection Reagent (in a 3:1 (v/v) ratio with respect to plasmid) and 2 µg of pFireflyLuc2P plasmid or 2 µg of the empty control vector. As a control HLE-B3 cells are incubated with FuGENE only. The following day 1 ml of fresh MEM medium, supplemented with 10% (v/v) FBS, 1% P/S and 1% (v/v) L-glutamine, is added so that each plate can reach 2 ml of total volume. 24 hours later cells are detached using 0.5 ml of a 0.05% trypsin/0.02% EDTA solution, transferred into 25 cm² flasks (T25), and incubated overnight at 37°C in a humidified 5% CO₂ atmosphere. Then the medium is replaced with MEM containing 20% FBS, 1% penicillin/streptomycin, 1% glutamine and 100 µg/ml hygromycin (complete medium) and, by virtue of the hygromycin resistance gene contained by the vectors, the selection of transfected cells occurs. Under these conditions, the cells are maintained in culture for about 30 days to let them replicate, thus becoming numerous enough to be stored at the concentration of 1×10^6 cells/ml within cryovials, that contain complete medium and 5% (v/v) DMSO, in liquid nitrogen, until further use. Except for the maintenance of 100 µg/ml hygromycin in the cell medium, cell culture conditions as well as cell preparation for experimental procedures are the same as described for not transfected HLE-B3 cell line in paragraphs 2.1 and 2.2.

2.23 Pro-inflammatory treatment of stably transfected HLE-B3 cells

Stably transfected HLE-B3 cells are seeded at 20,000 cells/cm² density in complete medium in 12- plate wells. After 72 hours complete medium is replaced with media characterized by different composition depending on the inflammatory stimulus used.

2.23.1 TNF- α treatment

Complete medium is replaced with MEM containing 0.5% (v/v) FBS, 2 mM L-glutamine, 50 µg/ml gentamycin and 100 µg/ml hygromycin. The following day cells are incubated with 0.2 nM TNF- α or, as control, 0.35 µg/ml human serum albumin (HSA) for 24 hours and then harvested.

2.23.2 4-HNE treatment

Complete medium is replaced with MEM containing 0.5% (v/v) FBS, 2 mM L-glutamine, 50 µg/ml gentamycin and 100 µg/ml hygromycin. After 24 hours, 30 µM or 40 µM 4-HNE is added to serum-free MEM supplemented with 2 mM L-glutamine, 50 µg/ml gentamycin and 100 µg/ml hygromycin and cells are harvested after 3, 6 or 24 hours of incubation. Stably transfected HLE-B3 cells incubated under the same conditions in the absence of 4-HNE are used as control.

2.23.3 D-glucose treatment

Complete medium is replaced with MEM containing 0.5% (v/v) FBS, 2 mM L-glutamine, 50 µg/ml gentamycin and 100 µg/ml hygromycin or glucose-deprived DMEM supplemented with 10% (v/v) FBS, 2 mM L-glutamine, 1% (v/v) P/S and 100 µg/ml hygromycin. The following day, fixed concentrations of D-glucose (20 and 75 mM in MEM containing 0.5% (v/v) FBS, 2 mM L-glutamine, 50 µg/ml gentamycin and 100 µg/ml hygromycin; 5, 25 and 50 mM in DMEM containing 10% (v/v) FBS, 2 mM L-glutamine, 1% (v/v) P/S and 100 µg/ml hygromycin) are added to the medium and cells are harvested after different times of incubation, as it will be deeply described in the Results section. If not differently specified, stably transfected HLE-B3 cells incubated under euglycaemic conditions are used as control. In addition, as previously described for HLE-B3 cells treatment with 4-HNE, the effect of sorbinil on D-glucose-induced NF-κB activation is assessed by pre-incubating stably transfected HLE-B3 cells for 24 hours with the inhibitor, before adding D-glucose. Cells are then harvested at different time points depending on the experimental condition adopted, as reported in the Results section.

2.24 Preparation of stably transfected HLE-B3 crude extracts for Firefly luciferase assay

According to the protocol provided by vector and transfection reagents manufacturer (Promega, Technical Bulletin 281 Revised 8/15), after treatment with different pro-inflammatory stimuli, the incubation medium is removed, and cells are rinsed with 1 ml PBS. Subsequently, 250 µl of Passive Lysis Buffer, previously diluted in ultra-pure water 1:5, are added to each well. Then, cells are incubated under agitation for 15 minutes at room temperature to enable cell lysis. The lysates are then collected into eppendorf tubes, and centrifugated at 14.000 x g for 30 seconds at 4 °C. Thus, the supernatant is retrieved, aliquoted and stored at -80°C, until further use.

2.25 Quantification of the Firefly luciferase expression

The activation of NF- κ B is evaluated by measuring the expression of the *Firefly* luciferase reporter gene which results in a luminescent signal detectable through a luminometer. In fact, the luciferase assay is based on the enzymatic activity of *Firefly* luciferase, which, in presence of O₂ and Mg²⁺, catalyses ATP-dependent D-luciferin oxidation to oxyluciferin, producing light emission centered at 560 nm (Fig. 46) (Promega, Technical Bulletin 281 Revised 8/15). The light emitted from this oxidation is directly proportional to the number of luciferase enzyme molecules, thus to the expression of the gene sequence in tandem with the reporter one.

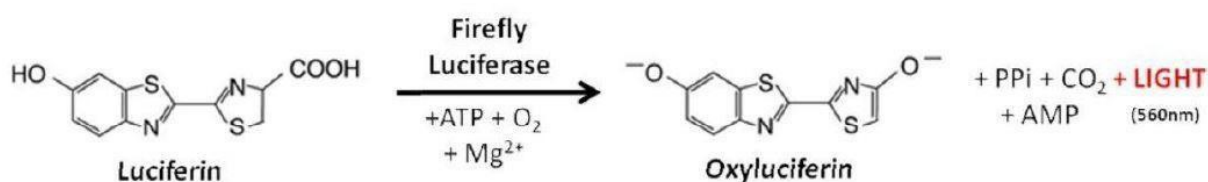


Figure 46 – Luciferin oxidation to oxyluciferin catalyzed by Firefly luciferase.

In particular, the quantification is expressed as the number of luciferase moles, that are measured at the luminometer, normalized to micrograms of total protein present in the sample, which is evaluated following Bradford's method. Thanks to this procedure, it is possible to compare the control samples with the treated ones, considering the differences in luciferase expression, whose increase is proportional to the enhancement of NF- κ B activation. In order to perform bioluminescent *Firefly* luciferase assay, 20 μ l of the cell lysates, that were obtained following the protocol described in the paragraph above, are equilibrated at room temperature and then transferred into a 96-well plate. The luminometer device is calibrated so that it injects 100 μ l of *Firefly* luciferase substrate into each well and soon after detects the subsequent luminescent signal from the sample (10 second injection and 2 second pre-measurement delay). The assay is performed at 37 °C and the gain of the photomultiplier tube is equal to 3600. The moles of luciferase are then calculated referring to a standard curve (Fig.47), that was obtained by using different quantities, in the mole range between 10⁻¹⁵ and 10⁻¹⁹, of a commercially available *Firefly* luciferase (QuantiL μ M® Recombinant Luciferase) and linking luminescence Log₁₀ with the negative Log₁₀ of the corresponding luciferase moles. Every value resulted from the analysis of three independent measurements. As expected, stably transfected HLE- B3 cells with the empty vector, do not exhibit any luminescent signal under pro-inflammatory stimulation.

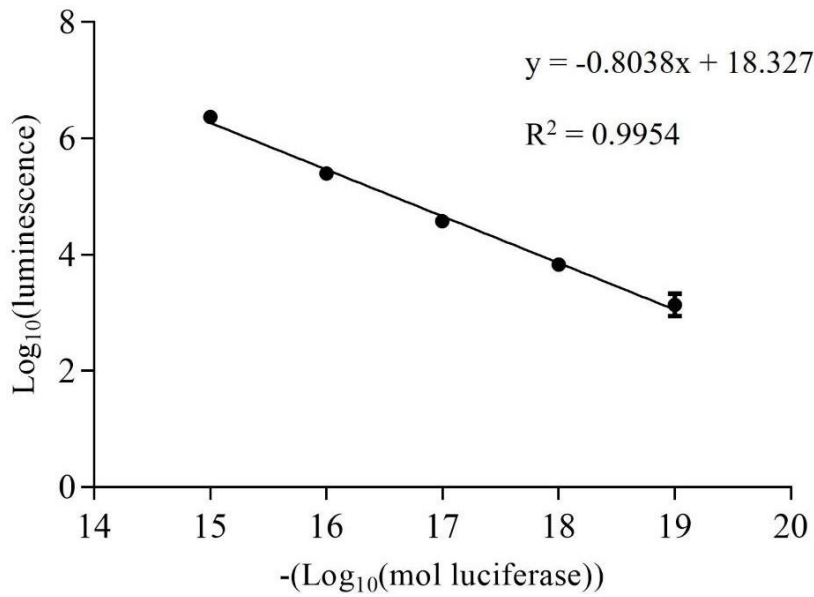


Figure 47 – Luciferase calibration curve for the quantification of moles of luciferase expressed. Data are reported as the mean \pm standard deviation (SD) of at least three measurements.

2.26 Statistical analysis

Data are expressed, if not otherwise specified, as mean \pm SEM and are the result of at least three independent experiments. Western blot data are analysed using R project software through two random effects linear regression model. Differences among groups are assessed through one-way Anova followed by Tukey post hoc test. Statistical analysis of other data is performed using GraphPad InStat 7.0 software through Student's t-test or one-way Anova with a Tukey or Dunnett post hoc test. Differences with $p \leq 0.05$ are considered statistically significant.

RESULTS

1. Optimization of experimental conditions for the treatment of HLE-B3 cells with 4-HNE

The ocular lens is a potential target of reactive oxygen species produced as by-products of cellular metabolism or photochemical reactions. In fact, constant exposure to high levels of irradiation provides a perfect environment for the generation in the ocular tissues of ROS that, in turn, are responsible for origination of lipid peroxidation products. Detection of arachidonic acid metabolites in the lens is associated with the presence of polyunsaturated fatty acids whose distribution, nevertheless, is not uniform throughout the lens (Borchman et al., 1995). Literature data report that in the lens epithelium there are at least 15 to 20 times more unsaturated lipids per milligram protein than in cortex and nucleus. Thus, human lens epithelial cells are particularly prone to generate under oxidative stress conditions reactive α,β -unsaturated aldehydes, such as 4-HNE, that have been shown to mediate oxidative stress-induced cell death leading to cataractogenesis (Choudhary et al., 2002). Because of their cytotoxicity, human lens epithelial cells should have appropriate detoxification mechanisms to metabolize such aldehydes, the major of which was reported to be the conjugation with GSH (Choudhary et al., 2003). However, as previously discussed, 4-HNE glutathionylated derivatives are reported to be the active molecules in mediating 4-HNE-induced inflammatory signalling via activation of PKC, MAPK and NF- κ B in different cell types (Yadav et al., 2010; Ramana and Srivastava, 2010). Human lens epithelial cells can therefore represent an ideal *in vitro* cell line model to investigate the metabolic pathways through which 4-HNE is detoxified that could be involved in the NF- κ B-mediated inflammatory response.

Some preliminary experiments have been performed in order to define the most appropriate

conditions for evaluating the pro-inflammatory effect of 4-HNE on HLE-B3 cells. This was relevant because it could be possible that some components of the cell culture medium were able to react with 4-HNE, thus preventing it to enter cells and consequently interfering with 4-HNE-triggered signal transduction pathways. Three different experimental conditions, corresponding to medium supplemented with 0.5% FBS (condition **A**), serum-free medium (condition **B**) or Krebs-Hanseleit bicarbonate buffer solution (condition **C**), have been considered. For each condition, HLE-B3 cell viability was first determined through the MTT assay obtaining different results. In fact, no significant reduction of cell viability was observed by incubating cells both under condition **A** and **B** for up to 8 hours (Fig. 48, panel A), while, in contrast, it significantly decreased after only 1 hour of incubation under condition **C** (Fig. 48, panel B).

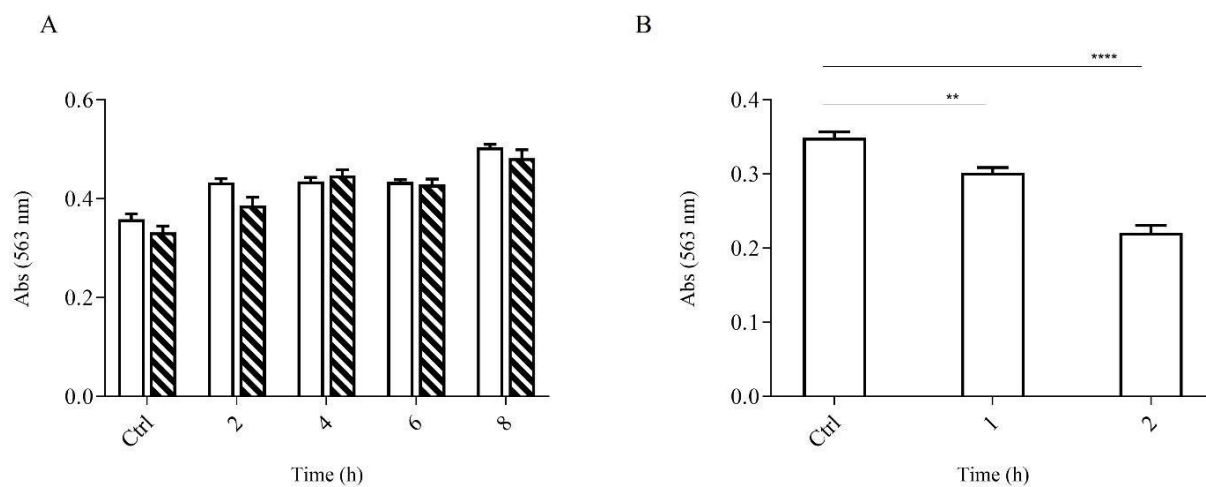


Figure 48 – MTT assay in HLE-B3 cells under three different experimental conditions. Panel A: cell viability was evaluated by MTT assay as described in Materials and methods section after incubating cells for the time indicated under condition A (solid bars) or condition B (hatched bars). Panel B: cells were incubated under condition C for the time indicated. In both panels Ctrl refers to MTT assay conducted on HLE-B3 cells before starting the treatment. Results are expressed as mean \pm SEM of at least six independent biological samples. Significance was evaluated with respect to control cells through one-way Anova followed by Tukey post hoc test (** $p \leq 0.01$, **** $p \leq 0.001$).

Furthermore, the ability of HLE-B3 cells to remove 4-HNE from the incubation medium was compared under the three different conditions (A, B and C) by treating cells with 30 μ M 4-HNE and measuring at different time of incubation the residual concentration of the aldehyde through a colorimetric assay as described in the Material and methods section. As reported in Figure 49, the rate of 4-HNE consumption under all the conditions applied was comparable, observing 20% of residual 4-HNE after 120 minutes of incubation.

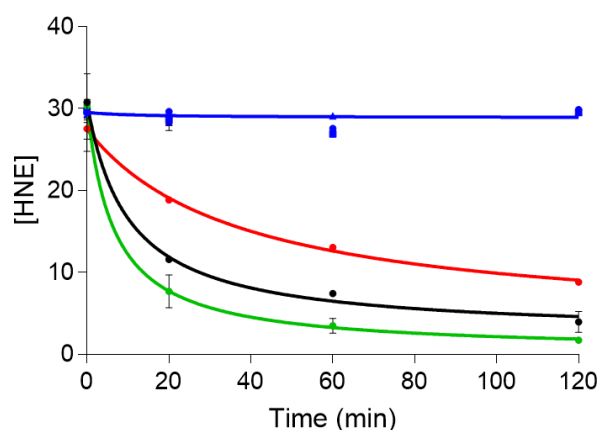


Figure 49 – Evaluation of 4-HNE residual concentration in different media. Residual concentration of 4-HNE under condition A (green line), condition B (black line) and condition C (red line) is plotted as a function of time. No removal of 4-HNE was observed in incubation media alone (blu circles, squares and triangles).

Finally, the pro-inflammatory effect of 4-HNE was evaluated in terms of increase in COX-2 expression that was detected by Western blotting analysis. HLE-B3 cells were incubated under condition **A** and **B** for 6 hours and under condition **C** for 2 hours followed by 4 hours in serum-free medium. The results evidenced a significant increase in COX-2 expression induced by 30 μ M 4-HNE in respect to control cells under all the conditions applied and also a significant difference in COX-2 protein levels by comparing fold change observed in condition **B** and **C** with that observed in condition **A**, that is assumed as a reference (Fig. 50). Thus, incubation of HLE-B3 cells in serum- deprived medium could represent the optimal experimental condition for investigating the pro- inflammatory effect of 4-HNE because it did not affect cell viability nor 4-HNE consumption and seems to be a good condition for observing the cellular inflammatory response induced by 4-HNE.

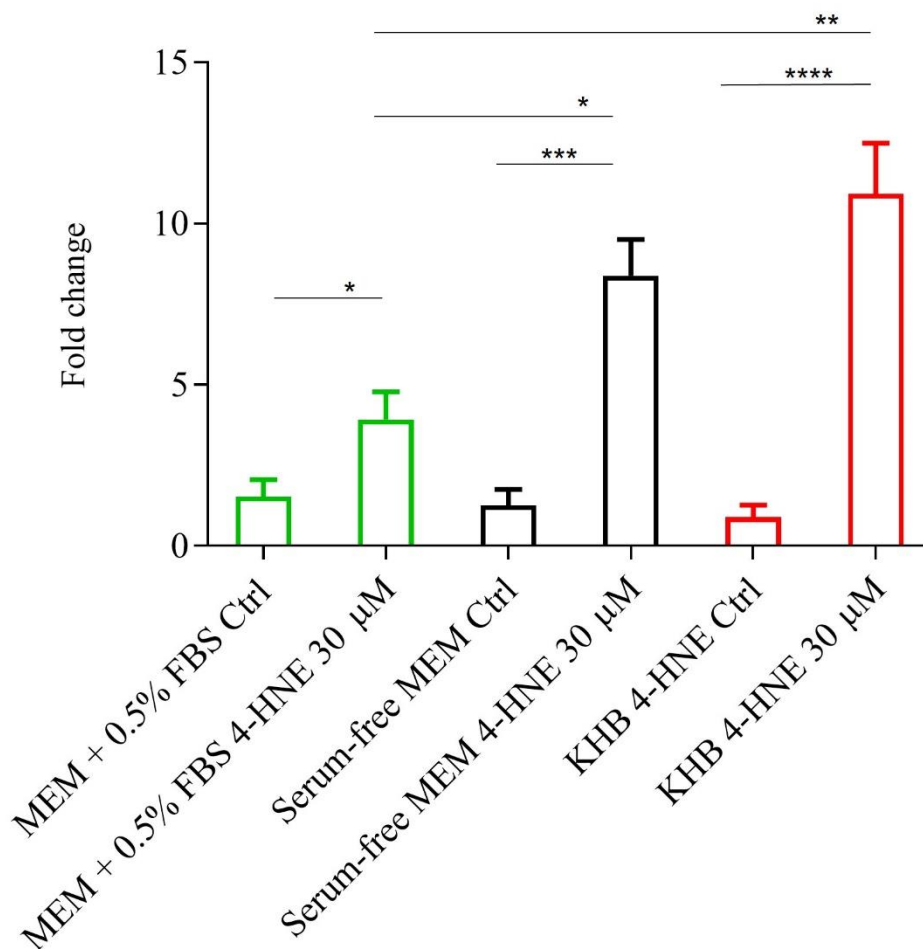


Figure 50 – Effect of different experimental conditions on 4-HNE-induced COX-2 expression. Fold increase in COX-2 protein levels in cells treated with 30 μ M 4-HNE with respect to untreated cells under the three different experimental conditions adopted. Results are expressed as mean \pm SEM of at least three independent experiments. Significance was evaluated in respect to condition A through one-way Anova followed by Tukey post hoc test (* $p \leq 0.05$ ** $p \leq 0.01$).

2. Inflammatory effect of 4-HNE in HLE-B3 cells

2.1 Time- and dose-dependent effect of 4-HNE

As previously described, literature data report that 4-HNE exerts hormetic effects on signalling in different cell types. Indeed, at low physiological levels (up to 10 μM), 4-HNE has been shown to induce cell proliferation activating pro-proliferative kinases, DNA and protein synthesis (Zarkovic et al., 1993) while at high concentrations (100 μM) it inhibits pro-proliferative mechanisms leading to apoptotic or necrotic cell death (Ruef et al., 2001). For this reason, the dose- and time-dependent effect of 4-HNE was evaluated on both cell viability and inflammatory process.

HLE-B3 cells were incubated with increasing concentrations of 4-HNE up to 50 μM in serum-free medium supplemented with 2 mM L-glutamine and 50 $\mu\text{g/ml}$ gentamycin and the number of viable cells was assessed after 6 and 24 hours of incubation by both MTT and crystal violet assay as described in Materials and methods section. The results reported in Figure 51 (panels A and B) evidenced a significant reduction of cell viability only at the highest concentrations tested, corresponding to 40 μM and 50 μM , after 24 hours of incubation. Treatment with 4-HNE for 6 hours, in contrast, did not significantly affect mitochondrial function nor cell viability, except for the concentration of 50 μM .

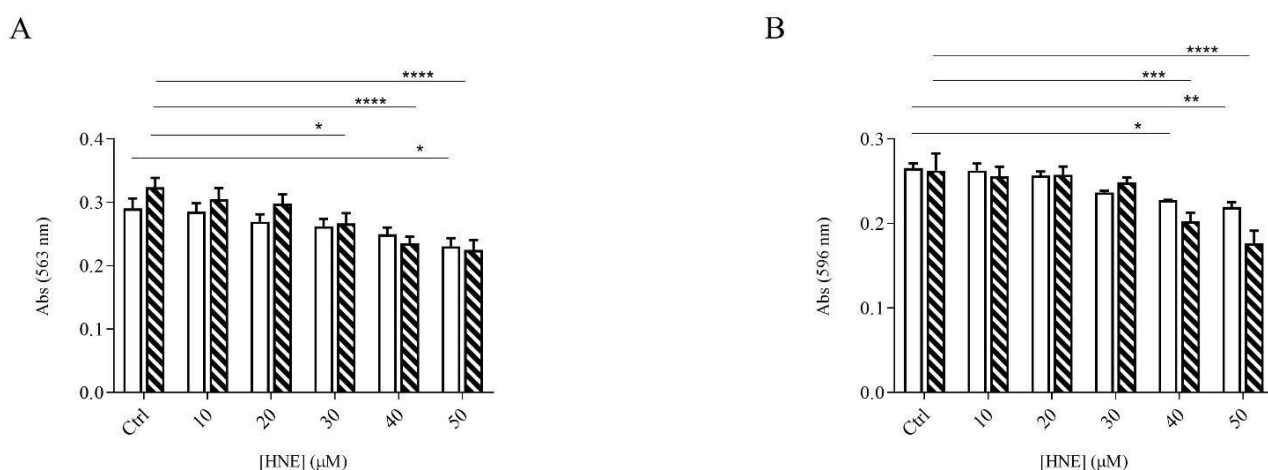


Figure 51 – Cell viability of HLE-B3 incubated with different 4-HNE concentrations. The figure reports MTT (panel A) and crystal violet (panel B) assay after incubating cells for 6 (solid bars) or 24 (hatched bars) hours with increasing 4-HNE concentrations. Results are expressed as mean \pm SEM of at least six independent biological samples. Significance was evaluated with respect to control cells incubated for the same time in the absence of the aldehyde. Statistical analysis was performed through one-way Anova followed by Dunnett post hoc test (* $p \leq 0.05$ ** $p \leq 0.01$ *** $p \leq 0.001$ **** $p \leq 0.0001$).

Furthermore, incubation of HLE-B3 cells with 30 μ M 4-HNE for different times up to 24 hours induced a significant increase in COX-2 expression after 2 hours, observing a maximum in the protein expression after 6 hours of exposure to 4-HNE and a subsequent decrease of protein level at longer incubations timing (Fig. 52). This result confirms a time dependence of COX-2 expression induced by 4-HNE in HLE-B3 cells, as reported for different cell types (Kumagai et al., 2015). Finally, in order to determine the range of 4-HNE concentration able to induce a significant inflammatory response, cells were exposed to different concentrations of the aldehyde (2-40 μ M), measuring after 6 hours through Western blotting analysis the increase in COX-2 protein levels in respect to control cells (Fig. 53).

Taking into account these results, 30 μ M and 40 μ M were chosen as 4-HNE concentrations for performing all the subsequent experiments because they were the concentrations of aldehyde able to trigger a significant inflammatory response in terms of COX-2 expression with a low effect on cell viability.

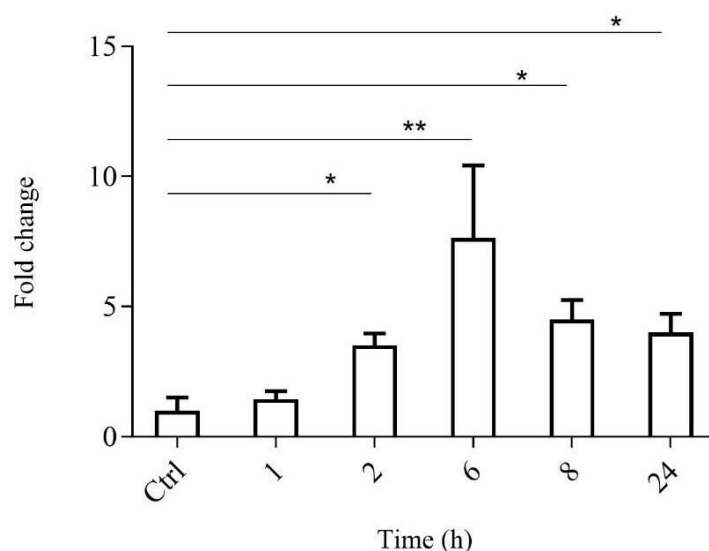


Figure 52 – Time-dependent effect of 4-HNE on the induction of COX-2 expression. HLE-B3 cells were incubated with 30 μ M 4-HNE for 1, 2, 6, 8 or 24 hours. Results are expressed as mean \pm SEM of at least three independent experiments. Significance was evaluated with respect to control cells incubated for 24 hours in the absence of the aldehyde. Statistical analysis was performed through one-way Anova followed by Tukey post hoc test (* $p \leq 0.05$ ** $p \leq 0.01$).

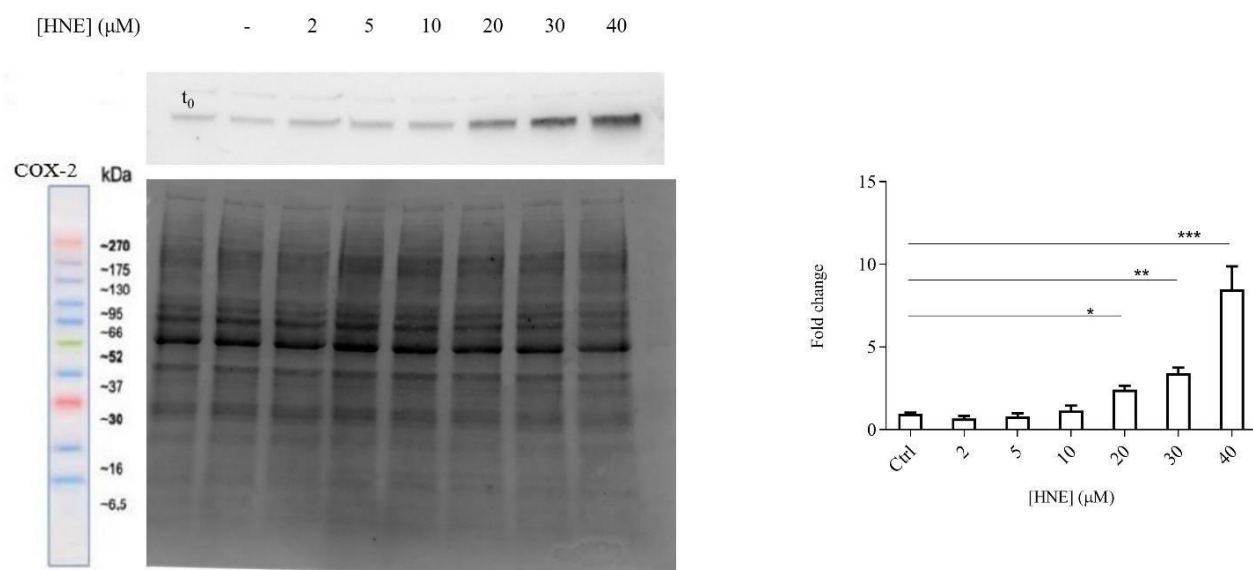


Figure 53 – Dose-dependent effect of 4-HNE on the induction of COX-2 expression. HLE-B3 cells were incubated with different concentrations of 4-HNE ranging from 2 μ M to 40 μ M. Results are expressed as mean \pm SEM of at least three independent experiments. Significance was evaluated with respect to control cells incubated for 6 hours in the absence of the aldehyde. Statistical analysis was performed through one-way Anova followed by Tukey post hoc test (* $p \leq 0.05$ ** $p \leq 0.01$ *** $p \leq 0.001$). The figure on the left reports an example of COX-2 immunoreactive bands that are normalized to total protein using the Stain free technology, as described in Materials and methods section.

2.2 Evaluation of the inflammatory effect of 4-HNE enantiomers

4-HNE has a chiral center at carbon 4 and exists as a racemic mixture of R- and S-enantiomers. It has been reported that 4-(R)-HNE and 4-(S)-HNE can differentially interact with cellular components showing different effects in biological tissues (Dabrowski et al., 2010) suggesting that they might differentially contribute to 4-HNE-induced inflammatory response. Thus, the dose-dependent effect of 4-(R)-HNE and 4-(S)-HNE on inducing an increase in COX-2 protein levels was examined by Western blotting. The comparison between the slopes of the two trendlines reported in Figure 54 showed that both enantiomers were individually able to induce the COX-2 expression, with no significant difference in their effect on the inflammatory process. This result indicates that the ability of 4-HNE to modulate the inflammatory signalling seems to be dependent only on the concentration of the aldehyde and not on its stereochemical configuration, since the same results were obtained using the same concentrations of racemic mixture of 4-HNE (Fig. 53).

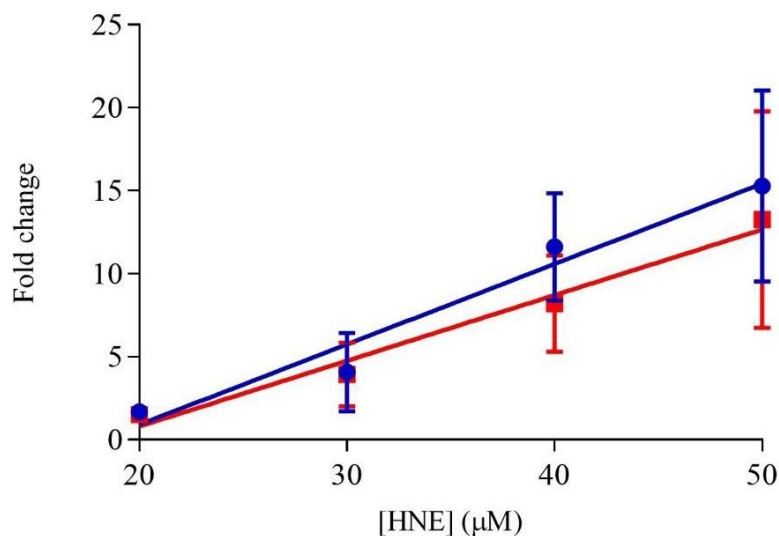


Figure 54 – Effect of 4-HNE enantiomers on COX-2 expression. In the figure is reported the fold increase of COX-2 protein levels over concentration of (R)-HNE (blue line) or (S)-HNE (red line) after 6 hours of incubation. The experimental data were interpolated using the linear regression analysis. A t-test comparing the slopes of the resulting trendlines was then performed, showing no significant differences between the slopes.

2.3 Determination of glutathione and glutathione adduct levels in HLE-B3 cells treated with 4-HNE

Literature data report that relatively high concentrations of 4-HNE induce an increase in oxidative stress with the subsequent inhibition of enzymatic antioxidant defence systems such as glutathione reductase and glutathione peroxidase activities leading to a reduction in intracellular GSH pool (Nakajima et al., 2002; Raza and John, 2006) and consequently to toxicity and apoptosis in different cell types, including human lens epithelial cells (Cheng et al., 2001; Cheng et al., 1999). It was also shown, nevertheless, that mild transient oxidative stress could induce in cultured retinal pigmented epithelial cells the increase in GST5.8 expression, a specific GST isozyme particularly abundant in human ocular tissues that catalyzes the conjugation of 4-HNE with GSH generating the GS-HNE adduct. This reaction represents one of the main cellular enzymatic detoxification pathways that acts as adaptive responses to oxidative stress (Cheng et al., 2001). For this reason, the intracellular glutathione content in HLE-B3 cells was measured performing a high-performance capillary electrophoresis analysis as described in Materials and Methods section and reported as nmol of glutathione normalized to total protein content. The intracellular glutathione levels were measured as total and reduced

glutathione and reported in Table 1. The oxidized glutathione levels, that include both GSSG and protein-glutathione mixed disulfides, were evaluated by the difference between the total glutathione and GSH values.

<i>GSH (nmol/mg protein)</i>	90 ± 14
<i>Total glutathione (nmol/mg protein)</i>	82 ± 19

Table 1 – Glutathione content in HLE-B3 cells. GSH and total glutathione levels are expressed as nmol/mg protein in HLE-B3 cells.

The comparison between GSH and total glutathione levels in HLE-B3 cells under basal conditions suggested that the cellular GSH/GSSG ratio was high, confirming the elevated antioxidant capacity of these cells.

The effect of 4-HNE treatment on glutathione levels in HLE-B3 cells was evaluated by incubating cells with 30 μ M or 40 μ M 4-HNE and harvesting them after 30 minutes, 1 hour, 3 hours or 6 hours of incubation. GSH and total glutathione levels were measured through HPCE in the corresponding ultrafiltrated samples, prepared following the protocol described in the Materials and Methods section, and in control samples obtained from untreated cells incubated for the same time under the same conditions. As shown in Figure 55, a significant decrease in both GSH and total glutathione levels was observed in HLE-B3 cells after 30 minutes and 1 hour of incubation with both concentrations of 4-HNE in respect to control cells, but the glutathione content resulted to be completely restored after 3 and 6 hours of incubation. These results suggest that the 4-HNE-induced decrease in intracellular glutathione content was due to the formation of the GS-HNE adduct. This could be also confirmed by the fact that in samples harvested at early times of incubation, namely with 30 μ M or 40 μ M 4-HNE for 30 minutes or with 40 μ M 4-HNE for 1 hour, HPCE analysis indicated the presence of a well resolved peak at the elution time of 5.3 minutes, which could correspond to GS-HNE (Fig. 56 and Fig. 57). This was also confirmed by the addition of a standard of GS-HNE to the cellular ultrafiltrate before the analysis (Fig. 58). The quantification of this intracellular metabolite in different samples were determined by referring to the calibration curve reported in Materials and Methods section (Fig. 41) and normalized to total protein content. The mean values \pm standard error were reported in Table 2. These data are consistent with those reported in a study performed by Cheng and

co-workers in a different cell line, showing that treatment of K562 cells 4-HNE induced the formation of GS-HNE with no significant oxidation of GSH (Cheng et al.,2001).

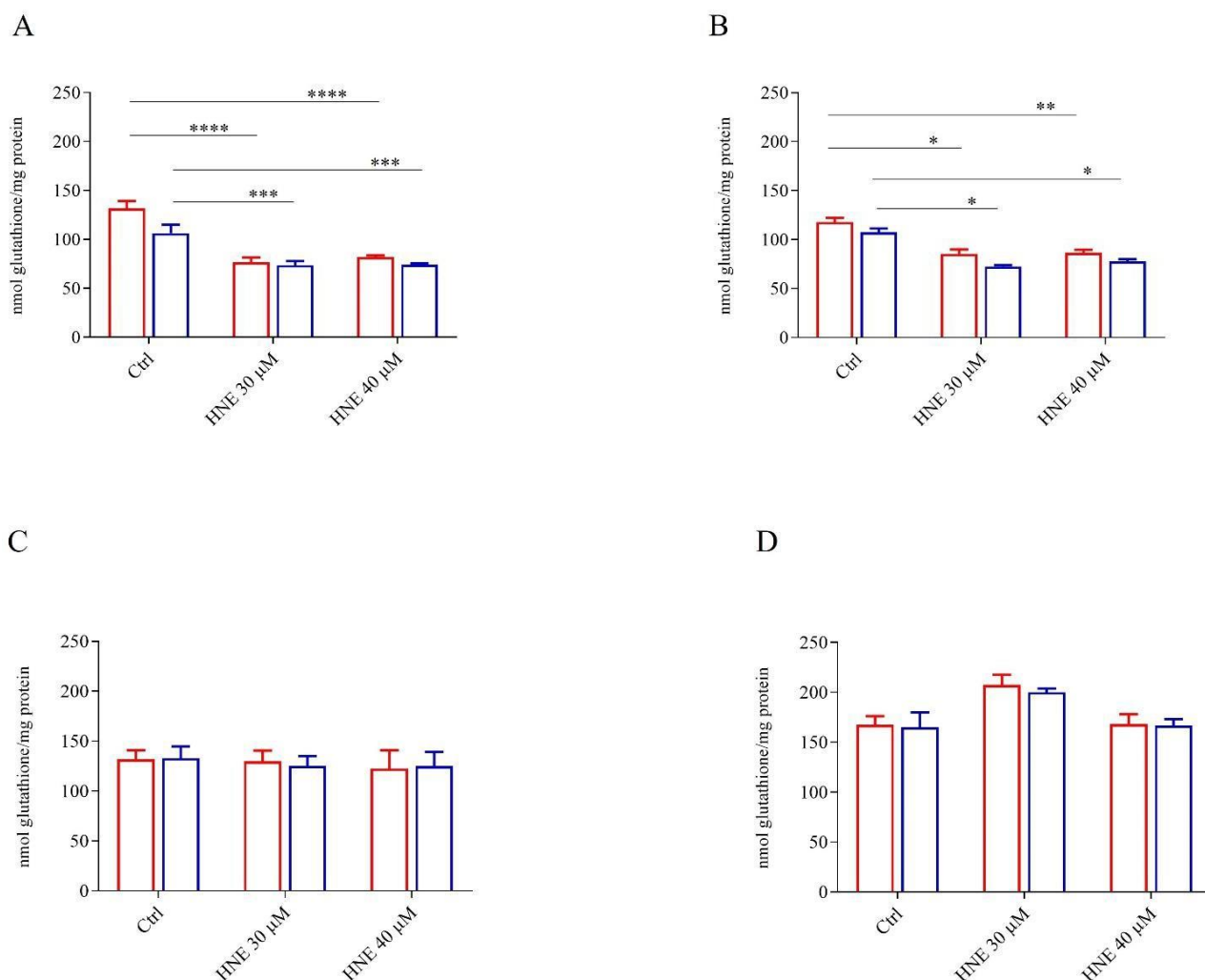


Figure 55 – Effect of 4-HNE on GSH and total glutathione intracellular content. GSH (red bars) and total glutathione (blue bars) levels were measured by HPCE analysis in ultrafiltrated crude extracts obtained as described in Materials and methods section of HLE-B3 cells incubated for 30 minutes (panel A), 1 hour (panel B), 3 hours (panel C) or 6 hours (panel D) with 30 μM or 40 μM 4-HNE. Results are expressed as mean ± SEM of at least three independent experiments. Significance was evaluated with respect to control cells incubated for different times in the absence of the aldehyde. Data groups have been compared through one-way Anova followed by Dunnett post hoc test (* $p \leq 0.05$, ** $p \leq 0.01$, *** $p \leq 0.005$, **** $p \leq 0.001$).

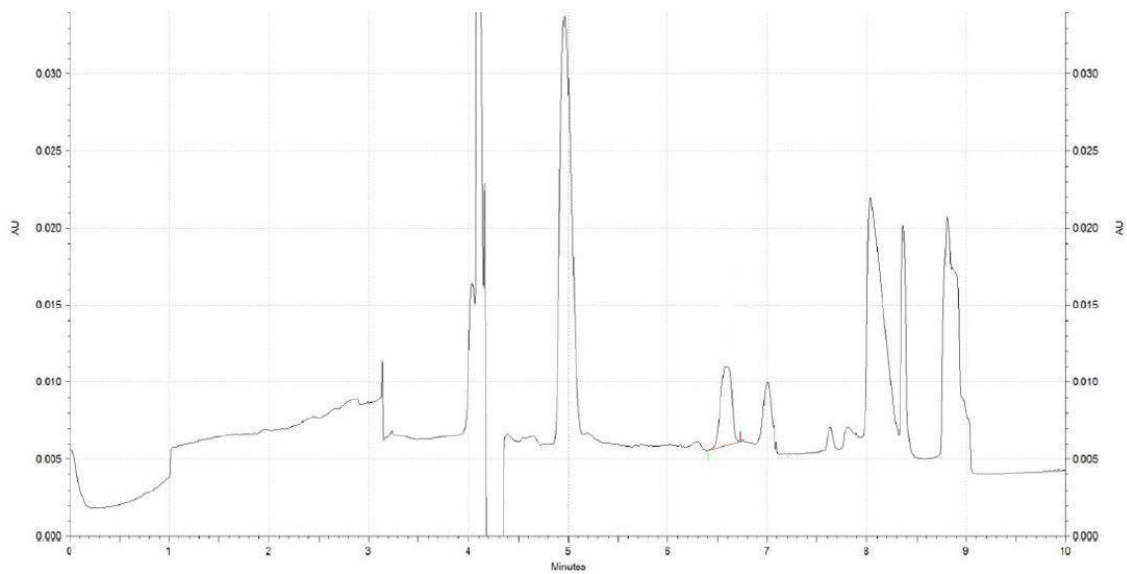


Figure 56 – Representative electropherogram of an ultrafiltrated crude extract obtained from untreated HLE-B3 cells.

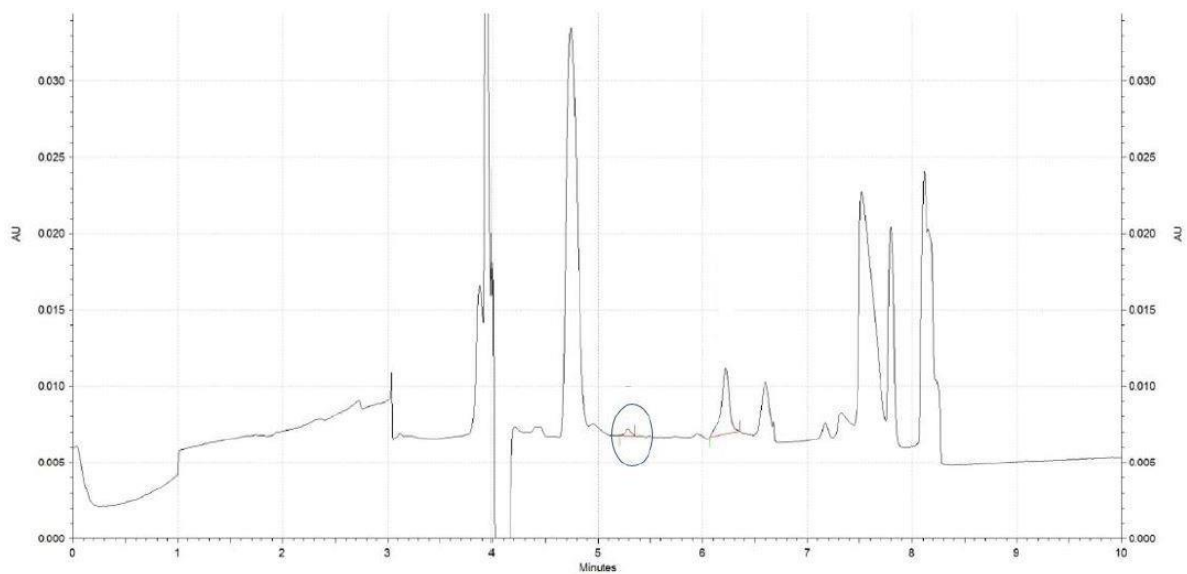


Figure 57 – Representative electropherogram of an ultrafiltrated crude extract obtained from HLE-B3 cells incubated for 30 minutes with 40 μ M 4-HNE. The blue circle indicates the peak that is associated with GS-HNE.

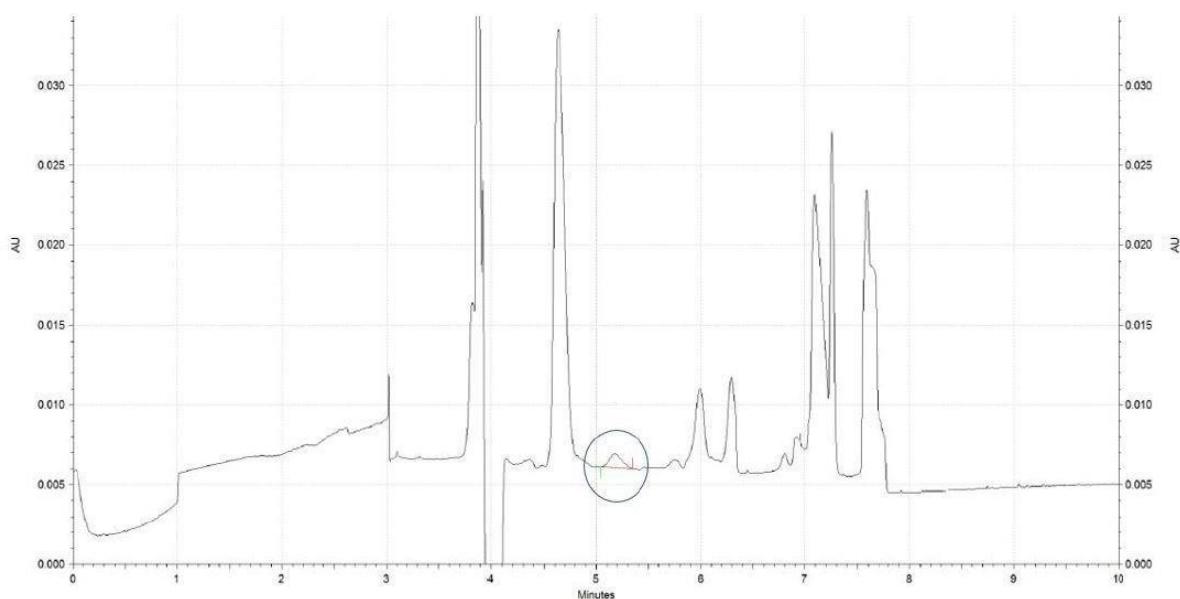


Figure 5840 – Representative electropherogram of an ultrafiltrated crude extract obtained from HLE-B3 cells to which 50 μ M GS-HNE as internal standard was added. The blue circle indicates the peak that is associated with GS-HNE.

<i>Incubation time</i>	<i>[4-HNE] (μM)</i>	<i>GSHNE (nmol/mg protein)</i>
30 minutes	30	6.1 ± 1.1
30 minutes	40	8 ± 0.8
1 hour	40	5.7 ± 2.9

Table 2 – Intracellular GS-HNE content in HLE-B3 cells incubated for different incubation times with 30 μ M or 40 μ M 4-HNE. GS-HNE levels expressed as nmol/mg protein.

2.4 Evaluation of the anti-inflammatory effect of two reductase activity inhibitors in HLE-B3 cells

4-HNE pro-inflammatory effect is assumed to be mediated also by 4-HNE metabolites produced by NADPH-dependent reductase activities, as reported in the Introduction section (Paragraph 2.5.1). For this reason, in order to clarify the role of these enzymes in the inflammatory response, the effect of the administration of two well-known NADPH-dependent reductase activity inhibitors, sorbinil and rutin, on the 4-HNE-induced increase in COX-2 expression was evaluated through Western blotting analysis as reported in Materials and

methods section. Before proceeding with 4-HNE treatment, HLE-B3 cells were pre-incubated with 100 μ M sorbinil or 100 μ M rutin for 1 hour in MEM supplemented with 0.5% FBS, 2 mM L-glutamine and 50 μ g/ml gentamycin. Afterwards, the medium was replaced with serum-deprived MEM supplemented with 2 mM L-glutamine and 50 μ g/ml gentamycin and 30 μ M or 40 μ M 4-HNE was added. HLE-B3 cells were incubated for 6 hours with the aldehyde and subsequently harvested. The anti-inflammatory effect of sorbinil or rutin was assessed using as control samples obtained by cells that were pre-incubated for 1 hour under the same conditions with only the solvent, DMSO, in which the inhibitors were dissolved at the final concentration applied (0.1% (v/v)) and, after medium replacement, cells were maintained for 6 hours with 30 μ M or 40 μ M 4-HNE.

Furthermore, only sorbinil efficacy was tested also through the simultaneous addition of the inhibitor and 4-HNE to the serum-free medium supplemented with 2 mM L-glutamine and 50 μ g/ml gentamycin, harvesting cells after 6 hours of incubation for the analysis of COX-2 expression. As control for the evaluation of the effect of the inhibitor on COX-2 expression induced by the aldehyde, cells were incubated for 6 hours with 4-HNE and 0.1% v/v DMSO.

The statistical analysis of Western blotting results confirmed, under all the conditions examined, the pro-inflammatory effect of 4-HNE that, nevertheless, was not abolished by treatment with sorbinil and with rutin either, as no statistically significant difference in COX-2 expression between inhibitor treated and control samples was observed, under all the conditions applied (Fig. 59, Fig. 60, and Fig. 61).

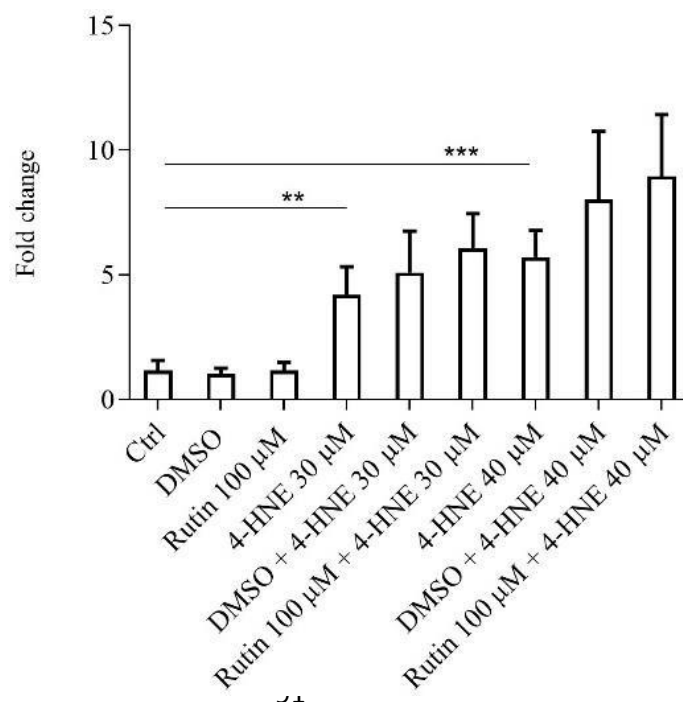


Figure 59 – Effect of 100 μ M rutin on the 4-HNE-induced inflammatory response. HLE-B3 cells were incubated for 1 hour with either rutin 100 μ M or 0.1% (v/v) DMSO in MEM supplemented with 0.5% FBS, 2 mM L-glutamine and 50 μ g/ml gentamycin and, after that the medium was replaced with serum-free MEM supplemented with 2 mM L-glutamine and 50 μ g/ml gentamycin cells were incubated with 30 μ M or 40 μ M 4-HNE for 6 hours. Results are expressed as mean \pm SEM of at least three independent experiments. Significance was evaluated with respect of control cells incubated in the absence of the aldehyde to evaluate the effect of 4-HNE or with respect to control cells incubated in the presence of 4-HNE and 0.1% (v/v) DMSO to test rutin efficacy. Statistical analysis was performed through one-way Anova followed by Tukey post hoc test (** $p \leq 0.01$ *** $p \leq 0.001$).

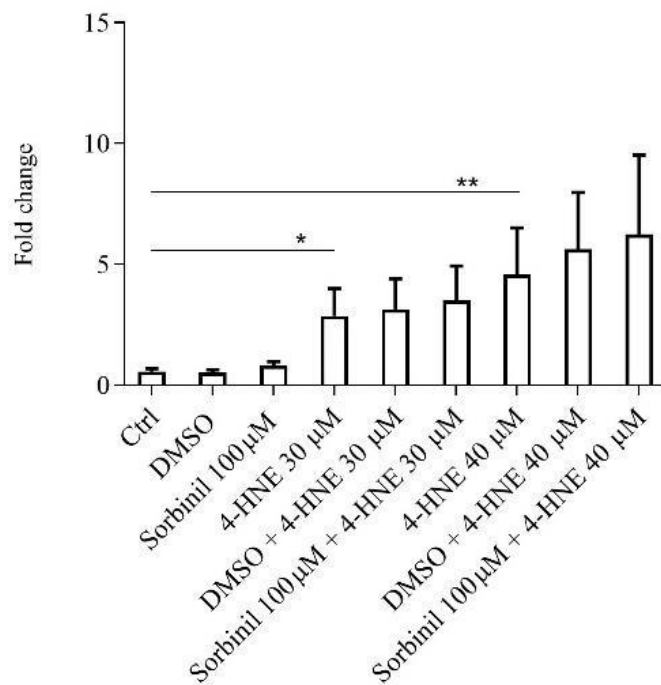


Figure 60 – Effect of 100 μ M sorbinil on the 4-HNE-induced inflammatory response. HLE-B3 cells were incubated for 1 hour with either sorbinil 100 μ M or 0.1% (v/v) DMSO in MEM supplemented with 0.5% FBS, 2 mM L-glutamine and 50 μ g/ml gentamycin and, after that the medium was replaced with serum-free MEM supplemented with 2 mM L-glutamine and 50 μ g/ml gentamycin, cells were incubated with 30 μ M or 40 μ M 4-HNE for 6 hours. Results are expressed as mean \pm SEM of measures obtained from at least three independent experiments. Significance was evaluated with respect to control cells incubated for 6 hours in the absence of the aldehyde to evaluate the effect of 4-HNE or with respect to control cells incubated with the presence of 4-HNE and 0.1% (v/v) DMSO to test sorbinil efficacy. Statistical analysis was performed through one-way Anova followed by Tukey post hoc test (* $p \leq 0.05$ ** $p \leq 0.01$).

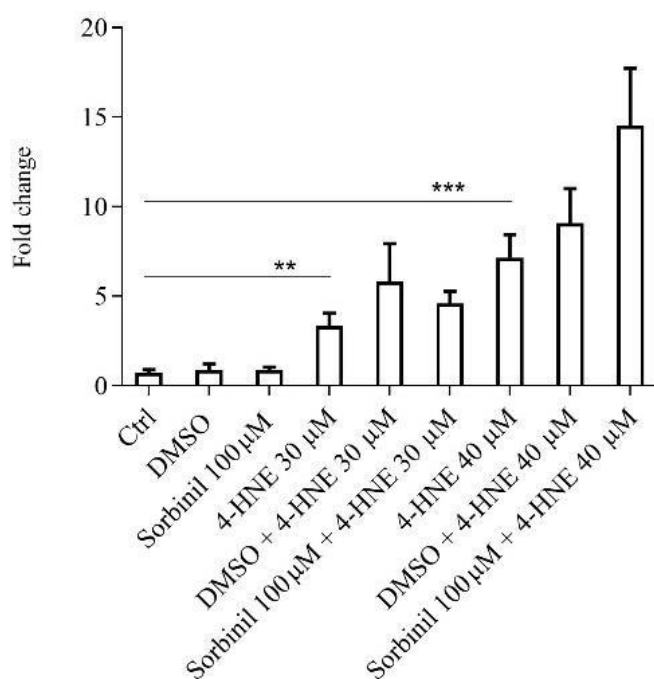


Figure 61 – Effect of 100 µM sorbinil on the 4-HNE-induced inflammatory response. HLE-B3 cells were incubated for 6 hours with either 100 µM sorbinil or 0.1% (v/v) DMSO in serum-deprived MEM supplemented with 2 mM L-glutamine and 50 µg/ml gentamycin as well as 30 µM or 40 µM 4-HNE. The results are expressed as mean ± SEM of measures on at least three independent experiments. Significance was evaluated with respect to control cells incubated for 6 hours in the absence of the aldehyde to evaluate the effect of 4-HNE or with respect to control cells incubated with the presence of 4-HNE and 0.1% (v/v) DMSO to test sorbinil efficacy. Statistical analysis was performed through one-way Anova followed by Tukey post hoc test (** p ≤ 0.01 *** p ≤ 0.001).

The results of Western blotting analysis of COX-2 protein levels revealed that neither sorbinil nor rutin were able to attenuate the 4-HNE pro-inflammatory effect. The susceptibility to sorbinil and rutin of enzymatic activities present in HLE-B3 cells and considered to mediate the inflammatory response was assessed. The efficacy of these molecules was evaluated through enzymatic assays performed with HLE-B3 crude extracts as described in the Materials and Methods section using L-idose as substrate that is known to be efficiently reduced by AKR1B1 (Balestri et al., 2015). The incubation of crude extracts with increasing concentrations of sorbinil caused an almost complete inhibition of reductase activity on L-idose (Fig. 62).

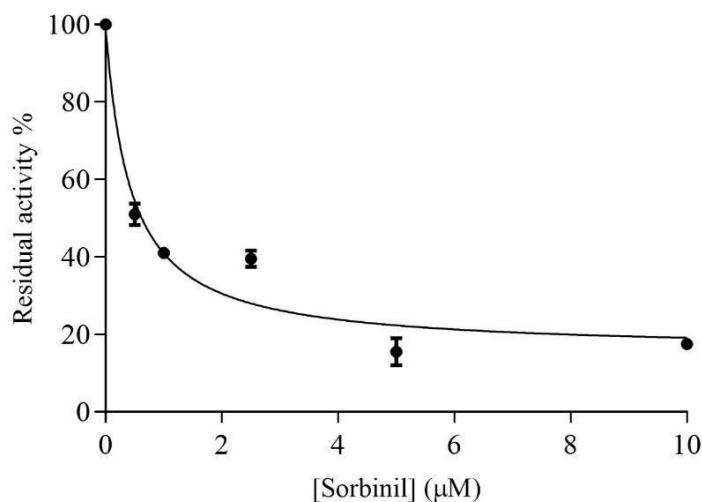


Figure 62 – Inhibitory effect of sorbinil on NADPH-dependent reductase activity of crude extracts of HLE-B3 cells. Enzymatic assays were performed in crude extracts as reported in Materials and methods section using 8 mM L-Idose as substrate. Results are reported as percentage of residual activity considering 100% the one measured in crude extracts of control cells in the presence of 0.5% (v/v) DMSO. For each concentration is reported mean \pm SD of three independent measures.

Furthermore, the effect of rutin, another inhibitor of AKR1B1, was evaluated by adding increasing concentrations of this molecule directly to the assay mixture containing 8 mM L-idose. Contrary to expectations, rutin did not exhibit a complete inhibition of reductase activity, as shown by the dose-inhibition curves reported in Figure 63.

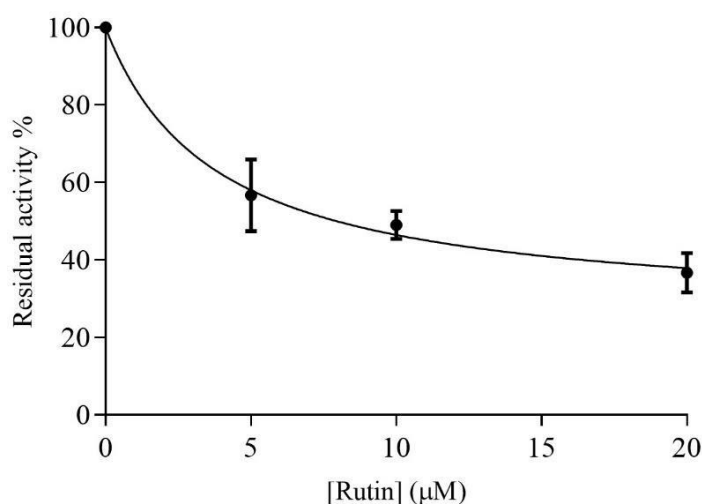


Figure 413 – Inhibitory effect of rutin on NADPH-dependent reductase activity of crude extracts of HLE-B3 cells. Enzymatic assays were performed in crude extracts as reported in Materials and methods section using 8 mM L-idose as substrate. Results are reported as percentage of residual activity considering

100% the one measured in crude extracts of control cells in the presence of 0.5% DMSO. For each concentration is reported mean \pm SD of three independent measures.

2.5 Evaluation of 4-HNE pro-inflammatory effect on stably transfected HLE-B3_F cell line

NF- κ B activation as a possible response of 4-HNE cellular treatment was evaluated in the stably transfected HLE-B3_F cell line by measuring *Firefly* luciferase expression as described in the Material and Methods section. In the same experimental conditions, the increase of COX-2 protein levels was also verified by Western blotting analysis in order to confirm the pro-inflammatory effect of 4-HNE in the HLE-B3_F cell line.

In order to assess whether HLE-B3_F cells could be effectively used as a model for evaluating NF- κ B activation, stably transfected cells were first incubated for 24 hours with 0.2 nM TNF- α , a pro-inflammatory cytokine that is a NF- κ B activator (Sartor, 1998). *Firefly* luciferase expression was quantified by referring to the standard curve reported in the Material and Methods section (Fig. 47) and expressed as the number of luciferase moles normalized to micrograms of total protein present in each sample. In accordance with theoretical expectations, TNF- α induced a significant increase in luciferase expression in respect to control samples (Fig. 64) which refer to cells incubated with 0.35 μ g/ml human serum albumin (HSA) that is used as a carrier protein for TNF- α solubilization in order to increase TNF- α stability under storage conditions.

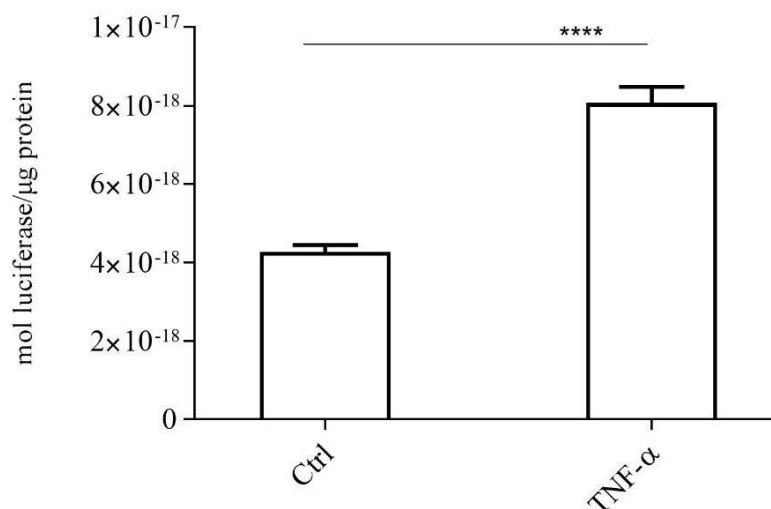


Figure 64 – Firefly luciferase reporter assay in stably transfected HLE-B3_F cells stimulated with 0.2

nM TNF- α . HLE-B3_F cells were incubated for 24 hours with either 0.2 nM TNF- α or 0.35 μ g/ml HAS as control cells. Results are reported as mol of luciferase measured normalized to micrograms of protein for each sample and are expressed as mean \pm SEM of at least six independent measures in three independent experiments. Statistical analysis was performed through unpaired Student t test (**** $p \leq 0.0001$).

After the confirmation that HLE-B3_F is a good model to evaluate NF- κ B activation, the effect of two different concentrations of 4-HNE, 30 μ M and 40 μ M, on *Firefly* luciferase expression at different time-points of incubation corresponding to 3, 6 and 24 hours was assessed. Data obtained from luciferase reporter assay analysis and reported in Figure 65 show that not only it was observed an increase of luciferase expression but also it seems to be progressively reduced in cells incubated with 4-HNE for up to 24 hours in respect to the corresponding control cells. Furthermore, as control it was confirmed that under the same experimental conditions 40 μ M 4-HNE was able to induce COX-2 expression like it has been previously reported for HLE-B3 cells (Fig. 65, panel D).

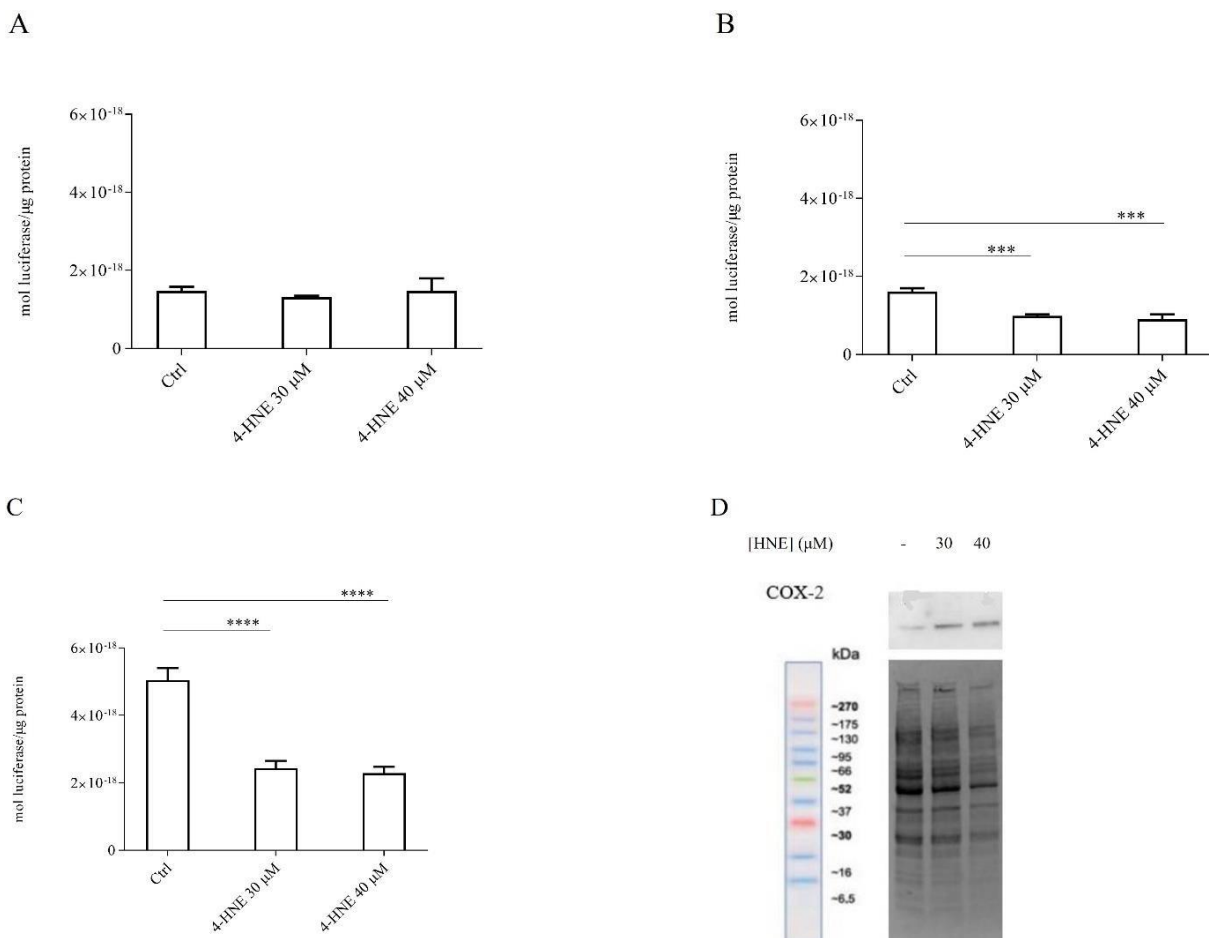


Figure 65 – Firefly luciferase reporter assay in HLE-B3_F cells incubated with 4-HNE. HLE-B3_F cells were incubated for 3, 6 or 24 hours (panel A, B and C, respectively) with 30 μ M or 40 μ M 4-HNE or in absence of the aldehyde (ctrl cells). Results are reported as mol of luciferase normalized to μ g of proteins for each sample and expressed as mean \pm SEM of measures of at least six independent experiments. Statistical analysis

was performed through one-way Anova followed by Dunnett post hoc test (** $p \leq 0.001$ **** $p \leq 0.0001$). In panel D is reported a Western blotting analysis of samples of HLE-B3_F cells incubated with 30 μM or 40 μM 4-HNE or in absence of the aldehyde for 6 hours as described in Materials and methods section.

3. Optimization of experimental conditions for the exposure of HLE-B3 cells to hyperglycaemic conditions

As previously reported, it is known that cataracts in humans is characterized by low cell density and apoptosis in lens epithelial cells. Many studies suggest that people with diabetes are more predisposed to develop cataracts but the exact mechanism underlying high glucose-induced human lens epithelial cells apoptosis remains unclear. High glucose is hypothesized to be the initiating agent which induces oxidative stress and activates AKR1B1 in the polyol pathway. Indeed, overexpression of AKR1B1 caused increased apoptosis and intracellular sorbitol and fructose concentrations and reduced cytosolic GSH levels in human lens epithelial cells exposed to elevated D-glucose levels. However, these effects resulted to be significantly inhibited by treatment with the AKR1B1 inhibitor fidarestat (Kubo et al., 2004). For this reason, HLE-B3 cells could represent a useful experimental model that may be used to investigate inflammation induced by high glucose levels and mediated by AKR1B1 and to evaluate eventually the anti-inflammatory activity of AKR1B1 inhibitors.

Since the experimental conditions for treatment of human lens epithelial cells with D-glucose vary considerably among different laboratories, the impact of different conditions on D-glucose-induced inflammatory response was initially examined. For each experimental condition tested, HLE-B3 cells were incubated with two different hyperglycaemic concentrations that were already known for being able to induce NF- κ B nuclear translocation (Ramana et al., 2003) and harvested in order to detect, by Western blotting analysis, changes in COX-2 expression.

HLE-B3 cells were initially pre-incubated for 24 hours in D-glucose-free DMEM supplemented with 10% FBS, 2 mM L-glutamine and 1% P/S. Before treatment with D-glucose, t_0 cells were harvested and cytosolic extract, namely t_0 , was prepared. The remaining part of cells was incubated with 5, 25 or 50 mM D-glucose for 24 hours and the increase in COX-2 expression was evaluated (Fig. 66). Western blotting analysis revealed that both normal and elevated D-glucose levels were able to induce a remarkable increase in COX-2 expression that, in addition, resulted to be comparable.

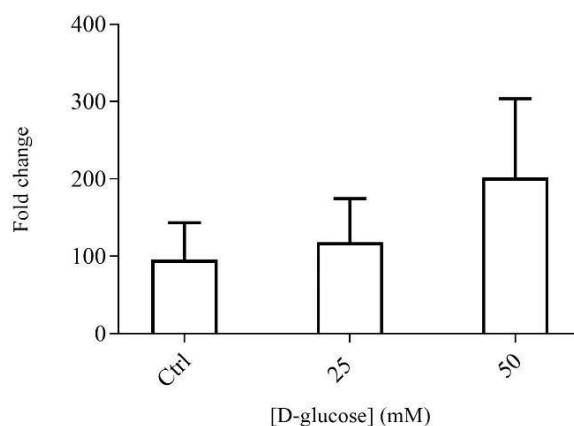


Figure 66 – Dose-dependent effect of D-glucose on the induction of COX-2 expression. HLE-B3 cells were incubated for 24 hours in glucose-deprived DMEM supplemented with 10% FBS, 2 mM L-glutamine and 1% (v/v) P/S and immediately harvested (t_0) or incubated for other 24 hours with 5, 25 or 50 mM D-glucose. Results are expressed as mean \pm SEM of at least three independent experiments. Significance was evaluated with respect to control cells incubated for 24 hours under euglycaemic conditions. Statistical analysis was performed through one-way Anova followed by Tukey post hoc test.

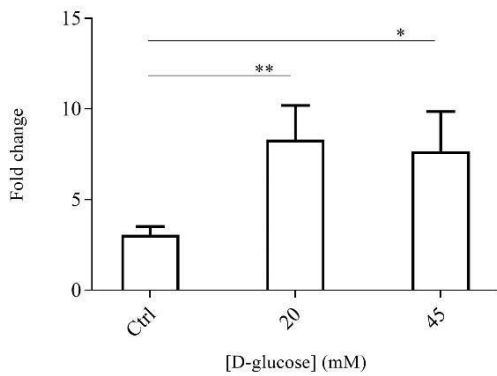
Since under this experimental condition it was observed no significant difference in COX-2 expression between hyperglycaemic and normoglycaemic conditions, that result to be able alone to induce an inflammatory response, different conditions were evaluated. Cells were therefore maintained for different incubation times in media that varied in their composition, as reported in Table 3, treated with 20 or 45 mM D-glucose and harvested after 24 hours. COX-2 expression under hyperglycaemic conditions was compared with that detected in control cells that were incubated under the same condition for the same time without adding D-glucose to the culture medium that contains 5 mM D-glucose.

	EXPERIMENTAL CONDITION
A	DMEM, 10% FBS, 2 mM L-glutamine, 1% P/S, 5 mM D-glucose, 24 hours
B	DMEM, 0.5% FBS, 2 mM L-glutamine, 1% P/S, 5 mM D-glucose, 24 hours
C	DMEM, 0.5% FBS, 2 mM L-glutamine, 50 μ g/ml gentamycin, 5 mM D-glucose, 24 hours
D	DMEM, 0.5% FBS, 2 mM L-glutamine, 50 μ g/ml gentamycin, 5 mM D-glucose, 48 hours
E	MEM, 0.5% FBS, 2 mM L-glutamine, 50 μ g/ml gentamycin, 24 hours

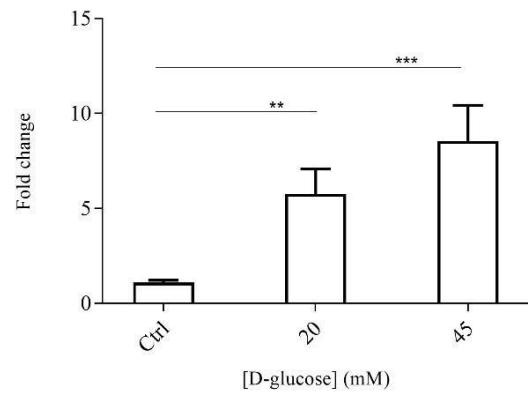
Table 3 – Different experimental conditions adopted for hyperglycaemic treatment of HLE-B3 cells.

As shown in figure 67, high glucose concentrations could induce, under all the experimental conditions tested, a significant increase in COX-2 protein levels that, nevertheless, resulted more marked under conditions C and E. These observations suggested that incubation of HLE-B3 cells for 24 hours in both DMEM and MEM containing 5 mM D-glucose, 0.5% FBS, 2 mM L-glutamine and 50 µg/ml gentamycin represents the most advantageous experimental conditions for evaluating the pro-inflammatory effect of D-glucose. However, the latter condition was chosen because it is the same previously used for 4-HNE treatment of HLE-B3 cells, allowing to eventually compare the inflammatory response induced by two different pro-oxidant stimuli.

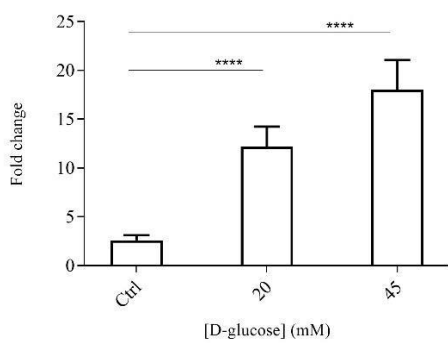
A



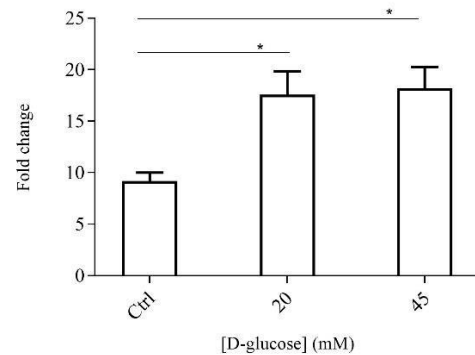
B



C



D



E

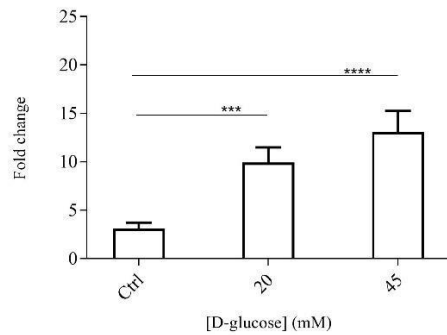


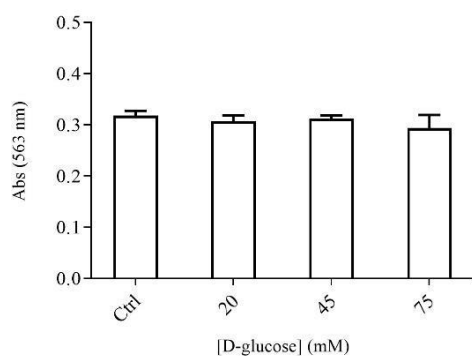
Figure 67 – Dose-dependent effect of D-glucose on the induction of COX-2 expression under different experimental conditions. HLE-B3 cells were incubated under condition **A** (Tab. 3) (panel A), condition **B** (Tab. 3) (panel B), condition **C** (Tab. 3) (panel C), condition **D** (Tab. 3) (panel D) or condition **E** (Tab. 3) (panel E) and immediately harvested (t_0) or incubated for other 24 hours with 20 or 45 mM D-glucose. Results are expressed as mean \pm SEM of at least three independent experiments. Significance was evaluated with respect to control cells maintained for 24 hours in the absence of D-glucose. Statistical analysis was performed through one-way Anova followed by Tukey post hoc test (* $p \leq 0.05$ ** $p \leq 0.01$ *** $p \leq 0.001$ **** $p \leq 0.0001$).

4. Pro-inflammatory effect of hyperglycaemic treatment on HLE-B3 cells

4.1 Evaluation of the cytotoxic effect of high glucose levels

Since it was reported that high glucose concentrations exert toxic effect on HLE-B3 cells (Ramana et al., 2003), it was verified if high glucose levels could be toxic for cells under the experimental conditions adopted. For this reason, HLE-B3 cells were incubated with increasing concentrations of D-glucose, corresponding to 20, 45 and 75 mM for 24 or 48 hours in MEM supplemented with 0.5% FBS, 2 mM L-glutamine and 50 $\mu\text{g}/\text{ml}$ gentamycin and cell viability was then evaluated by MTT assay, as described in Materials and methods section. As shown in Figure 68, all the glucose concentrations tested did not significantly affect cell survival.

A



B

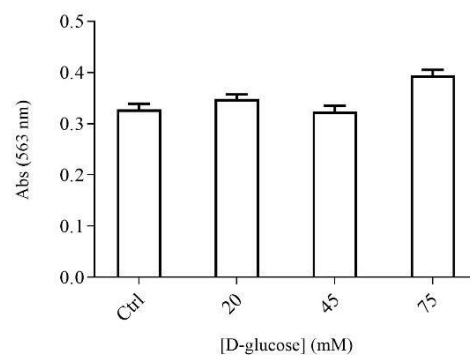


Figure 68 – Evaluation of toxic effect of different concentrations of D-glucose on HLE-B3 cells. Cell viability of cells incubated with 20, 45 or 75 mM D-glucose for 24 (panel A) or 48 (panel B) hours was evaluated by MTT assay as described in Materials and methods section. The results are expressed as mean \pm SEM of at least six independent biological samples. Significance was evaluated with respect to control cells incubated for the same time in the presence of 5 mM D-glucose. Statistical analysis was performed through one-way Anova followed by Tukey post hoc test.

4.2 Evaluation of time-dependent and dose-dependent effect of high glucose levels on COX-2 expression

The time-dependent effect of high glucose levels on the induction of the inflammatory response was evaluated by maintaining HLE-B3 cells for 24 hours in MEM supplemented with 0.5% FBS, 2 mM L-glutamine and 50 μ g/ml gentamycin and exposing them to 20 mM D-glucose for different time up to 48 hours. HLE-B3 cells were harvested at the end of incubation and the corresponding samples were analysed through Western blotting in order to measure COX-2 protein levels. Results reported in Figure 69 indicated that exposure to 20 mM D-glucose induced a significant increase in COX-2 expression after 16 hours of incubation in respect to cells that were maintained for the same time under euglycaemic conditions. Since it was observed a time-dependent increase of COX-2 levels, in all the following experiments cells were harvested for Western blotting analysis within 48 hours after treatment with D-glucose.

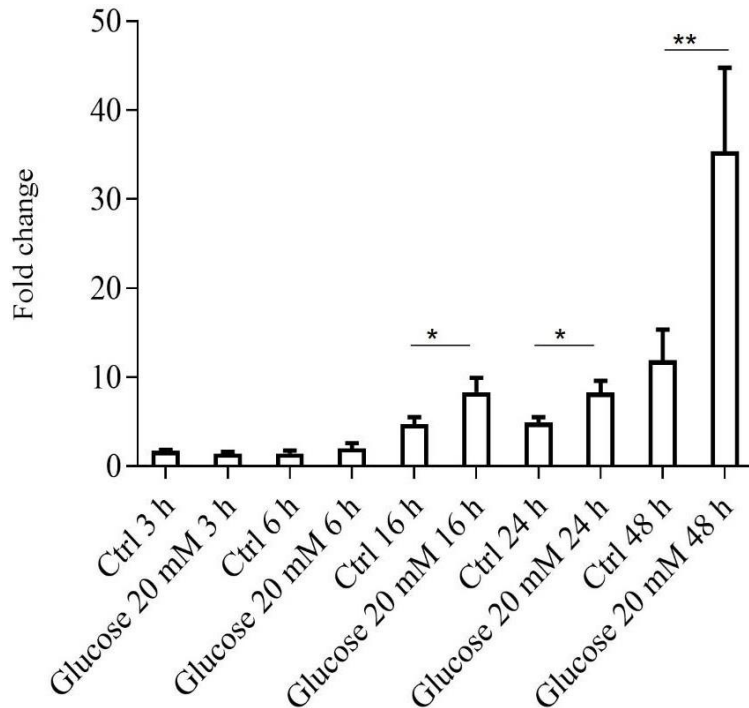


Figure 69 – Time-dependent effect of D-glucose on induction of COX-2 expression. COX-2 protein levels were measured by Western blotting in HLE-B3 cells maintained for 24 hours in MEM supplemented with 0.5% FBS, 2 mM L-glutamine and 50 µg/ml gentamycin and then exposed to 20 mM D-glucose for 3, 6, 16, 24 or 48 hours. All the values are the mean ± SEM of measures on at least three independent experiments. Significance was evaluated in respect to cells incubated for the same time under euglycaemic conditions through one-way Anova followed by Tukey post hoc test (* $p \leq 0.05$ ** $p \leq 0.01$).

Furthermore, the dose-dependent effect of high D-glucose levels on COX-2 expression was also evaluated by maintaining HLE-B3 cells for 48 hours in the presence of 20 mM or 75 mM D-glucose, considering that the incubation of cells with concentrations of D-glucose up to 75 mM resulted not to be cytotoxic (Fig. 68). In accordance with expectations, both the concentrations used were able to induce a significant increase in COX-2 protein levels in respect to cells incubated for the same time under euglycaemic conditions (Fig. 70).

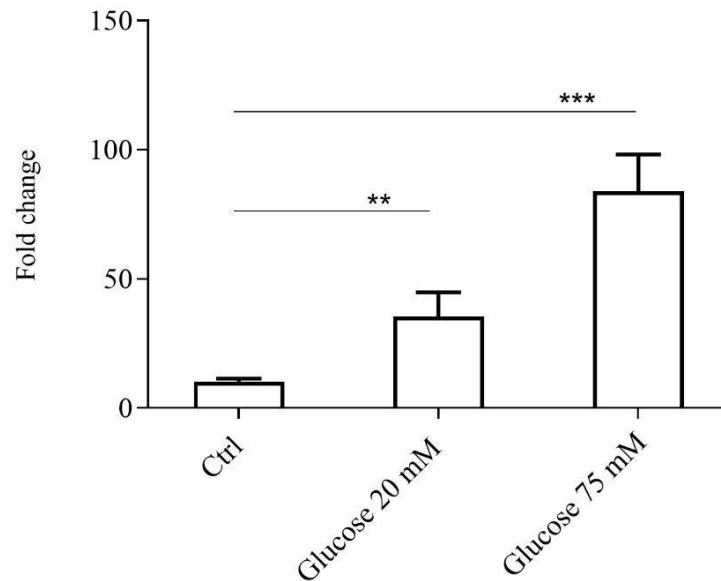


Figure 70 – Dose-dependent effect of high D-glucose concentrations on COX-2 expression. COX-2 protein levels were measured by Western blotting in HLE-B3 cells maintained for 24 hours in MEM supplemented with 0.5% FBS, 2 mM L-glutamine and 50 µg/ml gentamycin and then exposed to 20 mM or 75 mM D-glucose for 48 hours. All the values are the mean \pm SEM of measures on at least three independent experiments. Significance was evaluated in respect to cells incubated for the same time under euglycaemic conditions through one-way Anova followed by Tukey post hoc test (** $p \leq 0.01$ *** $p \leq 0.001$).

4.3 Evaluation of NF- κ B activation induced by high glucose levels in HLE-B3_F cells

Literature data report that some transcription factors, including NF- κ B, are involved in the regulation of COX-2 expression (Appleby et al., 1994; Kiritoshi et al., 2003). For this reason, the association between D-glucose-induced increase in COX-2 protein levels and NF- κ B activation was evaluated by measuring the increase in *Firefly* luciferase expression in HLE-B3_F cells stimulated with hyperglycaemic concentrations. Stably transfected HLE-B3 cells were therefore incubated with 20 mM D-glucose in MEM supplemented with 0.5% FBS, 2 mM L-glutamine, 50 µg/ml gentamycin and 100 µg/ml hygromycin for 24 or 48 hours in order to examine the time-dependent effect of high glucose levels on NF- κ B activation. The results, expressed as moles of luciferase normalized to micrograms of protein, evidenced no significant increase in NF- κ B activation in cells exposed to 20 mM D-glucose at both times of incubation (Fig. 71).

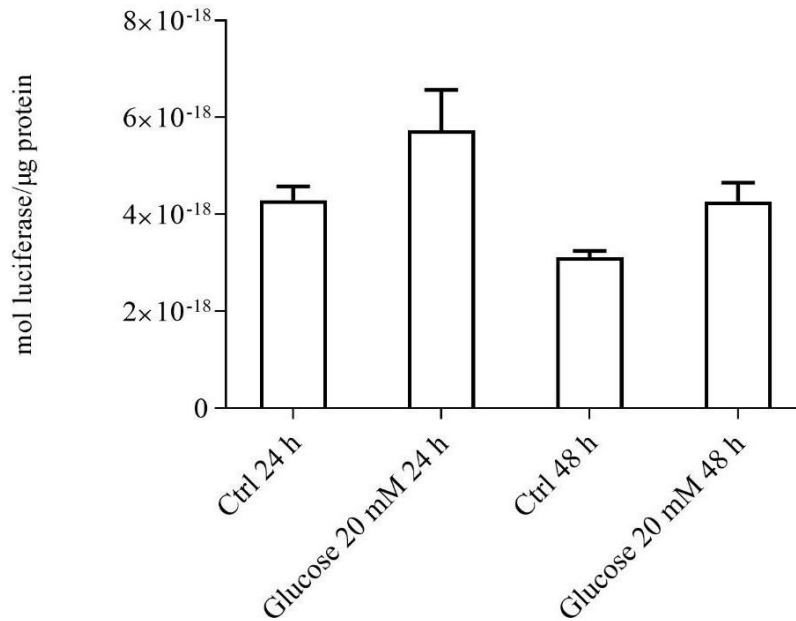


Figure 71 – Firefly luciferase reporter assay in stably transfected HLE-B3 cells stimulated with 20 mM D-glucose. Firefly luciferase expression was evaluated in HLE-B3_F cells incubated for 24 or 48 hours with 20 mM D-glucose in respect to control cells and reported as moles of luciferase normalized to micrograms of protein. Results are expressed as mean ± SEM of measures on at least twelve independent biological sample. Statistical analysis was performed through one-way Anova followed by Tukey post hoc test.

Since in the previous results was reported an increase in NF-κB activation after the treatment of cells with 20 mM D-glucose that however did not appear significant, more severe hyperglycaemic conditions were applied. HLE-B3_F cells were thus maintained for 24 hours in MEM containing 0.5% FBS, 2 mM L-glutamine, 50 μg/ml gentamycin and 100 μg/ml hygromycin. Then, 75 mM D- glucose was added to the incubation medium, and cells were harvested after 24 hours. The results obtained showed a significant increase in *Firefly* luciferase expression in response to the addition of D-glucose to the incubation medium (Fig. 72) with the induction of an inflammatory response that was also confirmed by Western blotting analysis of COX-2 expression. The significant increase in COX-2 protein levels is reported in Figure 73, thus confirming data obtained by the stimulation of HLE-B3 cells with 75 mM D-glucose (Fig. 70).

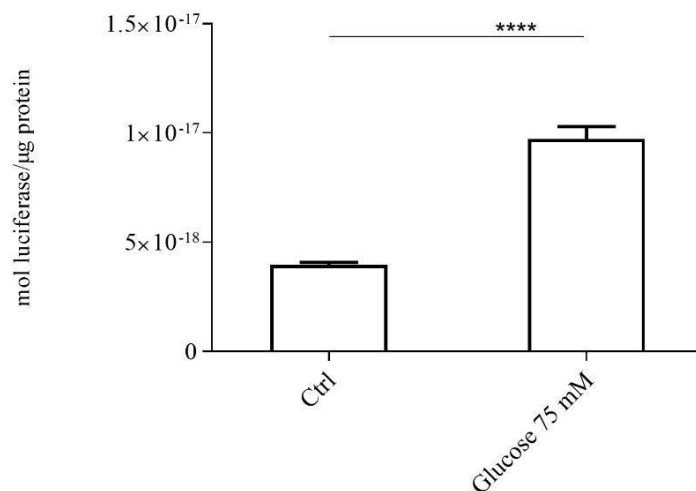


Figure 72 – Firefly luciferase reporter assay in HLE-B3_F cells stimulated with 75 mM D-glucose. Firefly luciferase expression was measured in HLE-B3_F cells incubated for 24 hours in MEM containing 0.5% FBS, 2 mM L-glutamine, 50 µg/ml gentamycin and 100 µg/ml hygromycin and maintained for 24 hours under euglycaemic or hyperglycaemic conditions. Results are expressed as mean ± SEM of measures on at least six independent biological samples. Statistical analysis was performed through unpaired Student’s t test (**** p ≤ 0.0001).

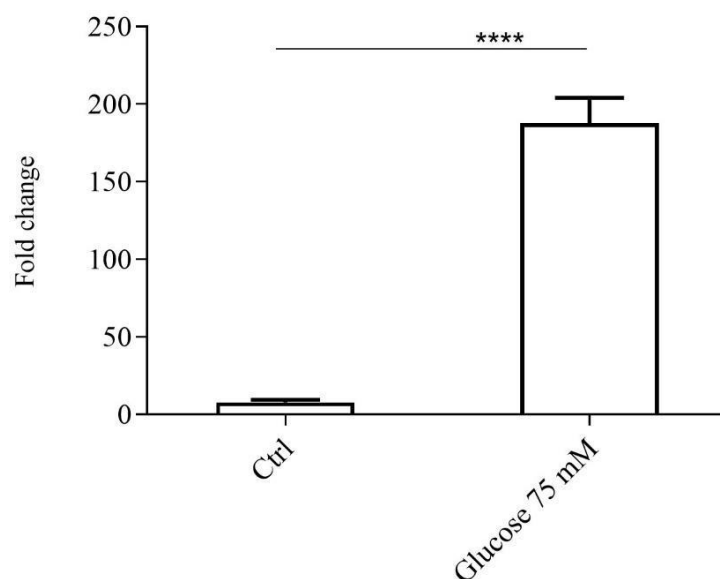


Figure 73 – Effect of hyperglycaemic conditions on COX-2 expression. COX-2 protein levels were measured by Western blotting in HLE-B3_F cells maintained for 24 hours in MEM supplemented with 0.5% FBS, 2 mM L-glutamine, 50 µg/ml gentamycin and 100 µg/ml hygromycin and then exposed to 75 mM D-glucose for 48 hours. All the values are the mean ± SEM of measures on at least three independent experiments. Significance was evaluated in respect to cells incubated for the same time under euglycaemic conditions through one-way Anova followed by Tukey post hoc test (**** p ≤ 0.0001).

4.4 Evaluation of the inhibitory effect of sorbinil on D-glucose pro-inflammatory effect

Since the aim of this work was assessing the involvement of AKR1B1 in the inflammatory signalling induced by hyperglycaemia, the effect of sorbinil on NF- κ B activation was evaluated. HLE-B3_F cells were incubated with either 50 μ M sorbinil or 0.1% (v/v) DMSO for 24 hours in MEM containing 0.5% FBS, 2 mM L-glutamine, 50 μ g/ml gentamycin and 100 μ g/ml hygromycin, at 37 $^{\circ}$ C, in a humidified 5% CO₂ atmosphere. Then, 75 mM D-glucose was added to culture medium and cells were harvested after 24 hours of incubation. As control, *Firefly* luciferase expression was measured in samples obtained from cells incubated only with 0.1% (v/v) DMSO or 50 μ M sorbinil, without adding D-glucose to the incubation medium. The results corroborated the elevated D-glucose levels- induced significant increase in *Firefly* luciferase expression that, nevertheless, was not reduced in the presence of sorbinil. Under this experimental condition, in contrast, a significant decrease in NF- κ B activation was observed in the presence of DMSO (Fig. 74).

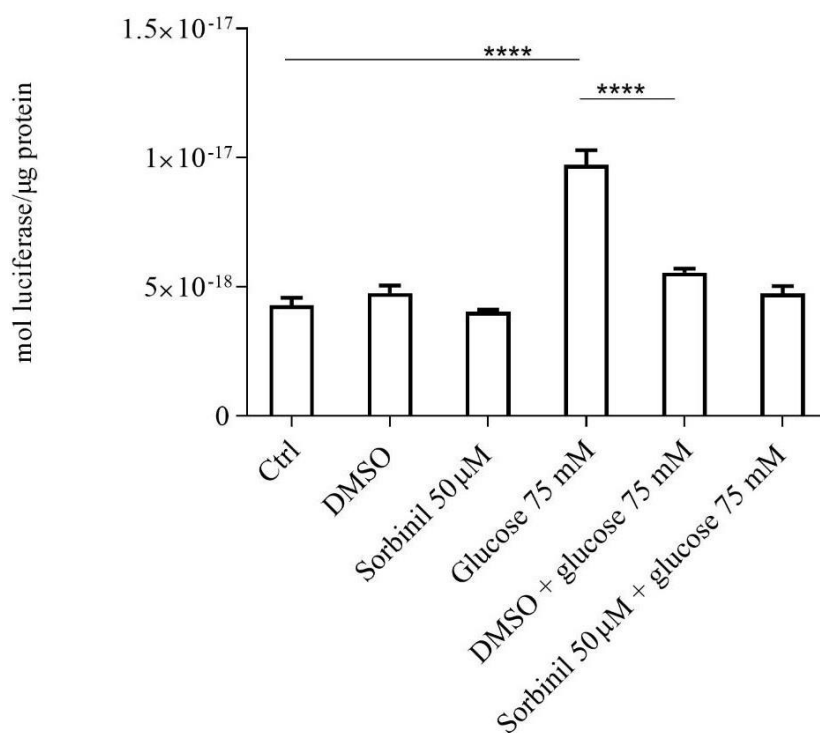


Figure 74 – Effect of sorbinil on Firefly luciferase expression in stably transfected HLE-B3 cells stimulated with 75 mM D-glucose. HLE-B3_F cells were incubated with either 0.1% (v/v) DMSO or 50 μ M sorbinil for 24 hours before adding 75 mM D-glucose and harvested after 24 hours. Results are expressed as mean \pm SEM of at least six independent biological samples. Significance was evaluated in respect to control cells maintained for 24 hours in MEM supplemented with 0.5% FBS, 2 mM L-glutamine, 50 μ g/ml gentamycin

and 100 µg/ml hygromycin under euglycemic conditions to evaluate the effect of D-glucose or in respect to cells incubated under hyperglycaemic conditions in the presence of 0.1% (v/v) DMSO to test sorbinil efficacy. Statistical analysis was performed through one-way Anova followed by Tukey post hoc test (**** $p \leq 0.0001$).

4.5 Evaluation of the inhibitory effect of DMSO on NF-κB activation induced by D-glucose

Since the majority of AKR1B1 and CBR1 inhibitors are hydrophobic molecules, DMSO seemed to be a suitable solvent to dissolve hydrophobic compounds guaranteeing their solubilization. For this reason, DMSO has been used as a solvent for all the inhibitors tested (sorbinil, rutin and epalrestat) in order to investigate their effects as anti-inflammatory agents. Nevertheless, DMSO at final concentration of 0.1% (v/v), that is reported to be safe for almost all cells, showed to significantly reduce the NF-κB transcriptional activity induced by treatment of HLE-B3_F cells with D-glucose (Fig. 36 and 37). Therefore, a range of DMSO concentrations (0.1, 0.05 and 0.02% (v/v)) was tested in order to identify a concentration that was still able to dissolve hydrophobic inhibitors but did not exhibit an anti-inflammatory action that could mask or interfere with the activity of the inhibitor. Stably transfected HLE-B3 cells were incubated for 24 hours with different concentrations of DMSO in MEM supplemented with 0.5% FBS, 2 mM L-glutamine, 50 µg/ml gentamycin and 100 µg/ml hygromycin, treated with 75 mM and harvested after 24 hours. As shown in Figure 75, the results obtained suggested that 0.1% (v/v) DMSO significantly reduced *Firefly* luciferase expression induced by high glucose levels, an effect that however was not observed at lower concentrations of the solvent.

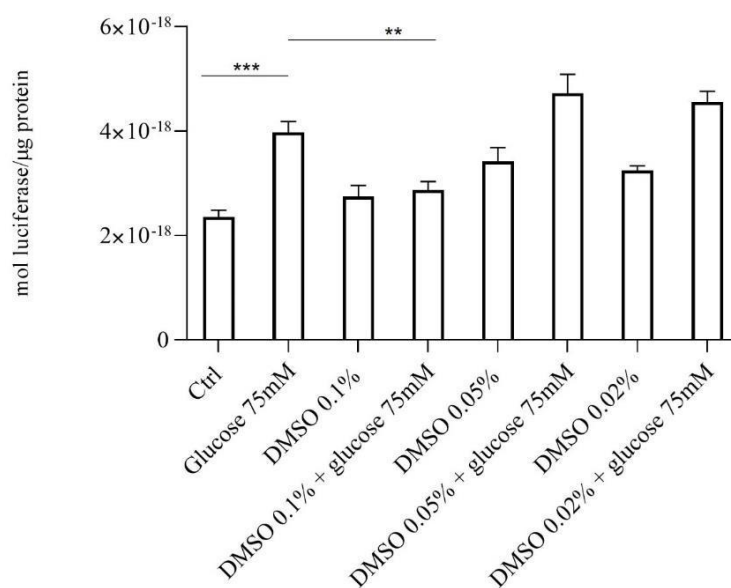


Figure 75 – Effect of different concentrations of DMSO on Firefly luciferase expression induced by 75 mM D-glucose. Firefly luciferase expression was quantified through luciferase reporter assay in HLE-B3_F cells maintained for 24 hours with 0.1, 0.05 or 0.02% (v/v) DMSO and incubated for 24 hours with 75 mM D-glucose. The results are expressed as mean \pm SEM of at least five independent biological samples. Significance was evaluated in respect to control cells maintained for 24 hours in MEM supplemented with 0.5% FBS, 2 mM L-glutamine, 50 μ g/ml gentamycin and 100 μ g/ml hygromycin under euglycaemic conditions to evaluate the effect of D-glucose or in respect to cells incubated under hyperglycaemic conditions to test the effect of DMSO. Statistical analysis was performed through one-way Anova followed by Tukey post hoc test (** $p \leq 0.01$ *** $p \leq 0.001$).

4.6 Evaluation of Firefly luciferase expression under D-glucose stimulation in glucose-deprived stably transfected HLE-B3 cells

Since the complexity of cellular response under hyperglycaemic conditions, also associated with oxidative stress, has been reported by literature data and in order to go deeper in understanding a possible role of aldose reductase, a different *in vitro* cell culture condition was finally considered. Therefore, stably transfected HLE-B3 cells were maintained for 24 hours in DMEM medium supplemented with 10% (v/v) FBS, 2 mM L-glutamine, 1% (v/v) P/S and 100 μ g/ml hygromycin, in glucose deprivation. Then, fixed concentrations of D-glucose corresponding to 5 mM, 25 mM and 50 mM were added to the medium and cells were harvested after 6, 16 or 24 hours. HLE-B3_F cells harvested after 24 hours of glucose deprivation and before starting the treatment with D-glucose were used as control. The luciferase reporter assay was performed according to the experimental procedure described in the Materials and methods section and the resultant increase in *Firefly* luciferase expression was reported in Figure 76. The results indicated that under this experimental condition both hyperglycaemic and euglycaemic concentrations were able to significantly activate NF- κ B after both 16 and 24 hours of incubation probably because glucose deprivation might induce a pre- activation of cellular response.

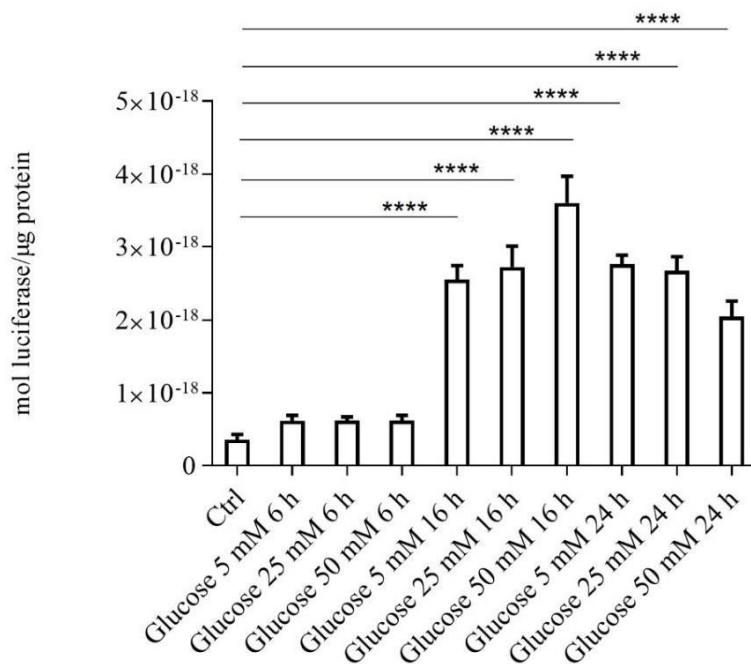


Figure 42 – Time-dependent effect of euglycaemic and hyperglycaemic conditions on Firefly luciferase expression. Firefly luciferase expression analysis was performed on HLE-B3_F cells treated with D-glucose (5 mM, 25 mM, 50 mM) for 6, 16 or 24 hours after having been maintained for 24 hours under glucose deprivation. The results are expressed as mean \pm SEM of at least six independent biological samples. Significance was evaluated in respect to control cells that were harvested before starting the treatment. Statistical analysis was performed through one-way Anova followed by Tukey post hoc test (**** $p \leq 0.0001$).

Finally, the effectiveness of sorbinil on NF- κ B activation induced by high glucose levels was also tested in HLE-B3_F cells exposed to euglycaemic and hyperglycaemic conditions after 24 hours of D-glucose deprivation. Cells were maintained for 24 hours in DMEM supplemented with 10% FBS, 2 mM L-glutamine, 50 μ g/ml gentamycin and 100 μ g/ml hygromycin without D-glucose in the presence with either 0.1% (v/v) DMSO or 50 μ M sorbinil. Then, they were incubated with 5, 25 or 50 mM D-glucose and harvested after 16 hours. Before starting the treatment with the inhibitor some cells were harvested and used as control (t_0 sample). The results obtained revealed a significant effect of DMSO in inhibiting NF- κ B transcriptional activity, as it was observed in previous experiments, as well as a slight anti-inflammatory effect of sorbinil (Fig. 77). For this reason, even though a relevant effect of DMSO upon *Firefly* luciferase expression was observed, this experimental condition appeared to be the most promising of all the ones that were applied for evaluating the effect of AKR1B1 inhibitors in abolishing the inflammatory response.

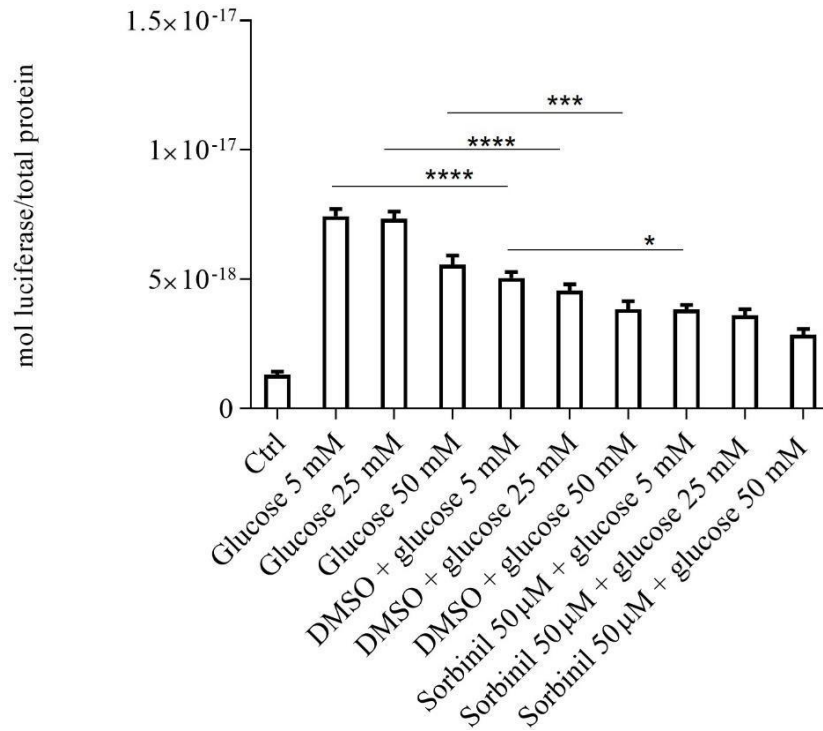


Figure 77 – Effect of sorbinil on Firefly luciferase expression induced by euglycaemic and hyperglycaemic conditions after 24 hours of glucose deprivation. Firefly luciferase expression was measured in stably transfected HLE-B3 cells initially deprived of glucose, incubated with either DMSO or 50 μM sorbinil 24 hours before D-glucose addition (5 mM, 25 mM, 50 mM) and harvested 16 hours later. Cells harvested before starting the treatment with D-glucose were used as control (t_0 sample). The results are expressed as mean \pm SEM of at least six independent biological samples. Significance was evaluated in respect to in respect to cells incubated with the same D-glucose concentration but in the presence of 0.1% (v/v) DMSO to test sorbinil efficacy. Statistical analysis was performed through one-way Anova followed by Tukey post hoc test (* $p \leq 0.05$ *** $p \leq 0.001$ **** $p \leq 0.0001$).

DISCUSSION AND CONCLUSIONS

Human lens epithelial cells are reported to have a well characterized defence system that supports antioxidant and detoxification processes. Indeed, HLE-B3 cells show remarkable levels of glutathione and exhibit an enzymatic pattern that metabolizes 4-HNE mainly through glutathionylation to generate the GS-HNE adduct. GS-HNE transformation, in turn, appears to be specifically related to NADPH-dependent activities that may be due to the synergistic action of CBR1 and AKR1B1 forming GS-DHN (Peroni et al., 2020). AKR1B1, in addition, as rate-limiting enzyme in the polyol pathway, under hyperglycaemic conditions, is responsible for reducing D-glucose to sorbitol using NADPH as cofactor leading to oxidative stress and subsequent tissue injury. Literature data report that both GS-DHN and the over-activation of the polyol pathway caused by hyperglycaemia stimulate the production and release of bioactive inflammatory mediators by promoting the phosphorylation and, consequently, the degradation of I κ -B α and the nuclear translocation of NF- κ B through various protein kinase cascades, such as MAPKs and PKC (Ramana et al., 2003; Ramana et al., 2006). Thus, both 4-HNE and high glucose levels lead to HLE-B3 cell death by triggering an inflammatory signalling in which AKR1B1 could play a key role as a mediator (Ramana et al., 2003). HLE-B3 cells have thus been chosen as a cellular model system to investigate the pro-inflammatory effect of these two endogenous stimuli that appear to be intertwined by AKR1B1 activity. Nevertheless, thanks to the several protective systems devoted to preserve lens normal physiology and homeostasis, human lens epithelial cells result to be strongly protected from both oxidative and glycative stress (Lou, 2003) as indicated by cell viability assays. Furthermore, it is worth noting that only HLE-B3 exposition to very high levels of either 4-HNE or D-glucose can significantly trigger the inflammatory response. Taking into account these results, it could be assumed that an efficient enzymatic pattern able to catalyse transformation of both aldehydes and D-glucose represents a significant factor that affects cells sensitivity to pro-inflammatory effect of these two stress sources. The results obtained from the measure of the residual 4-HNE concentration present in the different cell culture conditions applied show that 4-HNE is rapidly removed from the incubation medium, mostly within 2 hours. 4-HNE also promotes a transient induction of COX-2 with its maximum expression observed after 6 hours of incubation. This cellular response to 4-HNE appears to be affected only by 4-HNE concentration and not by its stereochemical configuration, that instead it is reported to be relevant in other biological processes, including phosphorylation of MAPK and apoptosis in cultured mouse hepatocytes (Dabrowski et al., 2010). In different cell lines the pro-inflammatory effect of the aldehyde is reported to be due not directly to 4-HNE but to its glutathionylated adducts (Ramana et al.,

2006) whose formation was also observed in our experimental conditions. In fact, HPLC analysis of ultrafiltrates of samples derived only from short periods of incubation with 30 or 40 μ M 4-HNE show the generation of a metabolite that could correspond, based on preliminary data, to GS-HNE. Since this molecule is not detectable in ultrafiltered samples obtained from cells incubated with 4-HNE for 3 or 6 hours, it could be assumed that this conjugate, once formed, is rapidly extruded in an ATP-dependent manner by RLIP76, a transporter that was demonstrated to contribute to detoxification of 4-HNE protecting HLE-B3 cells against toxic effects of oxidative stress (Sharma et al., 2003). This hypothesis is supported by data reported by Choudhary and colleagues that identified, after 1 hour of incubation, 4-HNE glutathionylated derivatives in the incubation medium of human lens epithelial cells (Choudhary et al., 2003). In fact, GS-HNE could be further metabolized by AKR1B1 and CBR1 to its corresponding alcohol that is reported to be extruded from cells (Choudhary et al., 2003) but also is known to activate the redox sensitive transcription factor NF- κ B (Yadav and Ramana, 2013). The results obtained by luciferase reporter assay indicate that 4-HNE is not able to induce NF- κ B activation in stably transfected HLE-B3 cells. In contrast, it appears to attenuate the basal NF- κ B transcriptional activity reported to be present in this cell line (Ramana et al., 2003) and actually measured also in HLE-B3 control samples under the experimental conditions applied. This evidence might be explained by the 4-HNE-mediated oxidative modification of amino acidic residues of *Firefly* luciferase that could compromise its enzymatic activity. In fact, it is known that this enzyme contains an average of seven free sulfhydryls per two 50 000-dalton polypeptides, some of which are located at or near the catalytic site (Lee and McElroy, 1969; Alter and DeLuca, 1986). The measurement of standard *Firefly* luciferase activity, after incubation with 4-HNE at different time points would allow to verify this hypothesis. On the other hand, 4-HNE might inhibit either NF- κ B nuclear translocation by interacting with upstream kinases or its transcriptional activity by directly modifying NF- κ B subunits (Sonowal and Ramana, 2019) in the N-terminal region of the Rel homology domain that is susceptible to modification induced by different pro-oxidant agents, including 4-HNE, affecting NF- κ B DNA binding ability (García-Piñeres et al., 2001). Based on our data, the induction of COX-2 expression by 4-HNE in the experimental conditions applied does not seem to depend on NF- κ B activation. Similar results are reported by Kumagai and colleagues who revealed that 4-HNE-induced COX-2 expression in rat epithelial RL34 cells was not related to NF- κ B but resulted from the stabilization of COX-2 mRNA mediated by the p38 mitogen-activated protein kinase signaling pathway (Kumagai et al., 2002).

As underlined above, AKR1B1 is considered to play a role in the mediation of NF- κ B activation (Ramana et al., 2006), thus the observed failure of both AKR1B1 inhibitors, sorbinil and rutin, in attenuating 4-HNE-induced COX-2 expression could also be considered as a further confirmation of a side role of NF- κ B in the induced inflammatory response. Similar to 4-HNE, prolonged exposure of HLE-B3 cells to hyperglycaemia is observed to trigger an inflammatory response leading to a glucose concentration-dependent and time-dependent induction of COX-2 expression. Hyperglycaemia appears to be associated with NF- κ B nuclear translocation in accordance with results obtained by Ramana and co-workers in the same cell line (Ramana et al., 2002). This effect could be due to the over-stimulation of the polyol pathway and the hyper-activation of AKR1B1 that cause the depletion of NAD⁺ and, as a consequence, the attenuation of NAD⁺-dependent deacetylase activity of sirtuin-1 (SIRT1), of which NF- κ B is a substrate. The acetylation status of this transcription factor is thus preserved and accumulation of acetyl-NF- κ B occurs, leading to increased expression of inflammatory genes, including COX-2 (Chang and Petrash, 2018).

Thus, in order to go deeper in understanding a possible role of AKR1B1 as a mediator of the inflammatory response under hyperglycemic conditions, the effectiveness of sorbinil on NF- κ B activation was evaluated. The *Firefly* luciferase expression induced by 75 mM D-glucose is not significantly reduced by the pre-incubation with sorbinil whose effect has to be compared with the one observed after pre-incubation of cells with DMSO alone. However, considering that the solvent alone (DMSO) is able to significantly reduce NF- κ B activation, this effect does not allow to highlight efficiently the effect of the inhibitor. An inhibitory effect of DMSO on inflammatory response is observed also when HLE-B3 cells are subjected to 24 hours of glucose deprivation and then exposed to different concentrations of D-glucose. In this case, however, a barely significant effect of 50 μ M sorbinil is observed. Thus, in order to reduce this effect, it will be necessary to use it at lower concentrations at which it is not observed a significant reduction of NF- κ B activation in cells stimulated by hyperglycaemic conditions. Since the aim of this work is evaluating the inflammatory response induced by 4-HNE and D-glucose on a human epithelial cells line and, in particular, clarifying the role of AKR1B1 in this response, some considerations have to be done for future applications of AKR1B1 inhibitors. These molecules are reported to be effectively used under several experimental conditions as anti-inflammatory compounds (Ramana et al., 2006), however it is still necessary to evaluate their bioavailability, although their use in these terms has not been widely characterized. In particular, the failure of all the inhibitor tested to reduce, at least partially, the inflammatory response indicates that

plasma membrane might be impermeable to these molecules, compromising their bioavailability for HLE-B3 cells.

REFERENCES

- Ahmed NK, Felsted RL, Bachur NR. Heterogeneity of anthracycline antibiotic carbonyl reductases in mammalian livers. *Biochem Pharmacol.* 1978; 27(23):2713-2719.
- Alary J, Fernandez Y, Debrauwer L, Perdu E, Guéraud F. Identification of intermediate pathways of 4-hydroxynonenal metabolism in the rat. *Chem Res Toxicol.* 2003; 16(3):320-327.
- Aldini G, Gamberoni L, Orioli M, Beretta G, Regazzoni L, Maffei Facino R, Carini M. Mass spectrometric characterization of covalent modification of human serum albumin by 4-hydroxy-trans-2-nonenal. *J Mass Spectrom.* 2006; 41(9):1149-1161.
- Alpert E, Gruzman A, Totary H, Kaiser N, Reich R, Sasson S. A natural protective mechanism against hyperglycaemia in vascular endothelial and smooth-muscle cells: role of glucose and 12-hydroxyeicosatetraenoic acid. *Biochem J.* 2002; 362(Pt 2):413-422.
- Alter SC, DeLuca M. The sulfhydryls of firefly luciferase are not essential for activity. *Biochemistry.* 1986; 25(7):1599-1605.
- American Diabetes Association. Classification and diagnosis of diabetes: standards of medical care in diabetes. *Diabetes Care.* 2018; 41(1):S13-27.
- Ansari NH, Bhatnagar A, Fulep E, Khanna P, Srivastava SK. Trolox protects hyperglycemia-induced cataractogenesis in cultured rat lens. *Res Commun Chem Pathol Pharmacol.* 1994; 84:93-104.
- Appleby SB, Ristimäki A, Neilson K, Narko K, Hla T. Structure of the human cyclooxygenase-2 gene. *Biochem J.* 1994; 302(3):723-727.
- Ayala A, Muñoz MF, Argüelles S. Lipid peroxidation: production, metabolism, and signaling mechanisms of malondialdehyde and 4-hydroxy-2-nonenal. *Oxid Med Cell Longev.* 2014; 2014:1-31.
- Bai J, Mei Y. Overexpression of aldehyde dehydrogenase-2 attenuates neurotoxicity induced by 4-hydroxynonenal in cultured primary hippocampal neurons. *Neurotox Res.* 2011; 19(3):412-422.
- Baldwin AS Jr. The NF-kappa B and I kappa B proteins: new discoveries and insights. *Annu Rev Immunol.* 1996; 14:649-683.
- Balestri F, Barracco V, Renzone G, Tuccinardi T, Pomelli CS, Cappiello M, Lessi M, Rotondo

- R, Bellina F, Scalonì A, Mura U, Del Corso A, Moschini R. Stereoselectivity of aldose reductase in the reduction of glutathionyl-hydroxynonanal adduct. *Antioxidants*. 2019; 8(10):502-519.
- Balestri F, Cappiello M, Moschini R, Rotondo R, Buggiani I, Pelosi P, Mura U, Del Corso A. L- Idose: an attractive substrate alternative to D-glucose for measuring aldose reductase activity. *Biochem Biophys Res Commun*. 2015; 456(4):891-895.
- Balogh LM, Roberts AG, Shireman LM, Greene RJ, Atkins WM. The stereochemical course of 4- hydroxy-2-nonenal metabolism by glutathione S-transferases. *J Biol Chem*. 2008; 283(24):16702- 16710.
- Bateman RL, Rauh D, Tavshanjian B., Shokat KM. Human carbonyl reductase 1 is an S-nitrosoglutathione reductase. *J Biol Chem*. 2008; 283(51):35756-35762.
- Bhatnagar A, Srivastava SK. Aldose reductase: congenial and injurious profiles of an enigmatic enzyme. *Biochem Med Metab Biol*. 1992; 48(2):91-121.
- Boleda MD, Saubi N, Farrés J, Parés X. Physiological substrates for rat alcohol dehydrogenase classes: aldehydes of lipid peroxidation, omega-hydroxyfatty acids, and retinoids. *Arch Biochem Biophys*. 1993; 307(1):85-90.
- Borhani DW, Harter TM, Petrash, JM. The crystal structure of the aldose reductase.NADPH binarycomplex. *J Biol Chem*. 1992; 267(34):24841-24847.
- Borchman D, Ozaki Y, Lamba OP, Byrdwell WC, Czarnecki MA, Yappert MC. Structural characterization of clear human lens lipid membranes by near-infrared Fourier transform Raman spectroscopy. *Curr Eye Res*. 1995; 14(6):511-515.
- Bosch Morell F, Flohé L, Marín N, Romero FJ. 4-Hydroxynonenal inhibits glutathione peroxidase: protection by glutathione. *Free Radic Biol Med*. 1999; 26(11-12):1383-1387.
- Bradford MM. A rapid and sensitive method for the quantitation of microgram quantities of proteinutilizing the principle of protein-dye binding. *Anal Biochem*. 1976; 72:248-254.
- Brambilla G, Sciabà L, Faggin P, Maura A, Marinari UM, Ferro M, Esterbauer H. Cytotoxicity DNA fragmentation and sister-chromatid exchange in Chinese hamster ovary cells exposed to the lipid peroxidation product 4-hydroxynonenal and homologous aldehydes. *Mutat Res Toxicol*. 1986; 171(2- 3):169-176.

Bringmann G, Gassen M, Schneider S. Toxic aldehydes formed by lipid peroxidation. I. Sensitive, gas-chromatography-based stereoanalysis of 4-hydroxyalkenals, toxic products of lipid peroxidation. *J Chromatogr A*. 1994; 670(1-2):153-160.

Brownlee M. The pathobiology of diabetic complications: a unifying mechanism. *Diabetes*. 2005; 54(6):1615-1625.

Burhans MS, Hagman DK, Kuzma JN, Schmidt KA, Kratz M. Contribution of adipose tissue inflammation to the development of type 2 diabetes mellitus. *Compr Physiol*. 2018; 9(1):1-58.

Caamaño J, Hunter CA. NF-kappaB family of transcription factors: central regulators of innate and adaptive immune functions. *Clin Microbiol Rev*. 2002; 15(3):414-429.

Camandola S, Scavazza A, Leonarduzzi G, Biasi F, Chiarotto E, Azzi A, Poli G. Biogenic 4-hydroxy-2-nonenal activates transcription factor AP-1 but not NF-kB in cells of the macrophage lineage. *Biofactors*. 1997; 6(2):173-179.

Castegna A, Lauderback CM, Mohammad-Abdul H, Butterfield DA. Modulation of phospholipid asymmetry in synaptosomal membranes by the lipid peroxidation products, 4-hydroxynonenal and acrolein: implications for Alzheimer's disease. *Brain Res*. 2004; 1004(1-2):193-197.

Castro JP, Jung T, Grune T, Siems W. 4-Hydroxynonenal (HNE) modified proteins in metabolic diseases. *Free Radic Biol Med*. 2017; 111:309-315.

Caviedes A, Maturana B, Corvalán K, Engler A, Gordillo F, Varas-Godoy M, Smalla KH, Batiz LF, Lafourcade C, Kaehne T, Wyneken U. eNOS-dependent S-nitrosylation of the NF-κB subunit p65 has neuroprotective effects. *Cell Death Dis*. 2021; 12(1):4.

Centers for Disease Control and Prevention (CDC). Prevalence of overweight and obesity among adults with diagnosed Diabetes United States, 1988-1994 and 1999-2000". *MMWR. Morbidity and Mortality Weekly Report*. 2004; 53(45):1066-1068.

Chang KC, Petrash JM. Aldo-Keto Reductases: Multifunctional Proteins as Therapeutic Targets in Diabetes and Inflammatory Disease. *Adv Exp Med Biol*. 2018; 1032:173-202.

Chaudhary P, Sharma R, Sharma A, Vatsyayan R, Yadav S, Singhal SS, Rauniyar N, Prokai L, Awasthi S, Awasthi YC. Mechanisms of 4-hydroxy-2-nonenal induced pro- and anti-apoptotic signaling. *Biochemistry*. 2010; 49(29):6263-6275.

- Chen ZJ. Ubiquitin signalling in the NF- κ B pathway. *Nat Cell Biol.* 2005; 7(8):758-765.
- Chen CH, Budas GR, Churchill EN, Disatnik MH, Hurley TD, Mochly Rosen D. Activation of aldehyde dehydrogenase-2 reduces ischemic damage to the heart. *Science.* 2008; 321(5895):1493- 1495.
- Chen HJ, Chung FL. Epoxidation of trans-4-hydroxy-2-nonenal by fatty acid hydroperoxides and hydrogen peroxide. *Chem Res Toxicol.* 1996; 9:306-312.
- Chen LF, Greene WC. Shaping the nuclear action of NF-kappaB. *Nat Rev Mol Cell Biol.* 2004; 5(5):392-401.
- Chen FE, Huang DB, Chen YQ, Ghosh G. Crystal structure of p50/p65 heterodimer of transcriptionfactor NF-kappaB bound to DNA. *Nature.* 1998; 391(6665):410-413.
- Chen LF, Mu Y, Greene WC. Acetylation of RelA at discrete sites regulates distinct nuclear functions of NF-kappaB. *EMBO J.* 2002; 21(23):6539-6548.
- Cheng JZ, Sharma R, Yang Y, Singhal SS, Sharma A, Saini MK, Singh SV, Zimniak P, Awasthi S, Awasthi YC. Accelerated metabolism and exclusion of 4-hydroxynonenal through induction of RLIP76 and hGST5.8 is an early adaptive response of cells to heat and oxidative stress. *J Biol Chem.* 2001; 276(44):41213-41223.
- Cheng JZ, Singhal SS, Saini M, Singhal J, Piper JT, Van Kuijk FJ, Zimniak P, Awasthi YC, Awasthi S. Effects of mGST A4 transfection on 4-hydroxynonenal-mediated apoptosis and differentiation of K562 human erythroleukemia cells. *Arch Biochem Biophys.* 1999; 372(1):29-36.
- Cheng JZ, Singhal SS, Sharma A, Saini M, Yang Y, Awasthi S, Zimniak P, Awasthi YC. Transfection of mGSTA4 in HL-60 cells protects against 4-hydroxynonenal-induced apoptosis by inhibiting JNK- mediated signaling. *Arch Biochem Biophys.* 2001; 392(2):197-207.
- Choudhary S, Srivastava S, Xiao T, Andley UP, Srivastava SK, Ansari NH. Metabolism of lipid derived aldehyde, 4-hydroxynonenal in human lens epithelial cells and rat lens. *Invest Ophthalmol Vis Sci.* 2003; 44(6):2675-2682.
- Choudhary S, Zhang W, Zhou F, Campbell GA, Chan LL, Thompson EB, Ansari NH. Cellular lipidperoxidation end-products induce apoptosis in human lens epithelial cells. *Free Radic Biol Med.* 2002; 32(4):360-369.

Choudhury S, Dyba M, Pan J, Roy R, Chung FL. Repair kinetics of acrolein- and (E)-4-hydroxy-2-nonenal-derived DNA adducts in human colon cell extracts. *Mutat Res.* 2013; 751-752:15-23.

Choudhury S, Pan J, Amin S, Chung FL, Roy R. Repair kinetics of trans-4-hydroxynonenal-induced cyclic 1,N²-propanodeoxyguanine DNA adducts by human cell nuclear extracts. *Biochemistry.* 2004; 43(23):7514-7521.

Cianfruglia L, Morresi C, Bacchetti T, Armeni T, Ferretti G. Protection of polyphenols against glyco-oxidative stress: involvement of glyoxalase pathway. *Antioxidants.* 2020; 9(10):1006.

Clyne AM. Endothelial response to glucose: dysfunction, metabolism, and transport. *Biochem Soc Trans.* 2021; 49(1):313-325.

Colleran A, Ryan A, O'Gorman A, Mureau C, Liptrot C, Dockery P, Fearnhead H, Egan LJ. Autophagosomal I κ B α degradation plays a role in the long term control of tumor necrosis factor- α -induced nuclear factor- κ B (NF- κ B) activity. *J Biol Chem.* 2011; 286(26):22886-22893.

Dabrowski MJ, Zolnerciks JK, Balogh LM, Greene RJ, Kavanagh TJ, Atkins WM. Stereoselective effects of 4-hydroxynonenal in cultured mouse hepatocytes. *Chem Res Toxicol.* 2010; 23(10):1601-1607.

Dalle Donne I, Carini M, Vistoli G, Gamberoni L, Giustarini D, Colombo R, Maffei Facino R, Rossi R, Milzani A, Aldini G. Actin Cys374 as a nucleophilic target of α,β -unsaturated aldehydes. *Free Radic Biol Med.* 2007; 42(5):583-598.

Dalleau S, Baradat M, Guéraud F, Huc L. Cell death and diseases related to oxidative stress: 4-hydroxynonenal (HNE) in the balance. *Cell Death Differ.* 2013; 20(12):1615-1630.

Dejardin E, Droin NM, Delhase M, Haas E, Cao Y, Makris C, Li ZW, Karin M, Ware CF, Green DR. The lymphotoxin- β receptor induces different patterns of gene expression via two NF- κ B pathways. *Immunity.* 2002; 17(4):525-535.

Delhase M, Hayakawa M, Chen Y, Karin M. Positive and negative regulation of I κ B kinase activity through IKK β subunit phosphorylation. *Science.* 1999; 284(5412):309-313.

Deng D, Xu C, Sun P, Wu J, Yan C, Hu M, Yan N. Crystal structure of the human glucose transporter GLUT1. *Nature.* 2014; 510:121-125.

Dixit BL, Balendiran GK, Watowich SJ, Srivastava S, Ramana KV, Petrash JM, Bhatnagar A, Srivastava SK. Kinetic and structural characterization of the glutathione-binding site of aldose reductase. *J Biol Chem.* 2000; 275(28):21587-21595.

Dodson M, Wani WY, Redmann M, Benavides GA, Johnson MS, Ouyang X, Cofield SS, Mitra K, Darley Usmar V, Zhang J. Regulation of autophagy, mitochondrial dynamics, and cellular bioenergetics by 4-hydroxynonenal in primary neurons. *Autophagy.* 2017; 13(11):1828-1840.

Dong J, Jimi E, Zhong H, Hayden MS, Ghosh S. Repression of gene expression by unphosphorylated NF-kappaB p65 through epigenetic mechanisms. *Genes Dev.* 2008; 22(9):1159-1173.

Doorn JA, Petersen DR. Covalent adduction of nucleophilic amino acids by 4-hydroxynonenal and 4-oxononenal. *Chem Biol Interact.* 2003; 143-144:93-100.

Doorn JA, Srivastava SK, Petersen DR. Aldose reductase catalyzes reduction of the lipid peroxidation product 4-oxonon-2-enal. *Chem Res Toxicol.* 2003; 16(11):1418-1423.

Eckl PM, Ortner A, Esterbauer H. Genotoxic properties of 4-hydroxyalkenals and analogous aldehydes. *Mutat Res Mol Mech Mutagen.* 1993; 290(2):183-192.

Esterbauer H, Schaur RJ, Zollner H. Chemistry and biochemistry of 4-hydroxynonenal, malonaldehyde and related aldehydes. *Free Radic Biol Med.* 1991; 11(1):81-128.

Esterbauer H, Zollner H, Scholz N. Reaction of glutathione with conjugated carbonyls. *Z Naturforsch C Biosci.* 1975; 30(4):466-743.

Fantuzzi G. Adipose tissue, adipokines, and inflammation. *J Allergy Clin Immunol.* 2005; 115(5):911-919.

Feoktistova M, Geserick P, Leverkus M. Crystal violet assay for determining viability of cultured cells. *Cold Spring Harb Protoc.* 2016.

Fernandes PH, Wang H, Rizzo CJ, Lloyd RS. Site-specific mutagenicity of stereochemically defined 1,N2-deoxyguanosine adducts of trans-4-hydroxynonenal in mammalian cells. *Environ Mol Mutagen.* 2003; 42(2):68-74.

Ferro M, Marinari UM, Poli G, Dianzani MU, Fauler G, Zollner H, Esterbauer H. Metabolism of 4-hydroxynonenal by the rat hepatoma cell line MH1C1. *Cell Biochem Funct.* 1988;

6(4):245-250.

Ferrucci L, Fabbri E. Inflammageing: chronic inflammation in ageing, cardiovascular disease, and frailty. *Nat Rev Cardiol*. 2018; 15(9):505-522.

Fiorentino T, Prioletta A, Zuo P, Folli F. Hyperglycemia-induced oxidative stress and its role in diabetes mellitus related cardiovascular diseases. *Curr Pharm Des*. 2013; 19(32): 5695–5703.

Forouhi, NG, Wareham NJ. Epidemiology of diabetes. *Medicine*. 2014; 42(12):698-702.

Frohnert BI, Long EK, Hahn WS, Bernlohr DA. Glutathionylated lipid aldehydes are products of adipocyte oxidative stress and activators of macrophage inflammation. *Diabetes*. 2014; 63(1):89-100.

Garavito RM, Malkowski MG, DeWitt DL. The structures of prostaglandin endoperoxide H synthases-1 and -2. *Prostaglandins Other Lipid Mediat*. 2002; 68–69:129–152.

García-Piñeres AJ, Castro V, Mora G, Schmidt TJ, Strunck E, Pahl HL, Merfort I. Cysteine 38 in p65/NF-kappaB plays a crucial role in DNA binding inhibition by sesquiterpene lactones. *J Biol Chem*. 2001; 276(43):39713-39720.

Gęgotek A, Skrzydlewska E. Biological effect of protein modifications by lipid peroxidation products. *Chem Phys Lipids*. 2019; 221:46-52.

Gerard-Monnier D, Erdelmeier I, Regnard K, Moze-Henry N, Yadan JC, Chaudiere J. Reactions of 1-methyl-2-phenylindole with malondialdehyde and 4-hydroxyalkenals. Analytical applications to a colorimetric assay of lipid peroxidation. *Chem Res Toxicol*. 1998; 11:1176-1183.

Ghosh S, Karin M. Missing pieces in the NF-kappaB puzzle. *Cell*. 2002; 109 Suppl:S81-96.

Ghosh G, van Duyne G, Ghosh S, Sigler PB. Structure of NF-k B p50 homodimer bound to a k B site. *Nature*. 1995; 373: 303-310.

Gilmore TD. Introduction to NF-κB: players, pathways, perspectives. *Oncogene*. 2006; 25(51):6680– 6684.

Gleissner CA, Galkina E, Nadler JL, Ley K. Mechanisms by which diabetes increases cardiovascular disease. *Drug Discov Today Dis Mech*. 2007; 4:131–140.

- Ghosh D, Weeks CM, Grochulski P, Duax WL, Erman M, Rimsay RL, Orr Jc. Three-dimensional structure of holo 3 α ,20 β -hydroxysteroid dehydrogenase: a member of a short-chain dehydrogenase family. *Proc Natl Acad Sci USA*. 1991; 88:10064-10068.
- Grela E, Kozłowska J, Grabowiecka A. Current methodology of MTT assay in bacteria – A review. *Acta Histochemica*. 2018; 120(4): 303–311.
- Giri B, Dey S, Das T, Sarkar M, Banerjee J, Dash SK. Chronic hyperglycemia mediated physiological alteration and metabolic distortion leads to organ dysfunction, infection, cancer progression and other pathophysiological consequences: An update on glucose toxicity. *Biomed Pharmacother*. 2018; 107:306-328.
- Graham A, Brown L, Hedge PJ, Gammack AJ, Markham AF. Structure of the human aldose reductase gene. *J Biol Chem*. 1991; 266(11):6872-6877.
- Grune T, Davies KJ. The proteasomal system and HNE-modified proteins. *Mol Asp Med*. 2003; 24(4- 5):195-204.
- Grune T, Merker K, Sandig G, Davies KJ. Selective degradation of oxidatively modified protein substrates by the proteasome. *Biochem Biophys Res Commun*. 2003; 305(3):709-718.
- Guéraud F. 4-Hydroxynonenal metabolites and adducts in pre-carcinogenic conditions and cancer. *Free Radic Biol Med*. 2017; 111:196-208.
- Guéraud F, Crouzet F, Alary J, Rao D, Debrauwer L, Laurent F, Cravedi JP. Enantioselective metabolism of (R)- and (S)-4-hydroxy-2-nonenal in rat. *BioFactors*. 2005; 24(1-4):97-104.
- Guichardant M, Taibi-Tronche P, Fay LB, Lagarde M. Covalent modifications of aminophospholipids by 4-hydroxynonenal. *Free Radic Biol Med*. 1998; 25(9):1049-1056.
- Guzman-Martinez L, Maccioni RB, Andrade V, Navarrete LP, Pastor MG, Ramos-Escobar N. Neuroinflammation as a common feature of neurodegenerative disorders. *Front Pharmacol*. 2019; 10:1008.
- Ha H, Lee HB. Reactive oxygen species as glucose signaling molecules in mesangial cells cultured under high glucose. *Kidney Inter Suppl*. 2000. 77:S19-S25.
- Hashimoto M, Sibata T, Wasada H, Toyokuni S, Uchida K. Structural basis of protein-bound endogenous aldehydes. Chemical and immunochemical characterizations of configurational

isomers of 4-hydroxy-2-nonenal-histidine adduct. *J Biol Chem.* 2003; 278(7):5044-5051.

Hayden MS, Ghosh S. Shared principles in NF- κ B signaling. *Cell.* 2008; 132(3):344-362.

Hayes JD, Flanagan JU, Jowsey IR. Glutathione transferases. *Annu Rev Pharmacol Toxicol.* 2005; 45:51-88.

Hers HG. The mechanism of the transformation of glucose in fructose in the seminal vesicles. *Biochem Biophys Acta.* 1956; 22(1):202-203.

Hiratsuka A, Hirose K, Saito H, Watabe T. 4-Hydroxy-2(E)-nonenal enantiomers: (S)-selective inactivation of glyceraldehyde-3-phosphate dehydrogenase and detoxification by rat glutathione S-transferase A4-4. *Biochem J.* 2000; 349(3):729-735.

Hiratsuka A, Tobita K, Saito H, Sakamoto Y, Nakano H, Oqura K, Nishiyama T, Watabe T. (S)- preferential detoxification of 4-hydroxy-2(E)-nonenal enantiomers by hepatic glutathione-S-transferase isoforms in guinea-pigs and rats. *Biochem J.* 2001; 355(1):237-244.

Hiroaki M, Eisenbarth GS. Genetics and environmental factors in endocrine/organ-specific autoimmunity: have there been any major advances? *Springer Semin Immunopathol.* 2002; 24:231- 242.

Hoesel B, Schmid JA. The complexity of NF- κ B signaling in inflammation and cancer. *Mol Cancer.* 2013; 12:86.

Honzatko A, Brichac J, Murphy TC, Reberg A, Kubatova A, Smoliakova IP, Picklo Sr. MJ. Enantioselective metabolism of trans-4-hydroxy-2-nonenal by brain mitochondria. *Free Radic Biol Med.* 2005; 39(7):913-924.

Hotamisligil GS, Shargill NS, Spiegelman BM. Adipose expression of tumor necrosis factor-alpha: direct role in obesity-linked insulin resistance. *Science.* 1993; 259:87-91.

Hu FB, Manson JE, Stampfer MJ, Colditz G, Liu S, Solomon CG, Willett WC. Diet, lifestyle, and the risk of type 2 diabetes mellitus in women. *N Engl J Med.* 2001; 345(11):790-797.

International Diabetes Federation, IDF. IDF Diabetes Atlas, 8th ed. Brussels, Belgium. 2017.

Ishii T, Itoh K, Ruiz E, Leake DS, Unoki H, Yamamoto M, Mann GE. Role of Nrf2 in the regulation of CD36 and stress protein expression in murine macrophages: activation by

oxidatively modified LDL and 4-hydroxynonenal. *Circ Res.* 2004; 94(5):609-16.

Ito F, Sono Y, Ito T. Measurement and clinical significance of lipid peroxidation as a biomarker of oxidative stress: oxidative stress in diabetes, atherosclerosis, and chronic inflammation. *Antioxidants.* 2019; 8(3):72.

Jez JM, Bennett MJ, Schlegel BP, Lewis M, Penning TM. Comparative anatomy of the aldo-keto reductase superfamily. *Biochem J.* 1997; 326 (Pt 3):625-636.

Ji C, Kozak KR, Marnett LJ. IkappaB kinase, a molecular target for inhibition by 4-hydroxy-2-nonenal. *J Biol Chem.* 2001; 276(21):18223-18228.

Johnson RJ, Rodriguez Iturbe B, Roncal Jimenez C, Lanaspa MA, Ishimoto T, Nakagawa T, Correa Rotter R, Wesseling C, Bankir L, Sanchez Lozada LG. Hyperosmolarity drives hypertension and CKD--water and salt revisited. *Nat Rev Nephrol.* 2014; 10(7):415-420.

Jörnvall H, Persson B, Krook M, Atrian S, González-Duarte R, Jeffery J, Ghosh D. Short-chain dehydrogenases/reductases (SDR). *Biochemistry.* 1995; 34(18):6003-6013.

Kahn BB, Flier JS. Regulation of glucose-transporter gene expression in vitro and in vivo. *DiabetesCare.* 1990; 13:548-564.

Kahn SE, Hull RL, Utzschneider KM. Mechanisms linking obesity to insulin resistance and type 2 diabetes. *Nature.* 2006; 444:840-846.

Kanayama M, Yamaguchi S, Shibata T, Shibata N, Kobayashi M, Nagai R, Arai H, Takahashi K, Uchida K. Identification of a serum component that regulates cyclooxygenase-2 gene expression in cooperation with 4-hydroxy-2-nonenal. *J Biol Chem.* 2007; 282(33):24166-24174.

Klip A, Tsakiridis T, Marette A, Ortiz PA. Regulation of expression of glucose transporters by glucose: a review of studies in vivo and in cell cultures. *FASEB J.* 1994; 8(1):43-53.

Kubo E, Urakami T, Fatma N, Akagi Y, Singh DP. Polyol pathway-dependent osmotic and oxidative stresses in aldose reductase-mediated apoptosis in human lens epithelial cells: role of AOP2. *Biochem Biophys Res Commun.* 2004; 314(4):1050-1056.

Kumagai T, Matsukawa N, Kaneko Y, Kusumi Y, Mitsumata M, Uchida K. A lipid peroxidation-derived inflammatory mediator: identification of 4-hydroxy-2-nonenal as a potential inducer of cyclooxygenase-2 in macrophages. *J Biol Chem.* 2004; 279(46):48389-

48396.

Kumagai T, Usami H, Matsukawa N, Nakashima F, Chikazawa M, Shibata T, Noguchi N, Uchida K. Functional interaction between cyclooxygenase-2 and p53 in response to an endogenous electrophile. *Redox Biol.* 2015; 4:74-86.

Laemmli UK. Cleavage of structural proteins during the assembly of the head bacteriophage T4. *Nature.* 1970; 227(5259):680-685.

Lee AY, Chung SS. Contributions of polyol pathway to oxidative stress in diabetic cataract. *FASEBJ.* 1999; 13(1):23-30.

Lee R, McElroy WD. Role and reactivity of sulfhydryl groups in firefly luciferase. *Biochemistry.* 1969; 8(1):130-136.

Lee SR, An EJ, Kim J, Bae YS. Function of NADPH oxidases in diabetic nephropathy and development of Nox inhibitors. *Biomol Ther (Seoul).* 2020; 28(1):25-33.

Lemieux N, Malfoy B, Forrest GL. Human carbonyl reductase (CBR) localized to band 21q22.1 by high-resolution fluorescence in situ hybridization displays gene dosage effects in trisomy 21 cells. *Genomics.* 1993; 15:169-172.

Leitinger N. Cholesteryl ester oxidation products in atherosclerosis. *Mol Aspects Med.* 2003; 24:239- 250.

Li Q, Sadhukhan S, Berthiaume JM, Ibarra RA, Tang H, Deng S, Hamilton E, Nagy LE, Tochtrop GP, Zhang GF. 4-Hydroxy-2(E)-nonenal (HNE) catabolism and formation of HNE adducts are modulated by β oxidation of fatty acids in the isolated rat heart. *Free Radic Biol Med.* 2013; 58:35- 44.

Li RL, Zhao WW, Gao BY. Advanced glycation end products induce neural tube defects through elevating oxidative stress in mice. *Neural Regen Res.* 2018; 13(8):1368-1374.

Lim JW, Kim H, Kim KH. Nuclear factor-kappaB regulates cyclooxygenase-2 expression and cell proliferation in human gastric cancer cells. *Lab Invest.* 2001; 81(3):349-60.

Liu W, Porter NA, Schneider C, Brash AR, Yin H. Formation of 4-hydroxynonenal from cardiolipin oxidation: intramolecular peroxy radical addition and decomposition. *Free Radic*

Biol Med. 2011; 50(1):166-178.

Liu T, Zhang L, Joo D, Sun SC. NF- κ B signaling in inflammation. *Signal Transduct Target Ther.* 2017; 2:17023.

Lou MF. Redox regulation in the lens. *Prog Retin Eye Res.* 2003; 22(5):657-682.

Luczaj W, Gęgotek A, Skrzydlewska E. Antioxidants and HNE in redox homeostasis. *Free Radic Biol Med.* 2017; 111:87-101.

Malek S, Huang DB, Huxford T, Ghosh S, Ghosh G. X-ray crystal structure of an I κ B β X NF- κ B p65 homodimer complex. *J Biol Chem.* 2003; 278:23094-23100.

Manolescu AR, Witkowska K, Kinnaird A, Cessford T, Cheeseman C. Facilitated hexose transporters: new perspectives on form and function. *Physiology.* 2007; 22:234-240.

Masferrer JL, Zweifel BS, Manning PT, Hauser SD, Leahy KM, Smith WG, Isakson PC, Seibert K. Selective inhibition of inducible cyclooxygenase 2 in vivo is anti-inflammatory and nonulcerogenic. *Proc Natl Acad Sci USA.* 1994; 91:3228-3232.

Matsunaga T, Shintani S, Hara A. Multiplicity of mammalian reductases for xenobiotic carbonyl compounds. *Drug Metab Pharmacokinet.* 2006; 21(1):1-18.

Mercurio F, DiDonato JA, Rosette C, Karin M. p105 and p98 precursor proteins play an active role in NF- κ B-mediated signal transduction. *Genes Dev.* 1993; 7(4):705-718.

Minko IG, Kozekov ID, Harris TM, Rizzo CJ, Lloyd RS, Stone MP. Chemistry and biology of DNA containing 1, N 2-deoxyguanosine adducts of the α,β -unsaturated aldehydes acrolein, crotonaldehyde, and 4-hydroxynonenal. *Chem Res Toxicol.* 2009; 22(5):759-778.

Mol M, Regazzoni L, Altomare A, Degani G, Carini M, Vistoli G, Aldini G. Enzymatic and non-enzymatic detoxification of 4-hydroxynonenal: Methodological aspects and biological consequences. *Free Radic Biol Med.* 2017; 111:328-344.

Moschini R, Peroni E, Rotondo R, Renzone G, Melck D, Cappiello M, Srebot M, Napolitano E, Motta A, Scaloni A, Mura U, Del Corso A. NADP(+)-dependent dehydrogenase activity of carbonyl reductase on glutathionylhydroxynonenal as a new pathway for hydroxynonenal detoxification. *Free Radic Biol Med.* 2015; 83:66-76.

Moschini R, Rotondo R, Renzone G, Balestri F, Cappiello M, Scaloni A, Mura U, Del Corso A. Kinetic features of carbonyl reductase 1 acting on glutathionylated aldehydes. *Chem Biol*

Interact. 2017; 276:127-132.

Mosmann T. Rapid colorimetric assay for cellular growth and survival: Application to proliferation and cytotoxicity assays. *J Immunol Methods.* 1983; 65(1–2): 55–63.

Mueckler M. Family of glucose transporter genes: implications for glucose homeostasis and diabetes. *Diabetes.* 1990; 39:6-11.

Muller CW, Rey FA, Sodeoka M, Verdine GL, Harrison SC. Structure of the NF- κ B p50 homodimer bound to DNA. *Nature.* 1995; 373:311-317.

Muzio G, Barrera G, Pizzimenti S. Peroxisome Proliferator-Activated Receptors (PPARs) and oxidative stress in physiological conditions and in cancer. *Antioxidants.* 2021; 10(11):1734.

Nair U., Bartsch H, Nair J. Lipid peroxidation-induced DNA damage in cancer-prone inflammatory diseases: a review of published adduct types and levels in humans. *Free Radic Biol Med.* 2007; 43:1109-1120.

Nakajima A, Yamada K, Zou LB, Yan Y, Mizuno M, Nabeshima T. Interleukin-6 protects PC12 cells from 4-hydroxynonenal-induced cytotoxicity by increasing intracellular glutathione levels. *Free Radic Biol Med.* 2002; 32(12):1324-1332.

Nakrani MN, Wineland RH, Anjum F. Physiology, Glucose Metabolism. *StatPearls.* 2021.

Nicholson T, Church C, Baker DJ, Jones SW. The role of adipokines in skeletal muscle inflammation and insulin sensitivity. *J Inflamm.* 2018; 15:9.

Niimi N, Yako H, Takaku S, Chung SK, Sango K. Aldose reductase and the polyol pathway in Schwann cells: old and new problems. *Int J Mol Sci.* 2021; 22(3):1031.

Ofei F, Hurel S, Newkirk J, Sopwith M, Taylor R. Effects of an engineered human anti-TNF- α antibody (CDP571) on insulin sensitivity and glycemic control in patients with NIDDM. *Diabetes.* 1996; 45:881–885.

Ohtsu A, Shibutani Y, Seno K, Iwata H, Kuwayama T, Shirasuna K. Advanced glycation end products and lipopolysaccharides stimulate interleukin-6 secretion via the RAGE/TLR4-NF- κ B-ROS pathways and resveratrol attenuates these inflammatory responses in mouse macrophages. *Exp Ther Med.* 2017; 14(5):4363-4370.

Okada K, Wangpoengtrakul C, Osawa T, Toyokuni S, Tanaka K, Uchida K. 4-Hydroxy-2-

nonenal-mediated impairment of intracellular proteolysis during oxidative stress. Identification of proteasomes as target molecules. *J Biol Chem.* 1999; 274(34):23787-23793.

Panahi G, Pasalar P, Zare M, Rizzuto R, Meshkani R. High glucose induces inflammatory responses in HepG2 cells via the oxidative stress-mediated activation of NF- κ B, and MAPK pathways in HepG2 cells. *Arch Physiol Biochem.* 2018; 124(5):468-474.

Parola M, Bellomo G, Robino G, Barrera G, Dianzani MU. 4-Hydroxynonenal as a biological signal: molecular basis and pathophysiological implications. *Antioxid Redox Signal.* 1999; 1(3):255-284.

Parola M, Robino G, Marra F, Pinzani M, Bellomo G, Leonarduzzi G, Chiarugi P, Camandola S, Poli G, Waeg G, Gentilini P, Dianzani MU. HNE interacts with JNK isoforms in human hepatic stellate cells. *J Clin Invest.* 1998; 102(11):1942-1950.

Perkins ND, Gilmore TD. Good cop, bad cop: the different faces of NF-kappaB. *Cell Death Differ.* 2006; 13(5):759-72.

Peroni E, Scali V, Balestri F, Cappiello M, Mura U, Del Corso A, Moschini R. Pathways of 4 - hydroxy-2-nonenal detoxification in a human astrocytoma cell line. *Antioxidants.* 2020; 9(5):385- 398.

Petras T, Siems WG, Grune T. 4-hydroxynonenal is degraded to mercapturic acid conjugate in rat kidney. *Free Radic Biol Med.* 1995; 19(5):685-688.

Poli G, Schaur RJ. 4-Hydroxynonenal in the pathomechanisms of oxidative stress. *IUBMB Life.* 2000; 50(4-5):315-321.

Poli G, Schaur RJ, Siems WG, Leonarduzzi G. 4-hydroxynonenal: a membrane lipid oxidation product of medicinal interest. *Med Res Rev.* 2008; 28(4):569-631.

Poligone B, Baldwin AS. Positive and negative regulation of NF-kappaB by COX-2: roles of different prostaglandins. *J Biol Chem.* 2001; 276(42):38658-38664.

Ramana KV. Aldose reductase: new insights for an old enzyme. *Biomol Concepts.* 2011; 2(1-2):103- 114.

Ramana KV, Bhatnagar A, Srivastava S, Yadav UC, Awasthi S, Awasthi YC, Srivastava SK. Mitogenic responses of vascular smooth muscle cells to lipid peroxidation-derived aldehyde 4-hydroxy-trans-2-nonenal (HNE): role of aldose reductase-catalyzed reduction of the HNE-

glutathione conjugates in regulating cell growth. *J Biol Chem.* 2006; 281(26):17652-17660.

Ramana KV, Fadl AA, Tammali R, Reddy AB, Chopra AK, Srivastava SK. Aldose reductase mediates the lipopolysaccharide-induced release of inflammatory mediators in RAW264.7 murine macrophages. *J Biol Chem.* 2006; 281(44):33019-33029.

Ramana KV, Friedrich B, Bhatnagar A, Srivastava SK. Aldose reductase mediates cytotoxic signals of hyperglycemia and TNF- α in human lens epithelial cells. *FASEB J.* 2003; 17(2):315-317.

Ramana KV, Srivastava SK. Aldose reductase: a novel therapeutic target for inflammatory pathologies. *Int J Biochem Cell Biol.* 2010; 42(1):17-20.

Raza H, John A. 4-hydroxynonenal induces mitochondrial oxidative stress, apoptosis and expression of glutathione S-transferase A4-4 and cytochrome P450 2E1 in PC12 cells. *Toxicol Appl Pharmacol.* 2006; 216(2):309-318.

Reddy AB, Tammali R, Mishra R, Srivastava S, Srivastava SK, Ramana KV. Aldose reductase deficiency protects sugar-induced lens opacification in rats. *Chem Biol Interact.* 2011. 191(1-3):346-350.

Reichard JF, Doorn JA, Simon F, Taylor MS, Petersen DR. Characterization of multidrug resistance-associated protein 2 in the hepatocellular disposition of 4-hydroxynonenal. *Arch Biochem Biophys.* 2003; 411(2):243-250.

Renes J, de Vries EG, Jansen PL, Muller M. The (patho)physiological functions of the MRP family.

Drug Resist Updat. 2000; 3(5):289-302.

Rittner HL, Hafner V, Klimiuk PA, Szweda LI, Goronzy JJ, Weyand CM. Aldose reductase functions as a detoxification system for lipid peroxidation products in vasculitis. *J Clin Invest.* 1999; 103(7):1007-1013.

Rolo AP and Palmeira CM. Diabetes and mitochondrial function: role of hyperglycemia and oxidative stress. *Toxicol Appl Pharmacol.* 2006; 212(2):167-178.

Rotondo R, Moschini R, Renzone G, Tuccinardi T, Balestri F, Cappiello M, Scaloni A, Mura U, Del Corso A. Human carbonyl reductase 1 as efficient catalyst for the reduction of glutathionylated aldehydes derived from lipid peroxidation. *Free Radic Biol Med.* 2016; 99:323-332.

Ruben SM, Klement JF, Coleman TA, Maher M, Chen CH, Rosen CA. I-Rel: a novel related protein that inhibits NF-kappa B transcriptional activity. *Genes Dev.* 1992; 6(5):745-760.

Ruef J, Moser M, Bode C, Kubler W, Runge MS. 4-Hydroxynonenal induces apoptosis, NF-kappaB activation and formation of 8-isoprostane in vascular smooth muscle cells. *Basic Res Cardiol.* 2001;96(2):143-150.

Ryseck RP, Bull P, Takamiya M, Bours V, Siebenlist U, Dobrzanski P, Bravo R. RelB, a new Rel family transcription activator that can interact with p50-NF-kappa B. *Mol Cell Biol.* 1992; 12(2):674- 684.

Sadhukhan S, Han Y, Jin Z, Tochtrop GP, Zhang GF. Glutathionylated 4-hydroxy-2-(E)-alkenal enantiomers in rat organs and their contributions toward the disposal of 4-hydroxy-2-(E)-nonenal in rat liver. *Free Radic Biol Med.* 2014; 70:78-85.

Sartor B. Specific NF- κ B blockade selectively inhibits tumour necrosis factor- α -induced COX-2 but not constitutive COX-1 gene expression in HT-29 cells. *Immunology.* 1998; 95(4):537-543.

Sattar N, Gill JM. Type 2 diabetes as a disease of ectopic fat? *BMC Med.* 2014; 12:123-129.

Schaur RJ. Basic aspects of the biochemical reactivity of 4-hydroxynonenal. *Mol Aspect Med.* 2003;24(4-5):149-159.

Schmidt JA, Birbach A. IkappaB kinase beta (IKKbeta/IKK2/IKBKB)--a key molecule in signaling to the transcription factor NF-kappaB. *Cytokine Growth Factor Rev.* 2008; 19(2):157-165.

Schmitz ML, Stelzer G, Altmann H, Meisterernst M, Baeuerle PA. Interaction of the COOH-terminal transactivation domain of p65 NF-kappa B with TATA-binding protein, transcription factor IIB, and coactivators. *J Biol Chem.* 1995; 270(13):7219-7226.

Schneider C, Porter NA, Brash AR. Routes to 4-hydroxynonenal: fundamental issues in the mechanisms of lipid peroxidation. *J Biol Chem.* 2008; 283(23):15539-15543.

Schneider C, Tallman KA, Porter NA, Brash AR. Two distinct pathways of formation of 4-hydroxynonenal. Mechanisms of nonenzymatic transformation of the 9- and 13-hydroperoxides of linoleic acid to 4-hydroxyalkenals. *J Biol Chem.* 2001; 276(24):20831-20838.

Sen R, Baltimore D. Multiple nuclear factors interact with the immunoglobulin enhancer sequences. *Cell*. 1986; 46(5):705-16.

Sen N, Paul BD, Gadalla MM, Mustafa AK, Sen T, Xu R, Kim S, Snyder SH. Hydrogen sulfide- linked sulfhydration of NF- κ B mediates its antiapoptotic actions. *Mol Cell*. 2012; 45(1):13-24.

Senftleben U. Activation by IKK α of a second, evolutionary conserved, NF-kappa B signaling pathway. *Science*. 2001; 293(5534):1495-1499.

Shanmugam N, Gaw Gonzalo IT, Natarajan R. Molecular mechanisms of high glucose-induced cyclooxygenase-2 expression in monocytes. *Diabetes*. 2004; 53(3):795-802.

Sharma R, Yang Y, Sharma A, Dwivedi S, Popov VL, Boor PJ, Singhal SS, Awasthi S, Awasthi YC. Mechanisms and physiological significance of the transport of the glutathione conjugate of 4 - hydroxynonenal in human lens epithelial cells. *Invest Ophthalmol Vis Sci*. 2003; 44(8):3438-3449.

Shringarpure R, Grune T, Mehlhase J, Davies KJ. Ubiquitin conjugation is not required for the degradation of oxidized proteins by proteasome. *J Biol Chem*. 2003; 278(1):311-318.

Singh S, Brocker C, Koppaka V, Chen Y, Jackson BC, Matsumoto A, Thompson DC, Vasiliou V. Aldehyde dehydrogenases in cellular responses to oxidative/electrophilic stress. *Free Radic Biol Med*. 2013; 56:89-101.

Singh T, Newman AB. Inflammatory markers in population studies of aging. *Ageing Res Rev*. 2011;10(3):319-329.

Singhal J, Singhal SS, Yadav S, Suzuki S, Warnke MM, Yacoub A, Dent P, Bae S, Sharma R, Awasthi YC, Armstrong DW, Awasthi S. RLIP76 in defense of radiation poisoning. *Int J Radiat Oncol Biol Phys*. 2008; 72(2):553-561.

Smith WL, DeWitt DL, Garavito RM. Cyclooxygenases: structural, cellular, and molecular biology.

Annu Rev Biochem. 2000; 69:145-182.

Smith W, Garavito R, DeWitt D. Prostaglandin endoperoxide H synthases (cyclooxygenases)-1 and -2. *J Biol Chem*. 1996. 271:33157-33160.

Son SM. Reactive oxygen and nitrogen species in pathogenesis of vascular complications of

diabetes. *Diabetes Metab J*. 2012; 36(3):190-198.

Song J, Yang X, Yan LJ. Role of pseudohypoxia in the pathogenesis of type 2 diabetes. *Hypoxia (Auckl)*. 2019; 7:33-40.

Sonowal H, Ramana KV. 4-Hydroxy-trans-2-nonenal in the regulation of anti-oxidative and pro-inflammatory signaling pathways. *Oxid Med Cell Longev*. 2019; 2019(Figure 1):1-17.

Srivastava SK, Ansari NH. Prevention of sugar-induced cataractogenesis in rats by butylated hydroxytoluene. *Diabetes*. 1988; 37:1505-1508.

Srivastava S, Chandra A, Bhatnagar A, Srivastava SK, Ansari NH. Lipid peroxidation product, 4-hydroxynonenal and its conjugate with GSH are excellent substrates of bovine lens aldose reductase. *Biochem Biophys Res Commun*. 1995; 217(3):741-746.

Srivastava SK, Ramana KV. Focus on molecules: nuclear factor-kappaB. *Exp Eye Res*. 2009; 88(1):2-3.

Srivastava SK, Ramana KV, Bhatnagar A. Role of aldose reductase and oxidative damage in diabetes and the consequent potential for therapeutic options. *Endocr Rev*. 2005; 26(3):380-392.

Steinmetz PR, Balko C, Gabbay KH. The sorbitol pathway and the complications of diabetes. *N Engl J Med*. 1973; 288(16):831-836.

Sun SC. The non-canonical NF- κ B pathway in immunity and inflammation. *Nat Rev Immunol*. 2017; 17(9):545-558.

Sunjic SB, Gasparovic AC, Jaganjac M, Rechberger G, Meinitzer A, Grune T, Kohlwein SD, Mihaljevic B, Zarkovic N. Sensitivity of osteosarcoma cells to concentration-dependent bioactivities of lipid peroxidation product 4-hydroxynonenal depend on their level of differentiation. *Cell*. 2021; 10(2):269.

Szablewski L. Diabetes mellitus: influences on cancer risk. *Diabetes Metab Res Rev*. 2014; 30(7):543-553.

Szablewski L. Distribution of glucose transporters in renal diseases. *J Biomed Sci*. 2017; 24(1):64.

Tammali R, Ramana KV, Srivastava SK. Aldose reductase regulates TNF-alpha-induced PGE2 production in human colon cancer cells. *Cancer Lett*. 2007; 252(2):299-306.

Tanabe T, Tohnai N. Cyclooxygenase isozymes and their gene structures and expression.

Prostaglandins Other Lipid Mediat. 2002; 68-69:95-114.

Tinguely JN, Wermuth B. Identification of the reactive cysteine residue (Cys227) in human carbonyl reductase. *Eur J Biochem.* 1999; 260(1):9-14.

Tumova S, Kerimi A, Porter KE, Williamson G. Transendothelial glucose transport is not restricted by extracellular hyperglycaemia. *Vascul Pharmacol.* 2016; 87:219-229.

Uchida K. 4-Hydroxy-2-nonenal: a product and mediator of oxidative stress. *Prog Lipid Res.* 2003;42(4):318-343.

Uchida K. HNE as an inducer of COX-2. *Free Radic Biol Med.* 2017; 111:169-172.

Vander Jagt DL, Kolb NS, Vander Jagt TJ, Chino J, Martinez FJ, Hunsaker LA, Royer RE. Substrate specificity of human aldose reductase: identification of 4-hydroxynonenal as an endogenous substrate. *Biochim Biophys Acta.* 1995; 1249(2):117-126.

Verma IM, Stevenson JK, Schwarz EM, Van Antwerp D, Miyamoto S. Rel/NF-kappa B/I kappa B family: intimate tales of association and dissociation. *Genes Dev.* 1995; 9(22):2723-2735.

Vermeulen L, De Wilde G, Van Damme P, Vanden Berghe W, Haegeman G. Transcriptional activation of the NF-kappaB p65 subunit by mitogen- and stress-activated protein kinase-1 (MSK1). *EMBO J.* 2003; 22(6):1313-1324.

Verzella D, Pescatore A, Capece D, Vecchiotti D, Ursini MV, Franzoso G, Alesse E, Zazzeroni F. Life, death, and autophagy in cancer: NF-κB turns up everywhere. *Cell Death Dis.* 2020; 11(3):210.

Vlassara H, Fuh H, Makita Z, Krungkrai S, Cerami A, Bucala R. Exogenous advanced glycosylation end products induce complex vascular dysfunction in normal animals: a model for diabetic and aging complications. *Prot Natl Acad Sci U S A.* 1992; 89(24):12043-12047.

Volpe CMO, Villar-Delfino PH, Dos Anjos PMF, Nogueira-Machado JA. Cellular death, reactive oxygen species (ROS) and diabetic complications. *Cell Death Dis.* 2018; 9(2):119.

Wermuth B. Purification and properties of an NADPH-dependent carbonyl reductase from human brain. Relationship to prostaglandin 9-ketoreductase and xenobiotic ketone reductase. *J Biol Chem.* 1981; 256(3):1206-1213.

Williamson JR, Chang K, Frangos M, Hasan KS, Ido Y, Kawamura T, Nyengaard JR, van den

Enden M, Kilo C, Tilton RG. Hyperglycemic pseudohypoxia and diabetic complications. *Diabetes*. 1993; 42(6):801-813.

Wilson DK, Bohren KM, Gabbay KH, Quioco FA. An unlikely sugar substrate site in the 1.65 Å structure of the human aldose reductase holoenzyme implicated in diabetic complications. *Science*. 1992; 257:81-84.

Wirth H, Wermuth B. Immunohistochemical localization of carbonyl reductase in human tissues. *J Histochem Cytochem*. 1992; 40(12):1857-1863.

Wong D, Teixeira A, Oikonomopoulos S, Humburg P, Lone IN, Saliba D, Siggers T, Bulyk M, Angelov D, Dimitrov S, Udalova IA, Ragoussis J. Extensive characterization of NF- κ B binding uncovers non-canonical motifs and advances the interpretation of genetic functional traits. *Genom Biol*. 2011; 12(7):R70.

World Health Organization, WHO. Global Report on Diabetes. 2016.

Xiao G, Harhaj EW, Sun SC. NF-kappaB-inducing kinase regulates the processing of NF-kappaB2 p100. *Mol Cell*. 2001; 7(2):401-409.

Xu XM, Tang JL, Chen X, Wang LH, Wu KK. Involvement of Two Sp1 Elements in Basal Endothelial Prostaglandin H Synthase-1 Promoter Activity. *J Biol Chem*. 1997; 272(11):6943-50.

Yadav UC, Ramana KV. Regulation of NF- κ B-induced inflammatory signaling by lipid peroxidation-derived aldehydes. *Oxid Med Cell Longev*. 2013; 2013:690545.

Yadav UCS, Srivastava SK, Ramana KV. Understanding the role of aldose reductase in ocular inflammation. *Curr Mol Med*. 2010; 10(6):540-549.

Yamamoto K, Arakawa T, Ueda N, Yamamoto S. Transcriptional roles of nuclear factor kappa B and nuclear factor-interleukin-6 in the tumor necrosis factor alpha-dependent induction of cyclooxygenase-2 in MC3T3-E1 cells. *J Biol Chem*. 1995; 270(52):31315-20.

Yan LJ. Pathogenesis of chronic hyperglycemia: from reductive stress to oxidative stress. *J Diabetes Res*. 2014; 2014:137919.

Yan LJ. Redox imbalance stress in diabetes mellitus: role of the polyol pathway. *Animal Model Exp Med*. 2018; 1(1):7-13.

Yang J, Gupta V, Tallman KA, Porter NA, Carroll KS, Liebler DC. Global, *in situ*, site-specific

- analysis of protein S-sulfenylation. *Nat Protoc.* 2015; 10(7):1022-1037.
- Yano M, Hasegawa G, Ishii M, Yamasaki M, Fukui M, Nakamura N, Yoshikawa T. Short-term exposure of high glucose concentration induces generation of reactive oxygen species in endothelial cells: implication for the oxidative stress associated with postprandial hyperglycemia. *Redox Rep.* 2004. 9:111-116.
- Yaribeygi H, Atkin SL, Sahebkar A. A review of the molecular mechanisms of hyperglycemia-induced free radical generation leading to oxidative stress. *J Cell Physiol.* 2019; 234(2):1300-1312.
- Yeung F, Hoberg JE, Ramsey CS, Keller MD, Jones DR, Frye RA, Mayo MW. Modulation of NF- κ B-dependent transcription and cell survival by the SIRT1 deacetylase. *EMBO J.* 2004; 23(12):2369-2380.
- Yin H, Xu L, Porter, NA. Free radical lipid peroxidation: mechanisms and analysis. *Chem Rev.* 2011; 111(10):5944-5972.
- Yoval Sánchez B, Rodríguez Zavala JS. Differences in susceptibility to inactivation of human aldehyde dehydrogenases by lipid peroxidation byproducts. *Chem Res Toxicol.* 2012; 25(3):722-729.
- Zarkovic N, Ilic Z, Jurin M, Schaur RJ, Puhl H, Esterbauer H. Stimulation of HeLa cell growth by physiological concentrations of 4-hydroxynonenal. *Cell Biochem Funct.* 1993; 11(4):279-286.
- Zhang H, Forman HJ. 4-hydroxynonenal-mediated signaling and aging. *Free Radic Biol Med.* 2017; 111:219-225.
- Zhang H, Forman HJ. Signaling by 4-hydroxy-2-nonenal: Exposure protocols, target selectivity and degradation. *Arch Biochem Biophys.* 2017; 617(12):145-154.
- Zhang T, Zhao Q, Ye F, Huang CY, Chen WM, Huang WQ. Alda-1, an ALDH2 activator, protects against hepatic ischemia/reperfusion injury in rats via inhibition of oxidative stress. *Free Radic Res.* 2018; 52(6):629-638.
- Zhong L, Liu Z, Yan R, Johnson S, Zhao Y, Fang X, Cao D. Aldo-keto reductase family 1 B10 protein detoxifies dietary and lipid-derived α , β -unsaturated carbonyls at physiological levels. *Biochem Biophys Res Commun.* 2009; 387(2):245-250.

Zhong H, May MJ, Jimi E, Ghosh S. The phosphorylation status of nuclear NF-kappa B determines its association with CBP/p300 or HDAC-1. *Mol Cell*. 2002; 9(3):625-636.

Zhong H, SuYang H, Erdjument-Bromage H, Tempst P, Ghosh S. The transcriptional activity of NF-kappaB is regulated by the IkappaB-associated PKAc subunit through a cyclic AMP-independent mechanism. *Cell*. 1997; 89(3):413-24.

Zimniak P. Detoxification reactions: relevance to aging. *Ageing Res Rev*. 2008; 7:281-300.

Zinatizadeh MR, Schock B, Chalbatani GM, Zarandi PK, Jalali SA, Miri SR. The Nuclear Factor Kappa B (NF-kB) signaling in cancer development and immune diseases. *Genes Dis*. 2020; 8(3):287-297.